RHODES UNIVERSITY

GEOLOGY DEPARTMENT

PRIMARY CONTROLS ON IRON AND MANGANESE DISTRIBUTION IN SPHALERITE OF THE GAMS FORMATION, GAMSBERG ZINC DEPOSIT, NAMAQUALAND, SOUTH AFRICA

By

Léo Poignant-Molina

Thesis presented in partial fulfilment of the requirements for the Degree of Master of Science in Economic Geology, Department of Geology, Rhodes University.

March 2018

Declaration

I declare that this thesis is my own work, and any authors have been accordingly acknowledged. It is being submitted in fulfilment of the Degree of Master of Science in Economic Geology at Rhodes University, Grahamstown, and has not been submitted before for the examination of any degree through any other university.

Léo Poignant-Molina
Student number: 17P8636

March 17th 2018

Abstract

The Gamsberg deposit is a 200 Mt zinc reserve belonging to the world class base metal-rich Aggeneys-Gamsberg mining district. A rifting environment permitted the development of four proximal SEDEX-type deposits whereby Gamsberg is localized in the eastern side of the district and characterised by a peculiar enrichment in manganese. This study investigates the geochemistry of sphalerite in the Gams Formation holding the economic units of the deposit. Microscopic petrography revealed that most of primary textures have been overprinted by recrystallization, alteration, replacement and deformational textures produced during the polyphase metamorphism of the Namaquan Orogeny. Therefore, EPMA analysis provided the bulk of information to define the geochemical distribution of sphalerite. A lateral variation was noticed throughout the Gams Formation, whereby the North orebody presents Zn-rich and Fe+Mn-poor sphalerite while the West and East orebodies contain Zn-poor and Fe-Mn-rich sphalerite. This feature has been interpreted as the association of a chemocline and a variation in the basin topography defining deep Mn+Fe-rich zones and shallow Mn+Fe-poor zones in the primitive basin. It is suggested that mineralized hot brines mixed with seawater developed the chemocline. The uneven topography shaped the geochemical variation between the actual orebodies.

Table of Content

List of Figures

List of Tables

Mineral Abbreviations

Alabandite	**Abd**
Galena	Gn
Garnet	Grt
Ilmenite	Ilm
Magnetite	Mag
Muscovite	Musc
Pyrite	Py
Pyrrhotite	Po
Quartz	Qz
Sillimanite	Sil
Sphalerite	Sp

after Siivola and Schmidt 2007

Acknowledgements

I would like to thank the people who contributed to the completion of this thesis.
First of all, I thank my supervisor Harilaos Tsikos for this opportunity and his constant guidance all along this study.
I thank the geological team of Vedanta Limited Ltd. for granting the possibility to work on the deposit, for the warm welcome during our stay and for the help provided. Special thanks to Archibald Moses and Patrick Spathelf for providing crucial expert assistance during core-logging and sampling.
The technical personnel of Rhodes University have my gratitude for the preparation of the samples and for the help during analysis session.

Also, thank you Lasni for all those pizza breaks and your sample hammering, thank you Rafa and Justine for the wonderful time spend together, thank you Julia for our quotidian talks and meals. Finally, thank you Julie for being my support all along!

1 INTRODUCTION

1.1 THE AGGENEYS-GAMSBERG MINING DISTRICT

The Gamsberg deposit is a zinc ore body located in the Northern Cape Province approximately 600km North North-West of Cape Town in South Africa. Gamsberg is included in the Aggeneys-Gamsberg mining district representing a cluster of four base metal deposits within a 30km distance (Figure 1). Black Mountain, Broken Hill, Big Syncline and Gamsberg form together the 5th biggest Zn+Pb-bearing basin in the world with a proven 30 Mt reserve of metals (Large et al 2002). The four deposits represent an accumulated estimation of 439 Mt at 3.60% Zn, 1.43% Pb, 0.21% Cu, and 21 g/t Ag (McClung et al. 2007). The Aggeneys-Gamsberg mining district is also the first lead and zinc production of South Africa (Du Toit 1998). The Gamsberg deposit is set on the eastern side of the mining district as a low grade, high tonnage deposit. The actual tonnage is 214 Mt of resource at 6 to 6.5% Zn (Vedanta Zinc International). Considering its excess of 10 Mt zinc, Gamsberg is classified as a supergiant sediment-hosted Zn-Pb deposit (Stalder 2004).

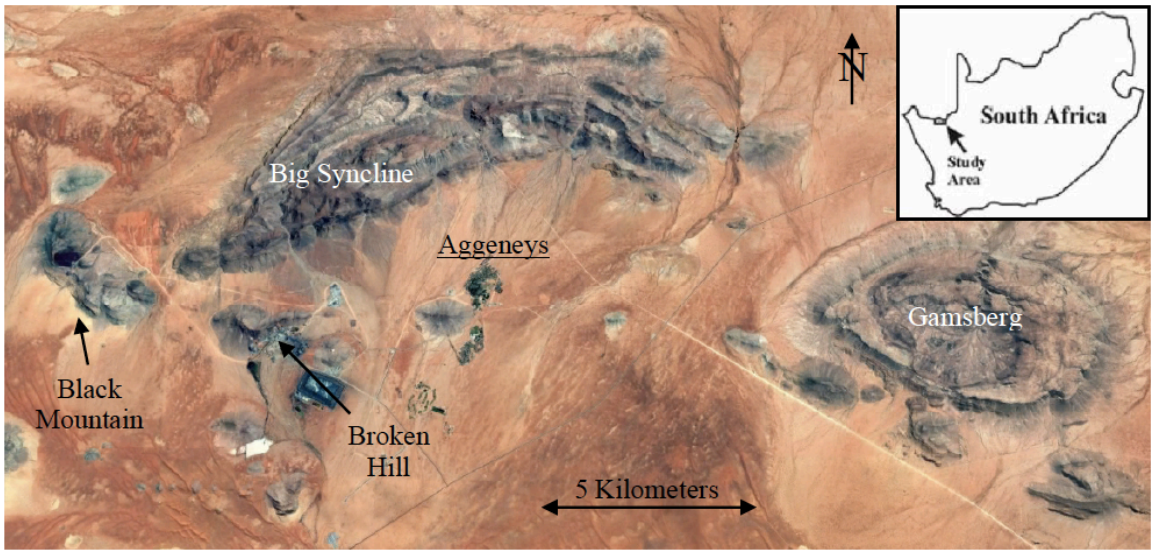

Figure 1: Satellite view of the Aggeneys-Gamsberg Mining District (Captured on Google Earth 25/05/2017). The deposits are localised in the dark inselbergs contrasting with the surrounding red sandy plane.

Historically, the first economic discovery was done in 1954 when R.G. Niemoller found a manganiferous iron ore deposit (hematite, barite, sillimanite) outcropping at the Gamsberg inselberg (Rozendaal 1975). In 1968, copper and zinc discoveries in the Prieska area led to exploration activities in the northwestern Cape Province and eventually encouraged a regional geological mapping of the Aggeneys-Pofadder area. An extensive magnetic survey over the Aggeneys-Gamsberg area highlighted a prominent magnetic anomaly over Gamsberg. A detailed mapping of the inselberg exposed a Pb-rich gossan outcrop (Stalder 2004). Surface drilling started on June 13th of 1972 (Rozendaal 1986). As a result, the 31st of December 1973, an official press release from the Ookiep Copper Company announced the discovery of a substantial sulfide deposit at Gamsberg: 93.5Mt of Zn-Pb ore grading at 7.41% and 0.55% respectively.

The high density of exploration activities produced sufficient data to refine the regional geology. During the same period, Joubert (1971, 1972, 1974) and Rozendaal (1975, 1977) published the basis for all the following geological research in the area.

Despite 20 years of exploration and discoveries, exploitation of the Aggeneys-Gamsberg mining district was very slow. Broken Hill was the first deposit with active mining operations. The exploitation started in 1979 with the joint ownership between Phelps Dodge and Gold Fields of South Africa Ltd. In 1998, Broken Hill resource was reaching its end, AngloAmerican Base Metals purchased the mining rights and continued the exploitation of the Broken Hill deposit through the Deeps extension. During the transition period toward the Deeps extension from 2001 to 2005, Anglo Base Metals decided to mine a lower grade orebody at Black Mountain to fill in the decreasing production (Williams and Holtzhausen 2001). Over these years, exploration drilling enlarged the resources of the Gamsberg deposit. Yet, exploitation was delayed several times due to the low zinc grade of the deposit combined with successive metallurgical, environmental, legislative and market issues (Stalder 2004, Shouwstra et al. 2010, Moses 2015). In May 2010, Vedanta Resources bought the portfolio of zinc assets of Anglo- American including the Gamsberg project and the Black Mountain mine. Since then, Vedanta continues mining the remaining resources from the Broken Hill Deeps and is planning to deepen the exploitation at Black

Mountain. Moreover, Vedanta cleared all previous issues at Gamsberg and started mine preparation in 2015 and ore exploitation via open-pit operations 29th of January 2018.

1.2 Aims of the Study

One of the issue that slowed development was the high concentration in manganese in sphalerite. This impacts the metallurgical processes and results in penalties (Schouwstra et al 2010, McClung and Viljoen 2011, Moses 2015). The typical recovery process uses froth flotation and refining by leaching followed by further electrowinning of the zinc. At Gamsberg, the manganese is leached with the zinc and incorporated in the final concentrate which diverged from the targeted recovery (Schouwstra et al. 2010). Another aspect of the deposit is the discontinuous occurrence of alabandite (MnS) associated with sphalerite. Alabandite shares similar mineralogical characteristics with sphalerite making it difficult to separate during the recovery processes and increasing the amount of manganese in the final zinc concentrate.

The economic valuation of the Gamsberg deposit depends partially on the capacity to extract the selected metal from the mineralized horizons. Zinc is the dominant commodity at Gamsberg, and the mineralogical and geochemical characteristics of sphalerite (ZnS) are essential information to reach an economic recovery grade. Manganese being a penalty element in the recovery processes, means that understanding the manganese distribution and behaviour in sphalerite is of particular interest for Vedanta Resources Limited. This thesis adds information in this area of concern.

Previous to this study, Vedanta Resource Limited carried out a geochemical analysis campaign on sphalerite from the North orebody resulting in a single distribution profile from the drillhole GAM107 being recorded (Figure 2). To complement this set of data, this study aims at providing a detailed investigation of samples from the West Ore body and to compare the two sets of geochemical profiles.

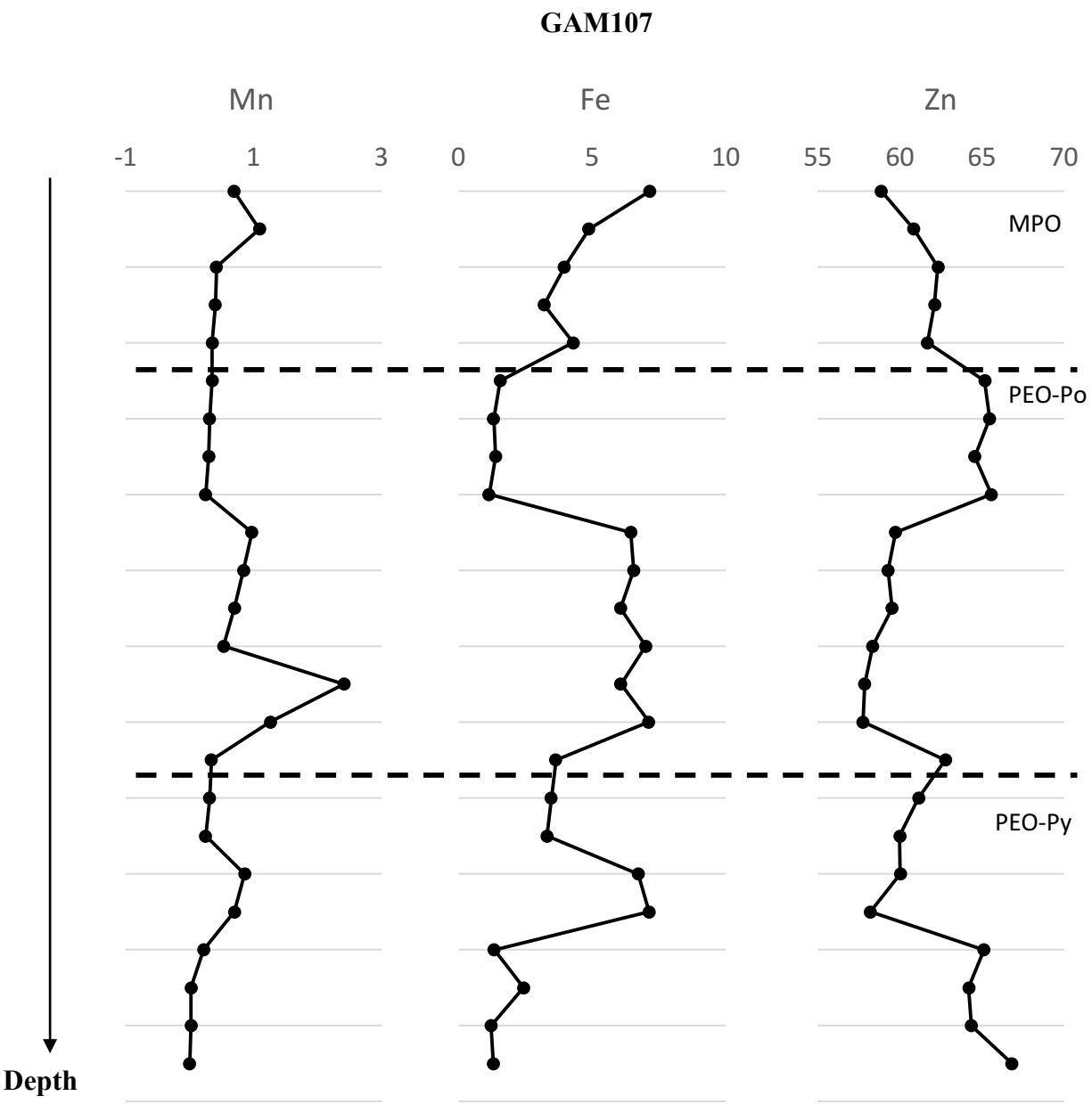

Figure 2: Manganese, zinc and iron distribution profiles (from sphalerite geochemistry) from drillhole GAM107 in the North orebody. All horizontal axis are in wt.% and the approximate depth is 25 meters with samples taken every meter. The nomenclature used in this figure has been defined by Vedanta, it represents the different units of the Gams Formation MPO: Magnetite ore, PEO-Po: Pyrrhotite ore and PEO-Py: Pyrite ore.

The said profile shows an erratic zinc concentration combined with high variability in the iron content and relatively low manganese concentration displaying irregular peaks.

In order to understand and define the geochemical distribution of iron and manganese, this study will investigate the geochemical signature of sphalerite in another section from the Gamsberg orebody. Should a continuity in the geochemical profile distribution be found, it will open up new areas of investigation:

i) Genetic implication

First of all, Fe and Mn distribution is most likely driven by genetic processes, the proven continuity would bring additional element for the depositional settings and would increase the understanding of the mineralization event which produced the Aggeneys-Gamsberg cluster of SEDEX-type deposits. Also, a genetic reconstruction of the basin leading to lateral geochemical prediction could be considered. Taken further, a general distribution of manganese could be drawn.

ii) Logistic and treatment for metallurgical process

An accurate localisation of Mn-poor and Mn-rich sphalerites could define different ore zones which could be treated separately during metallurgical processes. Both of the latter points can have considerable importance in a mining point of view.

1.3 METHODOLOGY

1.3.1 Sampling

To reproduce the profile from GAM107, drillhole GVD038 from the West orebody (Figure 3) was selected based on:

- Whole rock analysis showing high manganese concentration and typical Zn, Mn and S profiles.
- The presence of alabandite.
- The occurrence of a localized sulfidic quartzite unit with no microprobe data ever generated from sulfide species. This study gives the opportunity to interrogate this additional and apparently discontinuous unit.

- The chosen drillhole has the benefit that it present a complete sequence of all the different units of the mineralized formation of the deposit (the Gams Formation).

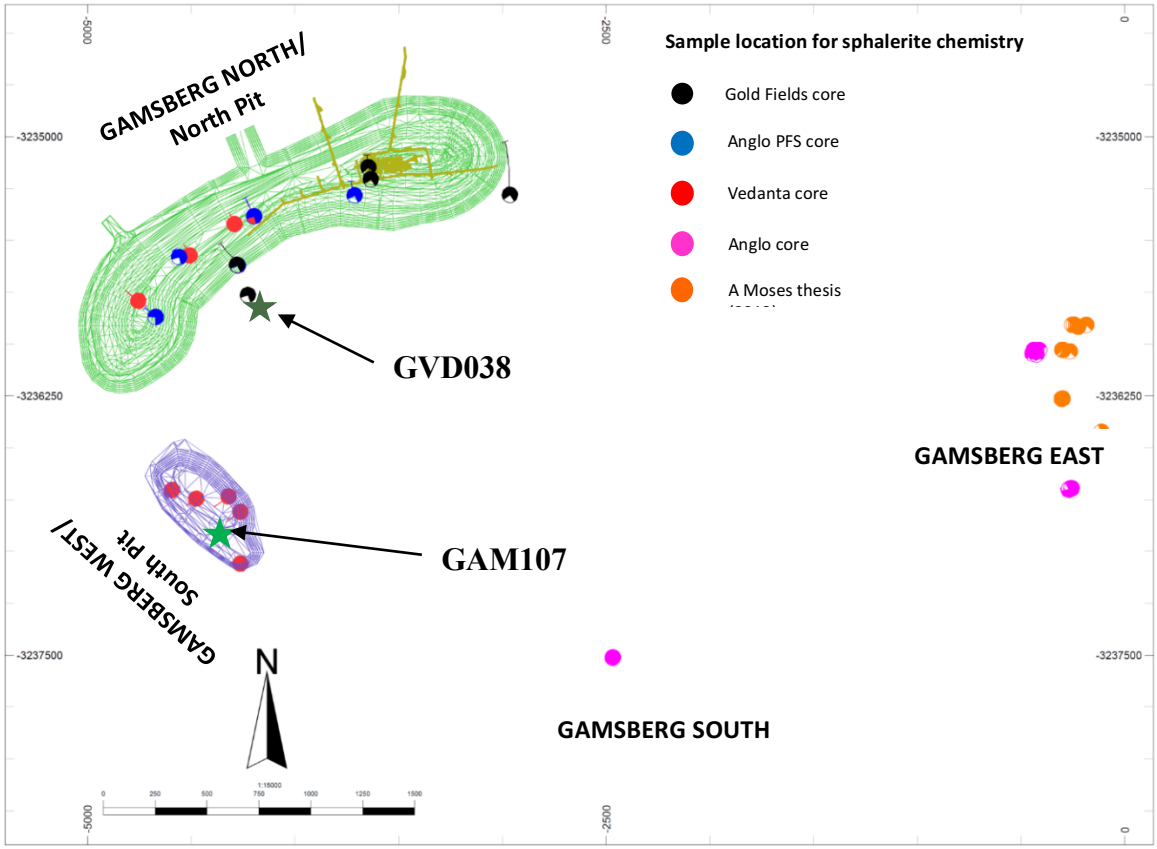

Figure 3: Locations of the two studied drillholes, GAM107 and GVD038, with other drillholes positions which their samples have been analysed for sphalerite chemistry.

The sampling of GVD038 focused on the Gams Formation containing the MPO, PEO(Po) and PEO(Py) units. Logging and sampling of the drillhole was performed in May 2017 by the author supported by his academic supervisor and by Vedanta Resources Limited geological representatives of the Gamsberg project. 34 samples were targeted representing homogeneous sphalerite-rich zones throughout 25m of the Gams Formation. Quartered-core samples were taken broadly every meter with a higher density of samples closer to the unit contacts to enhance the chemical variations observed in Figure 2. The distribution of the quartered-core samples is presented below in Table 1.

Table 1: Distribution of the samples in the GVD038 drillhole, in red are the units sampled.

Lithology of GVD038	Litho Code	From	To	Width	Number of Sample
Garnet-Amphibole-Pyroxene	GAP	56,69	61,31	4,62	0
Garnet-Amphibole-Quartz	GAQ	61,31	64,11	2,8	0
Garnet-Amphibole-Pyroxene	GAP	64,11	69,59	5,48	0
Garnet-Amphibole-Quartz	GAQ	69,59	72,47	2,88	0
Garnet-Magnetite-Quartz	GMQ	72,47	75,19	2,72	0
Garnet-Amphibole-Magnetite	GAM	75,19	78,07	2,88	2
Garnet-Magnetite Ore	MPO	78,07	84,97	6,9	7
Pyrrhotite Ore	PEO(Po)	84,97	93,77	8,8	8
Sulfidic Quartzite	SQZ	93,77	103,61	9,84	7
Pyrite Ore	PEO(Py)	103,61	108,06	4,45	6
Meta-pelite	PEL	108,06	110,4	2,34	4
Calc-silicate	CAS	110,4	-	-	0

The 34 samples were processed at the thin sectioning laboratory of the Geology Department at Rhodes University. As the main objective of the study was the sulphide fraction and particularly sphalerite, polished blocks were chosen rather than thin sections to focus on the sulfidic package. Therefore, 34 polished blocks have been produced for further analysis.

1.3.2 Analysis

A first microscopic petrographic approach has been selected to inspect the overall mineralogy, micro-structures and the textures occurring in the drillhole. The petrography was also performed to identify the sphalerite to analyse and to act as a support for the mineral chemical analyses. The microscopic observation was carried out in the Ore Petrography Laboratory of the Geology department at Rhodes University with a Leica DM

EP microscope on reflected light. Photographs have been taken using the Leica digital camera LEICA EC3 and the Leica Application Suite LAS EZ version 1.4.0.

Analyses were completed in September 2017. Initially, carbon coating was applied to all polished blocks. The coating was performed in the Electron Probe Microanalyzer Laboratory of the Geology Department at Rhodes University under the supervision of Dr Deon Van Niekerk, using the Q150T E High Vacuum Evaporator with film thickness monitor module. SEM spectroscopy was done on a selection of 15 polished blocks. This set of analyses provided a first-order qualitative and semi-quantitative overview of the geochemical elements of minerals present and permitted the differentiation of mineral species with similar optical properties and very fine particle size under microscopic observation. The SEM-EDS analysis was made with a VEGA TESCAN LMU associated with an Oxford Instruments INCA Penta FET x3 using the INCA 4.11 software in the Zoology and Entomology Department at Rhodes University.

Analysis using the Electron Probe Micro Analyzer (EPMA) were performed on sphalerite to produce the core of the data set for this study. Quantitative chemical analyses of sphalerite were obtained by using four wavelength dispersive spectrometers on a JEOL JXA-8230 electron probe micro-analyzer at Rhodes University. The beam was generated by a Tungsten cathode; 20 kV accelerating potential, 50 nA current, and a 10 μm beam size was applied. All elements were measured by counting K-alpha X-ray peaks. Counting times for Fe and Mn were 60 seconds on the peak, and 60 total on the background. Zinc and S were counted for 15s on- and off-peak. Commercial “SPI” standards were used for intensity calibration. The standards were sphalerite (S, Zn), pyrite (Fe), and metallic manganese (Mn). Iron and Mn were measured with a LIFL crystal. The data was collected with JEOL software. An automated ZAF algorithm was applied to correct for differential matrix effects.

2 BACKGROUND ON ORE FORMING PROCESSES

The four deposits forming the Aggeneys-Gamsberg district are classified as sedimentary exhalative (SEDEX) deposits, each displaying a distinct geochemical signature as part of a regional geochemical zoning pattern: Pb-Cu enrichment in the western part (Black Mountain, Broken Hill) contrasts with the eastern Zn-Mn-rich Gamsberg deposit, whereas Big Syncline has an intermediate geochemistry (Ryan et al. 1986). The occurrence of Pb-Zn-Cu has been commonly reported for SEDEX deposits (Emsbo 2010, Leach et al 2005, Large et al 2002) while the occurrence of high concentrations of manganese is not an ordinary feature. Understanding the mechanisms behind the ore forming processes is an essential step to interpret the high concentration of manganese at Gamsberg. This section provides the basement on SEDEX deposits genetic knowledge.

2.1 GENETIC PROCESSES FOR SEDEX DEPOSITS

The term SEDEX was introduced by Carne and Cathro (1982) as a contraction for "sedimentary exhalative". They based this nomenclature on the genetic process of sulfide-bearing sediments precipitating onto the seafloor from hydrothermal fluids by exhalation. This nomenclature is now widely accepted and used even when one deposit does not present evidence for exhalative process (Leach et al 2005). The bedded or laminated ore bodies hosted by fine-grained clastic rocks is the typical end product of this type of deposit (Holland 2005, Emsbo 2009, Leach et al 2005, Large et al 2002).

SEDEX deposit formation is driven by hydrothermal fluids carrying metals through the sedimentary basin toward the sea floor where sedimentation occurs, implying that the mineralization process is syn-sedimentary. Isotopic research on SEDEX deposits tends to indicate that the underlying sediments from the host basin are the source of metals (Emsbo 2010). To obtain those metals and ultimately produce a deposit, a conduit network has to permit fluid migration into a large volume of sediments during millions of years (whether continuously or episodically). The pathways are deep primary faults, commonly created during extension events, connected with the subsurface by secondary faulting systems. The

expulsion of fluids toward the subsurface happens by depressurisation. Different models exist to explain this pattern of migration (Emsbo 2010, Large et al 2002):

- The sedimentary compaction model presents a 2 to 3km-thick nearly impermeable cap of sediments covering the metal-rich fluids in the underlying sequence. The accumulation of sediments builds up pressure until an extensional tectonic event creates fault openings, allowing the fluids to break free upwards. This model is weakened by the limited accessibility of the fluids and the fact that it is problematic to account for the multiple events of mineralization often found in a SEDEX environment.

- The free convection model has a more dynamic approach to the system. At a first stage, fluids are again isolated under a low-permeable sediment cover but convective cells circulate the fluids within the underlying sediments scavenging metals. After a stress episode, faults breach the sedimentary cap, second-stage convective cells are created, and the metal-enriched fluids ascend toward the subsurface while marine water descends.

The marine environment where fluids are discharged is commonly a sub-basin with organic-rich muds (Large et al 2002). The fluid nature (temperature, pressure, pH and geochemistry) dictates the mobility and deposition of metals. Metal solubility and fluid salinity are closely associated because metals are transported via chloride complexes (Emsbo 2010). Fluid inclusions have provided essential data to define ideal fluid conditions: temperatures of 100 to 300°C and between 10 to 30 wt.% total dissolved solids (Leach et al 2005, Large et al 2002, Cooke et al 2000, Emsbo 2009). The most plausible source of salinity in the fluids is residual brines derived from seawater evaporation infiltrated in underlying sedimentary sequences. A shallow-confining platform environment located at 25° (±10°) plaeolatitude position presents compelling conditions to deliver large volumes of fluids (Emsbo et al 2010). The temperature increase needed for the ideal conditions of residual brines is achieved by the burial of sediments. The thickness

of the sedimentary cover should range from 2 to 5 km (Large et al 2002). Heat can also be produced by mafic intrusions (Large et al 2005).

The study conducted by Cooke et al (2000) identified two types of fluids generating the majority of SEDEX deposits based on their redox state:

- Reduced brines dominated by H_2S: here the temperature is thought to be moderate to high (200°-300°C), the salinity is moderate (around 10 wt.% NaCl), the presence of barite is common, and anomalous concentrations of Au and Sn have been noted.
- Oxidized brines dominated by SO_4^{2-}: in this instance the temperature is expected to be moderate to low (100°-200°C), salinity is high (above 15 wt.% NaCl), and a ferroan carbonaceous halo develops around the deposits.

One major difference between the two types of brines is the metal precipitation process. Once reduced brines are discharged on the basin floor, metals are precipitated via dilution of H_2S upon interaction with ambient seawater. With sulfate-rich oxidized brines, H_2S high concentrations have to be produced by sulfate reduction processes. Thermochemical sulfate reduction (TSR) and bacterial sulfate reduction (BSR) are the two likely operative processes. Further isotopic studies are necessary to clarify their role (Leach et al 2005, Large et al 2005). Still, the fact that TSR and/or BSR are needed for SEDEX deposits imparts key characteristics to the discharge basins. BSR requires the appearance of micro-organisms which proliferate better in a low temperature, aerially extensive brine pool (Large et al 2002, 2005). In the process, bacteria will produce organic matter which is commonly found in SEDEX deposits at levels as high as 10 wt.% total organic carbon (Emsbo 2010). With reduced brines, H_2S and H^- concentrations are already predominant, thus sulfate reduction is not a vital factor for metal precipitation. Therefore cooling, pH and increase in the concentration of sulfide will trigger precipitation of metals (Cooke et al 2000, Large et al 2002).

The works of Emsbo 2010, Large et al 2002, and Leach et al 2005 enlightened multiple recurrent geochemical signatures for SEDEX deposits. As metal concentration analysis is

mandatory in mining industry it is only natural that metal ratios are often used to delineate halos. Figure 4 presents the main metal zonations recovered at SEDEX deposits. Pb enrichment is noted nearby the feeder zone, while Zn concentration increases away from the vent complex. Thus, Zn/Pb ratio increasing outward the deposit is a common feature. Fe/Zn and Fe/Pb ratios have generally similar increasing behavior. On the opposite, Pb/Ag, Cu/(Zn+Pb) and SiO_2/Zn ratios decrease away from the same area.

Alteration is a function of the geological environment and will therefore always display a unique signature for each deposit. Still, recurrent patterns have been encountered and documented (Emsbo 2010, Leach et al 2005, Large et al 2002):

- Fe-Mn halos and thallium signatures are often developed around SEDEX deposits.
- Fe-Mn halos are better displayed in dolomitic environments.
- Trace element high values around the vent complex (Tl, Ag, As, Sb) are associated with the presence of sulfosalt minerals.
- Alteration can persist for tens of kilometers.
- Tourmaline, chlorite, muscovite, sericite, alkali feldspar, albite, carbonate, clay, quartz, siderite and sulfides (chalcopyrite, pyrrhotite, pyrite) are common alteration minerals.
- Silicification may be recorded post- or pre-mineralization.
- Isotopic analysis on carbonates around SEDEX deposits showed high values of $\delta^{18}O$ values and a lowering of $\delta^{13}C$ values. This trend is reversed for Irish-type deposits, skarn and Mississippi Valley Type (MVT) deposits.
- Weathering can develop a gossanous capping the deposits, it is especially noticed in Fe-rich environments as at Gamsberg.

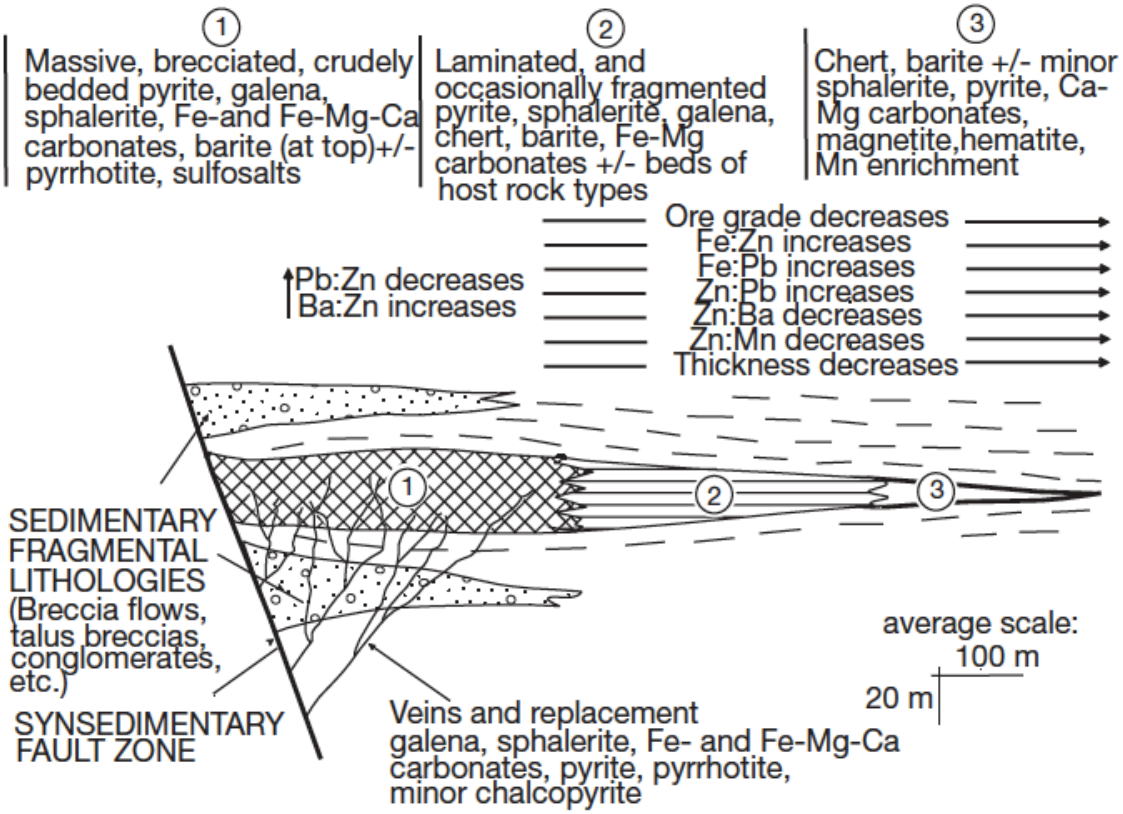

Figure 4: Idealized cross section of a SEDEX deposit with its geochemical zonations (adapted by Leach et al 2005 from Lydon 1996).

2.2 Broken Hill-type (BHT)

Broken Hill-type deposits is a sub-classification of SEDEX deposits presenting peculiar features. The Gamsberg deposit displays characteristics from BHT (metamorphic terrain, pyrrhotite-rich ore units, Zn high concentration, etc.) and SEDEX main category (presence of graphitic-rich metapelite, pyrite-rich ore units, association with barite, wide range of $\delta^{34}S$ ore values, etc.). Hence, Gamsberg can be described as an intermediary deposit between the two classes (Leach et al 2005, Emsbo 2010, Spry et al 2009).

The main feature of BHT deposits is the dominant metamorphic overprint affecting the host rocks without implying that all metamorphosed SEDEX deposits are BHT. Due to the metamorphic imprints, primary evidence is masked by complex alterations and the

understanding of BHT deposits is therefore arduous. Historically, BHT deposits were classified as metamorphosed equivalents of SEDEX deposits. The BHT classification is now recognized but the idea of BHT deposits being derived from SEDEX protoliths by metamorphism remains (Spry et al 2009, Cooke et al 2000). Nonetheless, several characteristics have been listed specific to BHT deposits (Walters 1998, Spry et al 2009, Emsbo 2010, Leach et al 2010, Large et al 2002):

- The high-grade metamorphic terrain is the common base, amphibolitic to granulite facies and deformation evidences are expected.
- The metasedimentary sequence presents a typical transition from rift related quartzo-feldspathic rocks to sag-phase related psammitic-pelitic rocks with the mineralization stacked between the two packages.
- Paleo- to Meso-Proterozoic terrains, which recorded a long thermal history, are more inclined to hold BHT deposits.
- Lithological associations with exhalites and magnetite are common with or along the ore strike.
- On the contrary, the association with pyrite and organic-rich components (graphite) is unlikely.
- Morphologies are dominated by low aspect ratio deposits (i.e. thickest ore bodies).
- Ore lenses are marked by a poor sulfur assemblage (galena-sphalerite-pyrrhotite, minor pyrite and variable magnetite) and often skarn-style mineralization associated with Fe-Mn-Ca-F gangue minerals.
- Pb/Zn ratios and Ag concentrations are higher than SEDEX deposits, the physical expression is a strong zonation from Pb-Ag to Zn.
- Geochemical signatures present very high Mn concentrations, high concentrations in Cd, Sb and Fe and localized increases in Cu, Au, Bi, As, W concentrations. The semi-regional presence of spessartine garnet is a typical evidence of the Mn halos.
- Sulfur isotopic analysis revealed a restricted range of $\delta^{34}S$ values.

A higher occurrence of manganese, recovered at Gamsberg, is typical for BHT deposits comparatively to classical SEDEX deposits. To explain the differences between BHT and SEDEX deposit characteristics, SEDEX genetic models are adjusted to fit the particularities of BHT deposits (including high Mn-concentration). Several debating models have been proposed for the formation of BHT deposits without any eclipsing the others (summarized by Large et al 2002). The creation of a comprehensive model is also weakened by the fact that each BHT deposit displays different particularities reflecting unique and complex successions of metamorphic and deformation events. Nonetheless, the spine of the SEDEX genetic model is the same: the rift environment generating deep-seated faults used as brines pathways until seafloor discharge in a clastic sedimentary basin are unchanged aspects. However, the geochemical signatures found in BHT lithologies are explained mainly by reduced ore-fluids discharging their transported metals in a relatively oxidized brine-pool for precipitation (see Figure 5). One major talking point is whether metamorphism and metasomatism occurred contemporaneously with the ore forming process or they represent later overprinting events which affected the ore body in place (Stalder 2004). This led Leach et al (2005) to make a distinction between BHT deposits formed by metamorphic and deformation events that rework a SEDEX entity and those produced by a distinct genetic model. Also, the presence of volcanic units surrounding some BHT deposits have led some authors to propose hybrid models that incorporate elements of a volcanosedimentary context (Jébrak and Marcoux 2008, Huston et al 2006).

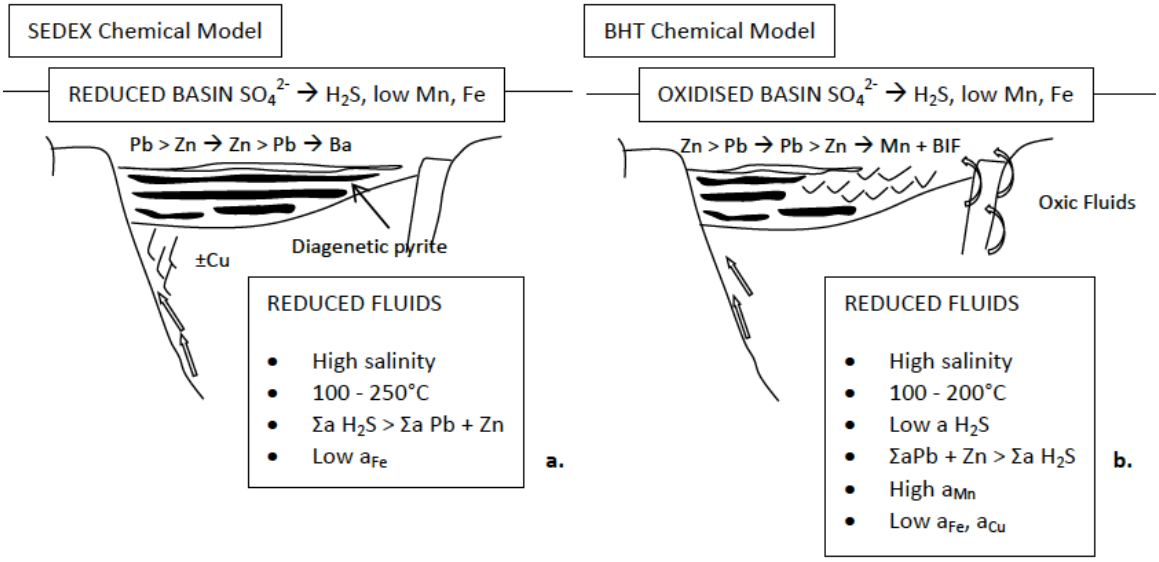

Figure 5: Geochemical models for a. SEDEX deposits and b. BHT deposits (adapted by Foulkes 2015 from Large et al 1996).

3 GEOLOGICAL BACKGROUND

3.1 THE NAMAQUA-NATAL PROVINCE

The Aggeneys-Gamsberg mining district is located in the Namaqua Sector in the north-western part of the Namaqua-Natal Mobile Belt of South Africa (Figure 6 and 7).

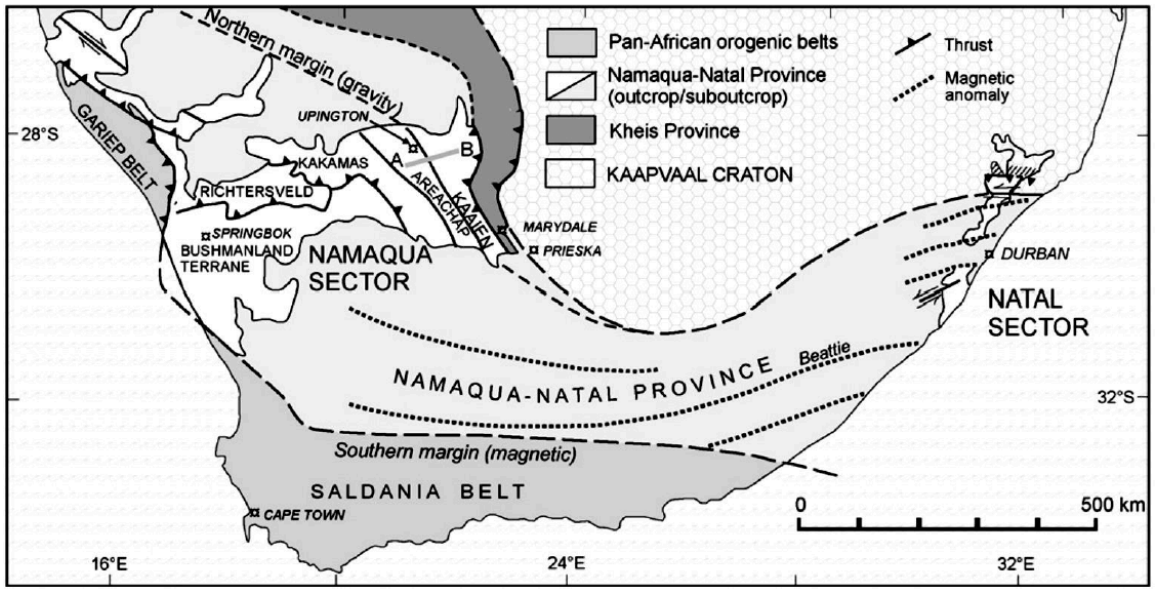

Figure 6: Geological setting of the Namaqua-Natal Province (Cornell et al 2006).

Lithological similarities recognized at the Natal Sector and at the Namaqua Sector associated with geophysical surveys helped drawing the belt boundaries (Joubert 1986, Cornell et al 2006, McCourt 2006). The Namaqua-Natal Mobile Belt or Namaqua-Natal Province is a ±400 km wide aggregation of medium to high-grade metamorphic terranes bound by shear zones and formed during the construction of the Rodinian supercontinent (Thomas et al 1994, McCourt et al 2006, Cornell et al 2006, Bailie et al 2007a, Dewey et al 2006). The Belt has been amalgamated on the southern and western borders of the Archean Kaapvaal Craton by compressional forces. On the western side of the Province, the Namaqua Sector or Namaqua Metamorphic Complex (Joubert 1986) is divided into five major subdivisions accreted together (Figure 7). This succession of terranes is characterized by medium- to high-grade metamorphosed volcano-sedimentary supracrustal sequences (±2000 Ma) frequently intruded by granitoids (±1200-1000 Ma) which recorded

several deformational events. North-west, the Richtersveld Terrane can be related to the western Kheis Province because it bears evidences of an ancient Kheisian block (Cornell et al 2006).

The Bushmanland Terrane contains the Zn-Pb-Cu-Ag deposits of the Aggeneys-Gamsberg district. Immediate to the east is the gneiss-granulite Kakamas Terrane, whereas the Areachap Terrane rocks further to the east are believed to be more juvenile (±1600-1300 Ma) and arc-related. The eastern side of the Namaqua Sector is defined by the Kaaien Terrane produced by arc-continent collision. At the easternmost extremity of the Namaqua Belt, the Kheis Province is also composed of volcano-sedimentary supracrustal sequences with an Archean basement in the south (Marydale Terrane). The Kheis Province can be represented as a buffer unit between the Namaqua orogeny and the Kaapvaal Craton. (Cornel et al 2006, Thomas et al 1994).

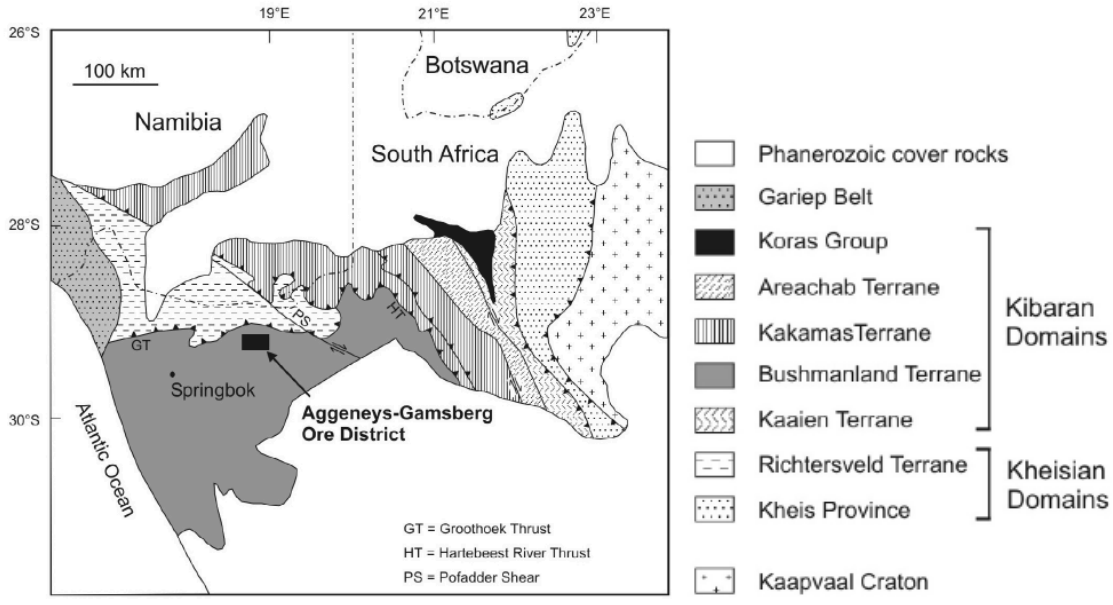

Figure 7: Geological setting of the Namaqua Province with its major subdivisions and localisation of the Aggeneys-Gamsberg Ore District (adapted by Stalder 2004 from Thomas 1994).

As introduced by Robb et al (1999), two major tectonic events shaped the morphology of the region, namely the Kibaran (±1.21-1.17 Ga) and Namaquan (±1.06-1.03 Ga)

orogenies. The Kibaran orogeny is the result of the collision between the Namaqua-Natal Belt and the Kaapvaal Craton whereas the Namaquan Orogeny is a later and more discrete heating event (Bailie et al 2007b, Robb et al 1999 and Dewey et al 2006). The two events are responsible for the metamorphic overprint in Namaqualand and for the granitoid intrusions which occurred at that time. The Kibaran event resulted in crustal thickening while the Namaquan event produced thermal reworking on the protoliths in place (Robb et al 1999, Thomas et al 1994).

3.2 The Bushmanland Terrane

The presence of four Zn-Pb deposits in the Bushmanland Terrane imparts a particular economic interest in this area. On surface, the Bushamanland Terrane is mostly represented by isolated mountains ("inselbergs") anchored on flat plains covered of reddish sand. Three main lithologies have been identified in the Buschmanland Terrane (Cornell et al 2006): a granitic dominated Kheisian basement overlain by supracrustal volcano-sedimentary sequences, and dispersed intrusions. The definition of the subdivisions is not unanimous; for example, Bailie (2007a) showed that several stratigraphic interpretations have been proposed for the supracrustal rocks of the Bushmanland Group. Those variations are a direct reflection of the differences observed between each area studied. For this study, the stratigraphy chosen (Figure 9) is based on the works of Stalder and Rozendaal (2004, 2005a) and adapted by the recent study of Moses (2015). This stratigraphy applies particularly well in the Aggeneys-Gamsberg area with a focus on the Gamsberg Zn deposit itself.

3.2.1 Granitic gneiss basement

The extent of the Bushmanland Kheisan basement is yet to be clarified (Cornell et al 2006). In the Aggeneys-Gasmberg area, Bailie et al (2007b) defined the Aggeneys Suite composed of three granitic gneisses suites representing the basement rocks (Figure 8). The **Achab Gneiss** is mostly exposed in the eastern part of the district. Coarse porphyroblasts of K-feldspar (microcline and microperthite), unusual SiO_2/Al_2O_3 ratios and inconsistent banding are the principal features of this unit. The **Aroams Gneis**s is widely developed on

the northeastern part of the district with an isolated appearance near Aggeneys but absent at Gamsberg. This unit presents augen textures composed of microcline and quartz. The Aroams Gneiss displays intrusive features indicating an affiliation with the intrusive entity of the Little Namaqualand Suite (Stalder and Rozendaal 2005a, Cornell et al 2006). The **Hoogoor Gneiss** is closely associated with the supracrustal sequences of the Bushmanland Group. This unit, also called "Pink Gneiss" or "Haramoep Gneiss" because of its characteristic pink color, is stratigraphically located between the other two gneisses and the Bushmanland Group. It displays equigranular rocks with higher biotite content, whereas foliations and augen textures are not recurrent. Because of the physical distinctions with the Achab and Aroams gneissic rocks, the presence of discontinuous schist layers from the overlying unit and the close proximity with the supracrustal sequences, the Hoogoor Gneiss has often been included into the Bushmanland Group.

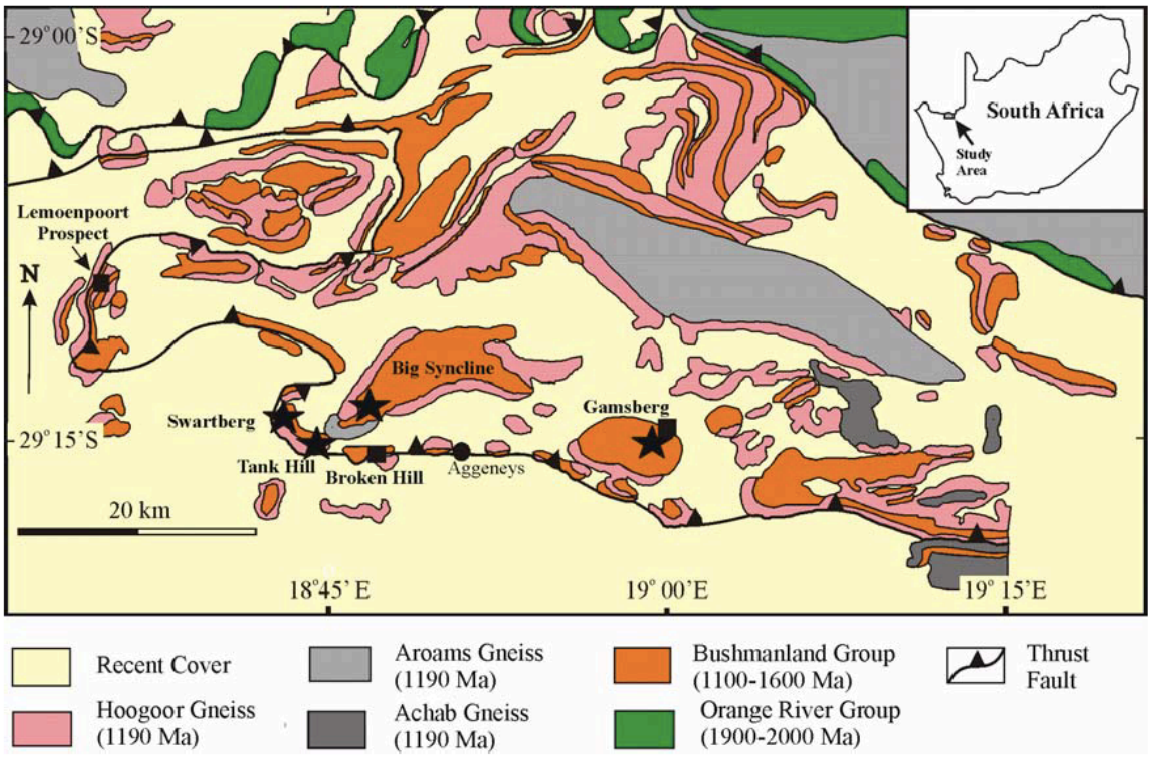

Figure 8: Geological setting of the Aggeneys-Gamsberg ore district. Stars and squares are not relevant for this study (McClung 2006).

3.2.2 Supracrustal sequences of the Bushmanland Group

The **Namies Schist** is the first unit of the supracrustal sequences of the Bushmanland Group. Sitting on the granitic gneiss basement, this unit is a well-foliated aluminous metapelitic schist dominated by quartz, k-feldspar, biotite, muscovite and sillimanite. Its average thickness is 80m and it has a sharp, conformable contact with the overlaying **Pella Quartzite** unit (Ryan et al 1986, Stalder and Rozendaal 2005a). The latter is an alternation between a dark recrystallized quartzite and a milky white recrystallized quartzite interbedded by thin lenses of aluminous schist (Rozendaal 1986). In the study area, the Pella Quartzite went through structural duplication and its thickness varies from 5 to 900m (Ryan et al 1986). The Namies Schist and the Pella Quartzite have been grouped to define the Wortel Formation (Bailie 2007a, McClung 2006). Stalder and Rozendaal (2005a) interpret the Wortel Formation as a metamorphosed sequence of a shallow-water quartz arenite and mudstone with an organic ("black shale") component.

Overlaying the Wortel Formation with a sharp contact is the **Gams Formation,** which is the Zn-Pb-Cu-Ag-bearing unit of the stratiform ore bodies in the region. Also called Aggeneys Ore Formation, the Gams Formation is another metapelitic schist with a complex mineralogy interbedded by quartzite, calc-silicate rocks, barite horizons and iron formations (Ryan et al 1986, Stalder and Rozendaal 2005a). The Gams Formation is a 200m thick unit subdivided into the A, B and C members (Rozendaal 1975). As this formation is the object of this study, a more detailed description is drawn in a later section.

Capping the Bushmanland Group is an unconformity that separates the Gams Formation from the **Nousees Mafic Gneiss** (Rozendaal 1975) **or Koeris Gneiss** (McClung 2006). This is a succession of metapsammitic schist, conglomerate, amphibolite and quartz-feldspar-muscovite gneiss (Stalder and Rozendaal 2005a, McClung et al 2007). This unit is particularly well developed at Gamsberg (400-500m thick). The end member of this formation and thus the youngest depositional unit of the Bushmanland Group is an amphibolite (Stalder and Rozendaal 2005a). The Gams Formation and Nousees Mafic Gneiss together constitute the Kouboom Formation (Bailie 2007a, McClung et al 2007).

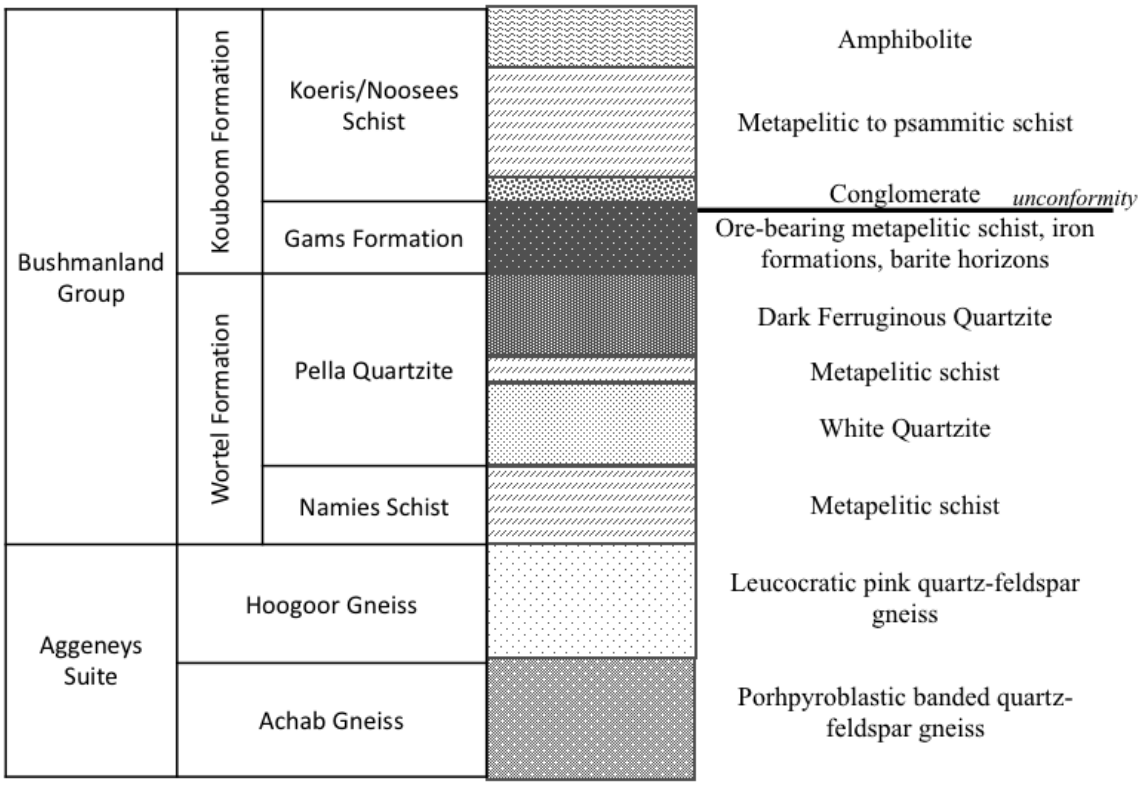

Figure 9: Simplified Stratigraphy of the Aggeneys-Gamsberg district after Stalder and Rozendaal (2005a).

3.3 Structure and Metamorphism

As stated by Joubert (1971), the Bushmanland Terrane and by extension the Aggeneys-Gamsberg ore district experienced polyphase deformation events which resulted in metamorphosed and structurally complex terrains. Those features are direct physical characteristics produced by the Kibaran and Namaquan orogenies (Robb et al 1999).

For many studies covering the tectonic history of the Aggeneys-Gamsberg ore district (Ryan et al 1986, Willner 1995, Bailie 2007b, Thomas et al 1994, Cornell et al 2006), the structural analysis made by Joubert (1971) remains the most widely accepted work detailing the different deformation phases. D1 to D5 are the five deformations phases summarized by Bailie et al (2007b). D1 is represented by an overprinted tight isoclinal (F1) folds. D2 produced recumbent isoclinal north-east plunging fold (F2) and structural duplication by thrusting. D2 was the most intense deformational event and is associated

with the higher grade of metamorphism (M2) in the region. D3 corresponds to a large scale open-asymmetric east-north-east striking (F3) folds. D4 is related to north-trending monoclinal folds and north to north-west faults. Finally, D5 produced north-east-trending strike-slip faults and shear zones.

The Namaqualand Metamorphic Complex has been affected by a high-temperature low-pressure event (M2) which produced the metamorphic grades from upper amphibolite to granulite facies and a successive retrograde metamorphism (M3) producing overprinted greenschist and amphibolite facies (Willner 1995, Cornell et al 2006). Textures display that the peak of metamorphism was prolonged after the main deformational event D2 but ceased before the D3 episode (Stalder and Rozendaal 2005b, Willner 1995). Based on the mineralogical assemblage encountered in the Bushmanland Terrane, the pressure-temperature conditions mentioned by Cornell and others (2006) frame the northern upper amphibolite facies (biotite-quartz-sillimanite) to 650-700°C, 4 kbar and the southern granulite facies (cordierite-garnet-K-feldspar-quarts, hercinyte-quartz) to 830°C, 5-7 kbar.

In the central portion of the Province, the Aggeneys-Gamsberg area was submitted to a clockwise P-T-t path associated with amphibolite metamorphic facies through the highest deformational event (D2) (Stalder and Rozendaal 2004, McClung et al 2007, Bailie et al 2007b, Willner 1995). At Gamsberg, Rozendal (1975) based on cordierite-sillimanite-K-feldspar and quartz-muscovite assemblages constrained the pressure-temperature conditions for the pro-grade metamorphism at 2.8-4.5 kbar and 630-670°C. This places the deposit in the upper amphibolite facies, close with the granulite border because of the presence of infrequent orthopyroxenes (Rozendaal 1975). Retrograde, cooler (550-600°C) metamorphism is witnessed by the presence of sorosilicates (epidote, zoisite) and chlorites (Rozendaal 1975, Willner 1995).

Metamorphism and deformation in the Aggeneys-Gamsberg district had major effects on the morphology and mineralogy of the ore bodies which consequently complicate the mining operations (Rozendaal 1975, 1986, Ryan et al 1986, Stalder and Rozendaal 2002).

3.4 GEOLOGY OF THE GAMSBERG DEPOSIT

Located in the Northern Cape Province, east of Aggeneys, the Gamsberg Zn deposit is restricted to a 7 km long and 5 km large inselberg (Rozendaal 1986). The stratiform ore horizon referred as the Gams Formation is hosted in meta-volcano-sedimentary sequences of the Bushmanland Group and has been submitted to regional scale polyphase deformation and medium- to high-grade metamorphism (Rozendaal 1986, Stalder and Rozendaal 2005a, McClung et al 2007, Rozendaal et al 2017). The tectonic events shaped the deposit in a large sheath-fold structure (Stalder and Rozendaal 2005b). The complex morphology of the deposit is explained by the tectonic history of the basin (Moses 2015, Stalder and Rozendaal 2004). Three phases of deformation (F1, F2 and F3) occurred subsequently to form the circular shape of Gamsberg while preserving the orebody due to plastic conditions of the metasedimentary units (Figure 10). F1 is represented by a north-south synformal folding occurring conjointly with F2 east-west synformal folding to produce the large sheath-folding of the basin. Later, F3 represents a north-east vertical synform folding event superimposed on the pre-existing structures. The result is the development of a large NE-inclined basin-shaped structure (Stalder and Rozendaal 2004).

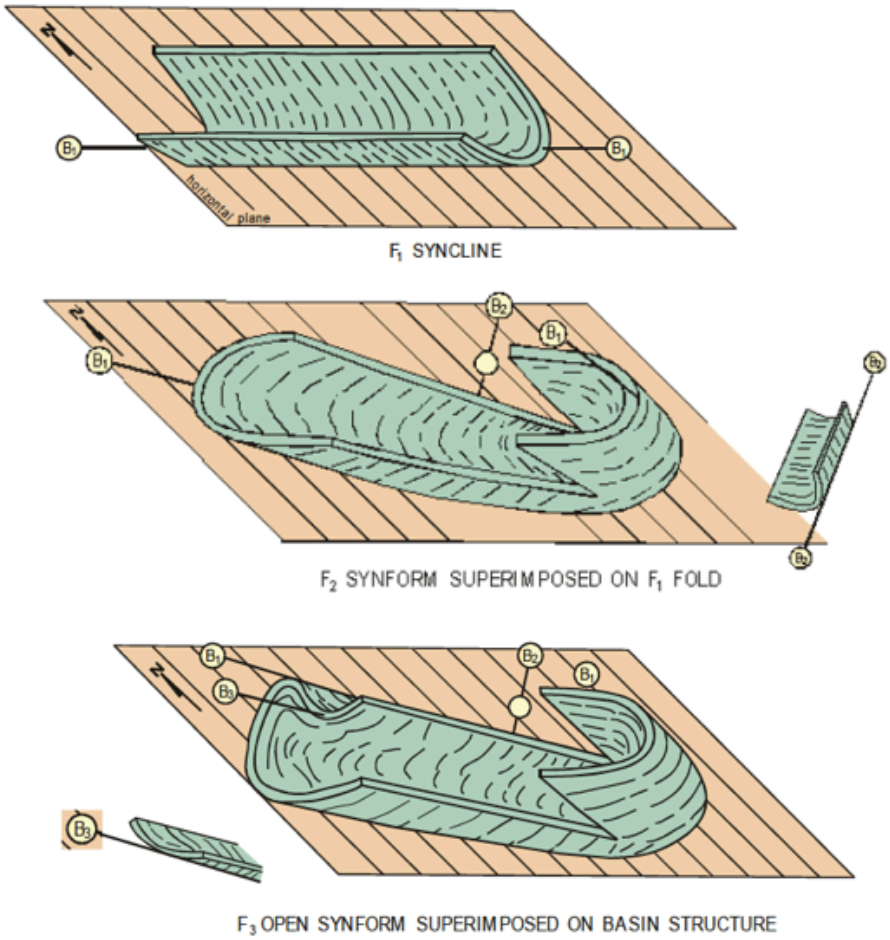

Figure 10: Representation of the three phases of deformation (F1, F2, F3) responsible for the Gamsberg Zn deposit morphology (originally from Rozendaal 1975 and 1977 and adapted from Moses 2015).

Over the years, exploration campaigns improved the geological understanding of the Gamsberg deposit. It is now divided into four ore bodies: North, West, South and East (Figure 11). One structural feature resulting from the deformational events is that the East orebody is associated with the "Overturned Limb" and is stratigraphically inversed compared to the others. The stratigraphy at Gamsberg is relatively similar to the one presented regionally (Figure 9 and 12); the Bushamnland Group is composed of the successions of metapelitic schist, quartzite and amphibolite units overlying the Hoogoor Gneiss basement.

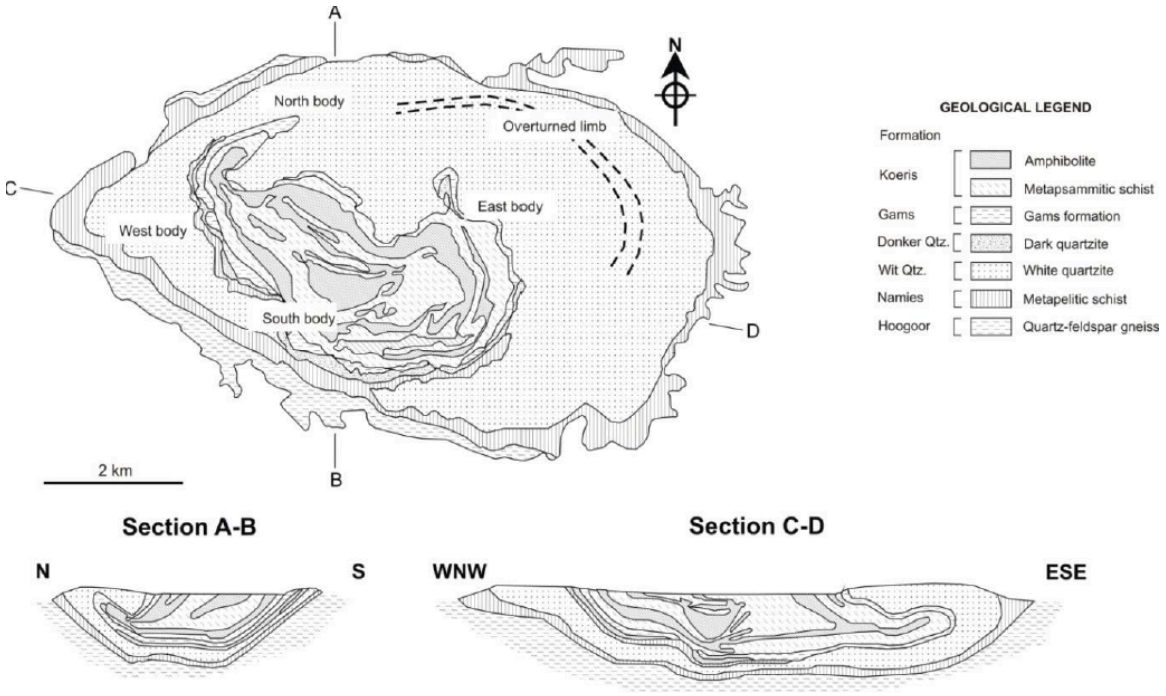

Figure 11: Geological setting and stratigraphy of the Gamsberg deposit (adapted by Moses 2015 from Stalder and Rozendaal 2004).

The mineralized Gams Formation is divided into three members (Figure 12). The A member starts with a gradational unit from the underlying quartzite (A1) to become a garnet-pyroxene-amphibole-magnetite unit (A2), a carbonate-quartz-garnet-clinopyroxene marble represents A3 and a relatively banded clinopyroxene-garnet-feldspar-quartz rock end the member (A4). The B member is the main mineralized unit. Sulphides are included into a basal layer of quartz-sericite-sillimanite schist (B1) and an overlaying calc-silicate-hosted ore-rich unit (B2). The C member is characterized by a dominance by oxides (magnetite, hematite) over sulfides and a complex assemblage of Fe-Mn silicate and silicate-carbonate facies metasediments (C1 and C2 units) (Rozendaal 1986, Stalder and Rozendaal 2004). Lithological departures from the above have been outlined by a collection of studies and include: barite horizons identified in the upper portion of the Gams Formation; calderitic garnet and franklinitic spinel restricted in the C2 unit; apatite nodules defining a marker unit above the B2 unit; and graftonite and wulfenite reported in iron formations (McClung et al 2007, Stalder and Rozendaal, 2002, 2004, 2005a, 2005b). Another particularity is the unique presence of a sulfidic quartzite intercalated in the B1

unit of the West oredoby which will be part of the mineralised rocks included in this study (Figure 12).

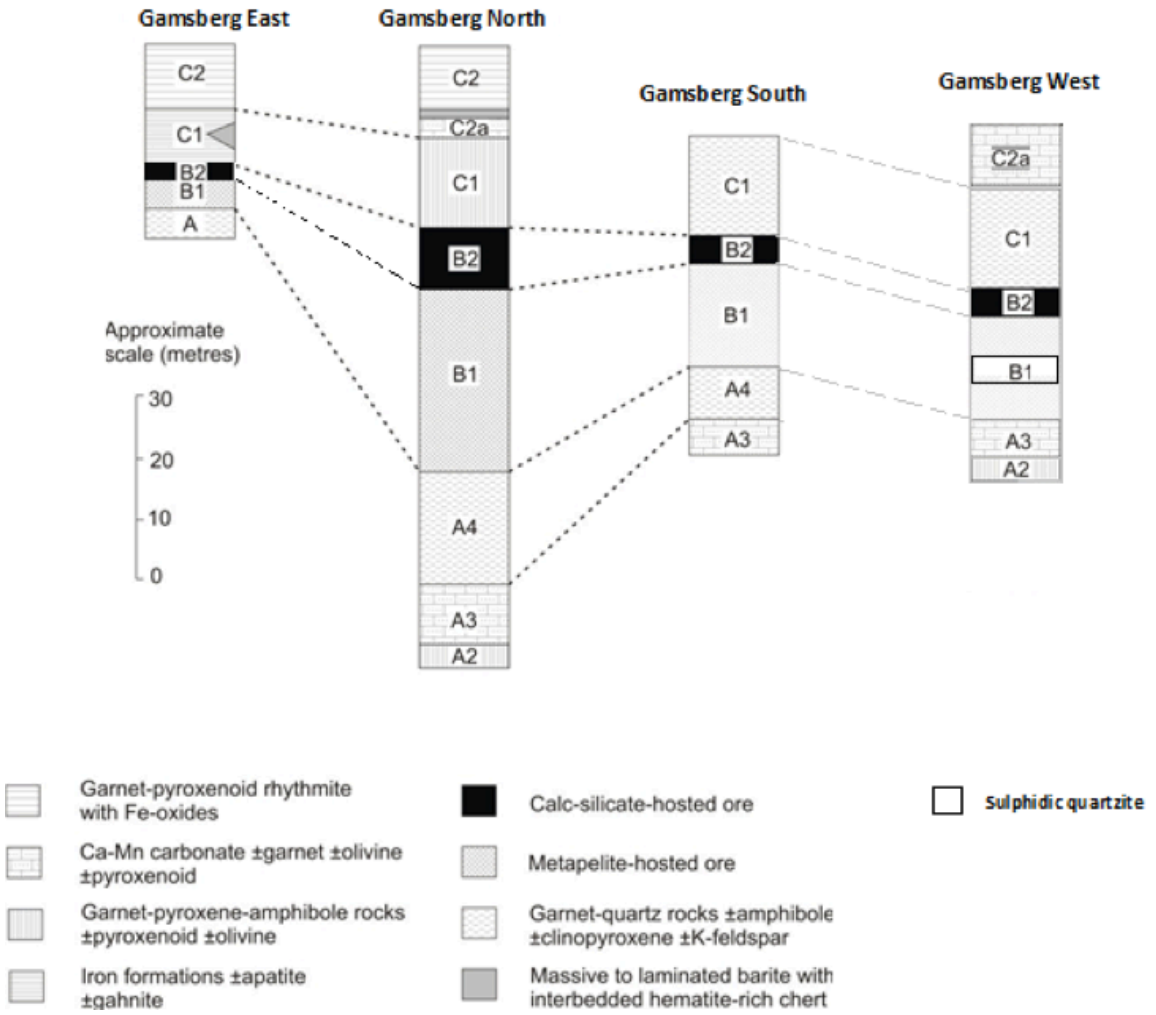

Figure 12: Comparison of the Gams Formation stratigraphy for each orebody at the Gamsberg Zn deposit (unpublished report Vedanta 2017).

4 PETROGRAPHIC APPROACH

This section does not aim to draw a complete microscopic petrography of the Gams Formation but focuses on the six units of the Gams Formation encountered in the GVD038 drillhole and more specifically on their sulfide-rich zones. This specific focus most certainly placed a lot less focus on the petrography of gangue mineral features in favour of the development on sulfides and iron oxides. This omission is arguably not so critical in view of the numerous previous studies characterizing the host rocks of the Gams Formation (Rozendaal 1975, Rozendaal 1986, Stalder 2004, Stalder and Rozendaal 2004, 2005a, 2005b, McClung et al 2007, McClung and Viljoen 2011, Foulkes 2014). The present petrographic study served as the necessary benchmark for the description and identification of the sulfides targeted for the subsequent mineral chemical aspects of this study. The petrographic work was coupled with SEM-EDS analysis where necessary to differentiate minerals with close or similar optical properties in reflected light and thus allow confident determination of different mineral species.

Table 2: Comparison of nomenclature used in the drillhole GVD038 for the Gams Formation and list of samples by unit.

	Nomenclature		
Lithology Vedanta	Vedanta	Literature	Samples
Garnet-Amphibole-Magnetite	GAM	C2	18A, 18B
Garnet-Magnetite Ore	MPO	C1	20A, 20B, 21A, 22A, 24A, 25A, 25B
Pyrrhotite Ore	PEO(Po)	B2	26A, 26B, 26C, 27A, 29A, 29B, 31A, 31B
Sulfidic Quartzite	SQZ	SQZ	33A, 34A, 34B, 35A, 36A, 37A, 38A
Pyrite Ore	PEO(Py)	B1	40A, 40B, 40C, 41A, 42A, 42B
Meta-pelite	PEL	B1	43A, 44A, 44B, 44C
Calc-silicate	CAS	A3	-

The stratigraphy used in this study (Figure 12) utilises the nomenclature drawn from the relevant literature. Table 2 above presents the equivalent nomenclature used by Vedanta at Gamsberg.

4.1 Mineralogy and Textures: C2 unit

This unit is the topmost one of the Gams Formation at the West orebody. The mineralogical assemblage of C2 is dominated by a massive equigranular package of gangue minerals, iron oxides and sulfides. A generally granoblastic texture defines the samples observed with minerals sizing from 0.5 to 3mm.

Gangue minerals are predominantly garnet, quartz, amphibole and pyroxenoid. Garnets are easily recognisable macroscopically as honey-brown to reddish nodules and microscopically as polygonal grains that are sub-idiomorphic to xenomorphic depending how much deformation obscured the primary texture. Qualitative SEM scans reveal that the geochemistry of garnets has high Mn content associated with varying Al and Fe contents, suggesting spessartine or calderite as key garnet species. Quartz crystals are xenomorphic often bearing inclusions of other gangue minerals, sulfides and iron oxides. Pyroxenoids are mostly dominated by rhodonite denoted by a high Mn content through SEM-EDS analysis, a slightly darker grey plus more common anhedral-shaped crystals differentiate them from garnets in reflected light. Amphibole has previously been reported in the C2 unit (see Table 2) but was not encountered in the selected areas observed. Amphiboles are found in varying proportion in the different units of the Gams Formation, from major to minor amounts in the form of fine- to medium-grained sub-euhedral crystals with common high manganese concentrations (Stalder 2004). Clinopyroxene, K-feldspar, chlorite, zoisite and calcite were also reported in the C2 unit in major to minor amounts but were not seen in the selected samples (Rozendaal 1986).

Sulfides minerals are dominated by pyrrhotite, sphalerite and a minor presence of pyrite. Pyrrhotite and sphalerite form anhedral flakes closely associated together, often developed interstitially to gangue minerals as concentrated aggregates. Being more ductile, sphalerite

and pyrrhotite are more severely affected by deformation which caused the softer sulfides to plastically migrate in grain boundaries and micro-fractures (Figure 13.d). Pyrite is found mainly fine- to medium-grained in inclusions in coarser pyrrhotite.

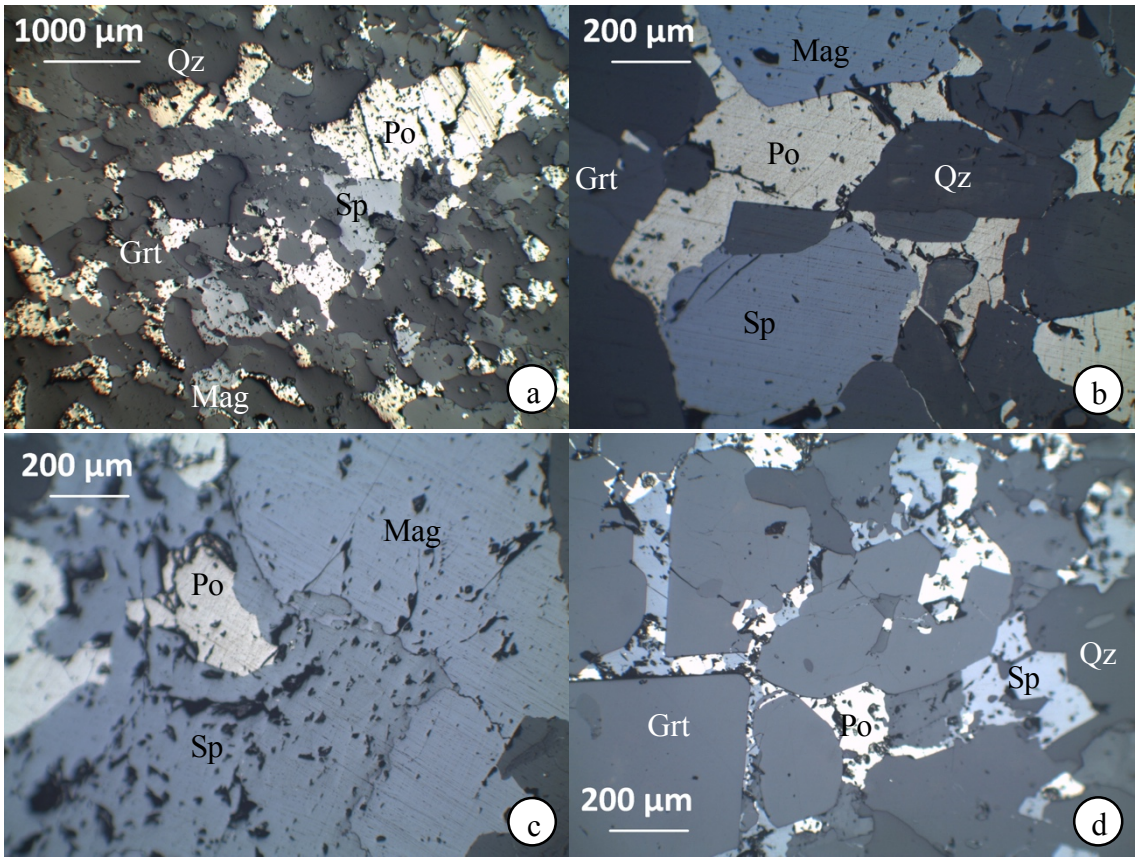

Figure 13: Microscopic photographs in reflected light of: (a) Typical granoblastic package (sample 18B). (b) Close-up on the predominant mineralogical package (sample 18A). (c) Close association of iron oxides and sulfides (sample 18A). (d) Sulfides and iron oxides aggregates interstitial to gangue minerals (sample 18B).

Iron oxides are represented by hematite and magnetite whilst ilmenite occurs as an accessory mineral phase. Hematite is the predominant iron oxide in the C2 unit but is gradationally replaced by magnetite toward the bottom of the unit. Evidence of such martitisation has been found throughout the Gams Formation (Stalder 2004). Deformational pressures tend to bring together minerals with similarly compliant behavior in the same areas, therefor iron oxides are often closely located with sulfides. As sulfides, hematite and magnetite form xenomorphic aggregates showing sharp to confounded

contacts with other minerals. Ilmenite is observable as fine exsolutions in magnetite, which is distinguishable due to the different tints between the two mineral phases. SEM-EDS analysis revealed a relatively high Mn content in ilmenite. Magnetite and hematite have similar optical properties in plain-polarised reflected light with sphalerite (Figure 13.c), but they present a slight lighter grey comparatively to the latter. In many instances, SEM-EDS analysis was particularly helpful in the differentiation of these species when grain sizes were too small.

4.2 Mineralogy and Textures: C1 unit

Underlying the previous C2 unit, the C1 unit has a similar mineralogical assemblage, and the general granoblastic texture with quartz, garnet, iron oxides and sulfides is maintained (Figure 14.a). Gangue minerals present the same overall morphologies, the major constituents (quartz and garnet) are mostly medium-grained, sub-idiomorphic to xenomorphic shaped crystals sometimes bearing multiple inclusions of iron oxides and sulfides. Sulfides and iron oxide sizes vary from fine- to coarser-grained aggregates. The intergrowth between mineral phases presented in Figure 14 shows either sharp curved contacts or composite contacts which have been interpreted before as evidence of simultaneous recrystallization (Stalder 2004). A breccia texture has been encountered in one sample, presumably due to intense deformation resulting in competent minerals being broken into fine grains while ductile mineral phases such as sphalerite, becoming more "agglomerated" in a brittle matrix (Figure 14.c). In some sulfide- and oxide-poor domains, opaque mineral species are finely grained (0.1mm) and disseminated within the gangue mineral matrix. Sporadically, scattered thin quartzite veins cross-cut the mineralogy, probably as the result of late deformational event.

As in the C2 unit, pyrite can be found as accessory idiomorphic to sub-idiomorphic crystals often associated with pyrrhotite. Fine-grained nodules of apatite conserve the chemical signature of phosphorus at Gamsberg. Some of the iron oxide contacts are characterised by fine-grained ilmenite (Figure 14.d). Other accessory minerals have been reported in the

literature as minor components namely gahnite, graphite, amphibole, K-feldspar, biotite, muscovite, chlorite (Stalder 2004), but these were not sought in the selected samples.

The fundamental distinction contrasting the C1 and C2 units comes from the gradational contact between the B and C members, which is marked by a decrease of gangue minerals and iron oxides to the benefit of sulfides. Therefore, a gradual decrease is noticeable in the amount of spessartine-calderite garnet and iron oxides toward the bottom of the unit. Moreover, as evidence of the increase in base metal sulfides; the average modal distribution of sphalerite is higher in the C1 unit samples than in the C2 unit samples, and the abundance of base metals appears to have led to the localised development also of some anhedral coarse galena with its characteristic triangular cleavage pits (Figure 14.b).

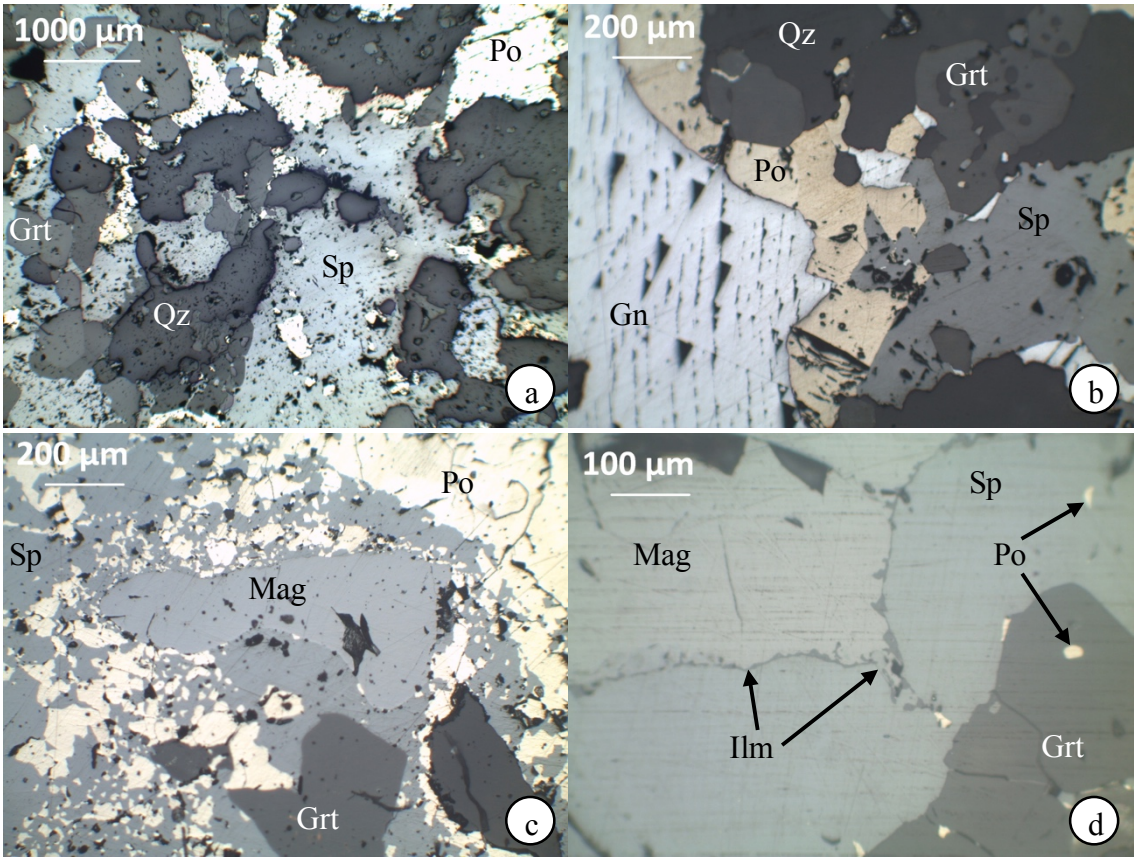

Figure 14: Microscopic photographs in reflected light of: (a) Granoblastic mineralogical package (sample 20A). (b) Close-up on the mineralogical package with galena triangular cleavage (sample 24A). (c) Breccia texture: sphalerite matrix associated with "shredded" pyrrhotite, sub-euhedral garnet and magnetite (sample 21A). (d) Ilmenite at the boundaries between magnetite and sphalerite (sample 22A).

4.3 MINERALOGY AND TEXTURES: B2 UNIT

The bulk of the base metal mineralisation is held in the B member of the Gams Formation with the upper B2 unit containing the higher ore grades. Figure 15.a presents the typical sulfidic package of the mineralization: it is mainly composed of fine- to medium-grained anhedral sphalerite and pyrrhotite with minor amount of sub-euhedral to euhedral pyrite. Galena and chalcopyrite are also found in small amounts. Quartz and garnet are again major constituents of the gangue minerals as medium-grained sub-euhedral crystals often bearing multiple inclusions. As in the C1 unit, micro-scaled quartz veinlets occur sporadically (Figure 15.a). Quartz and garnet are followed in modal abundance by subordinate amphibole and micas (biotite and muscovite) forming xenomorphic elongated grains sometimes closely associated with sulfides (Figure 15.e). The higher concentration of micas is located in planes of oriented silicates and sulfides displaying a foliation. This feature is enhanced by preferred orientation of the grains suggesting an inherited deformational alignment, and by alternating layers of variable mineralogical composition manifested as micro- to meso-banding. Micas are altered into chlorite most probably due to retrograde metamorphism. Sillimanite is present typically as elongated anhedral crystals. Apatite, K-feldspar, zircon, zoisite and clinozoisite have been detected as fine- to medium- grained accessory minerals.

The relationship between sulfides revealed multiple petrographic textures resulting from the polyphase metamorphism which occurred on the deposit scale. As stated before, sulfides are mainly developed as aggregates concentrated in preferred areas. The breccia texture found in the C1 unit is once again observable, denoted by fine-grained pyrite and gangue minerals closely dispersed within a sphalerite matrix (Figure 15.b). Annealing grain boundaries of pyrite grains included into anhedral sphalerite (Figure 15.c) is a recurrent feature occasionally displaying poikiloblastic pyrite grains when apparent resorption reached an advanced stage. Comparatively, sphalerite can be observed in coarser pyrite aggregates (Figure 15.d) which could have been mobilized during deformational event. In some places, micro-folding is recorded by alteration, cleavage and/or inclusions in the

sulfides which exhibit complex patterns (Figure 15.f) indicating a late deformational event post-dating the ore mineralization.

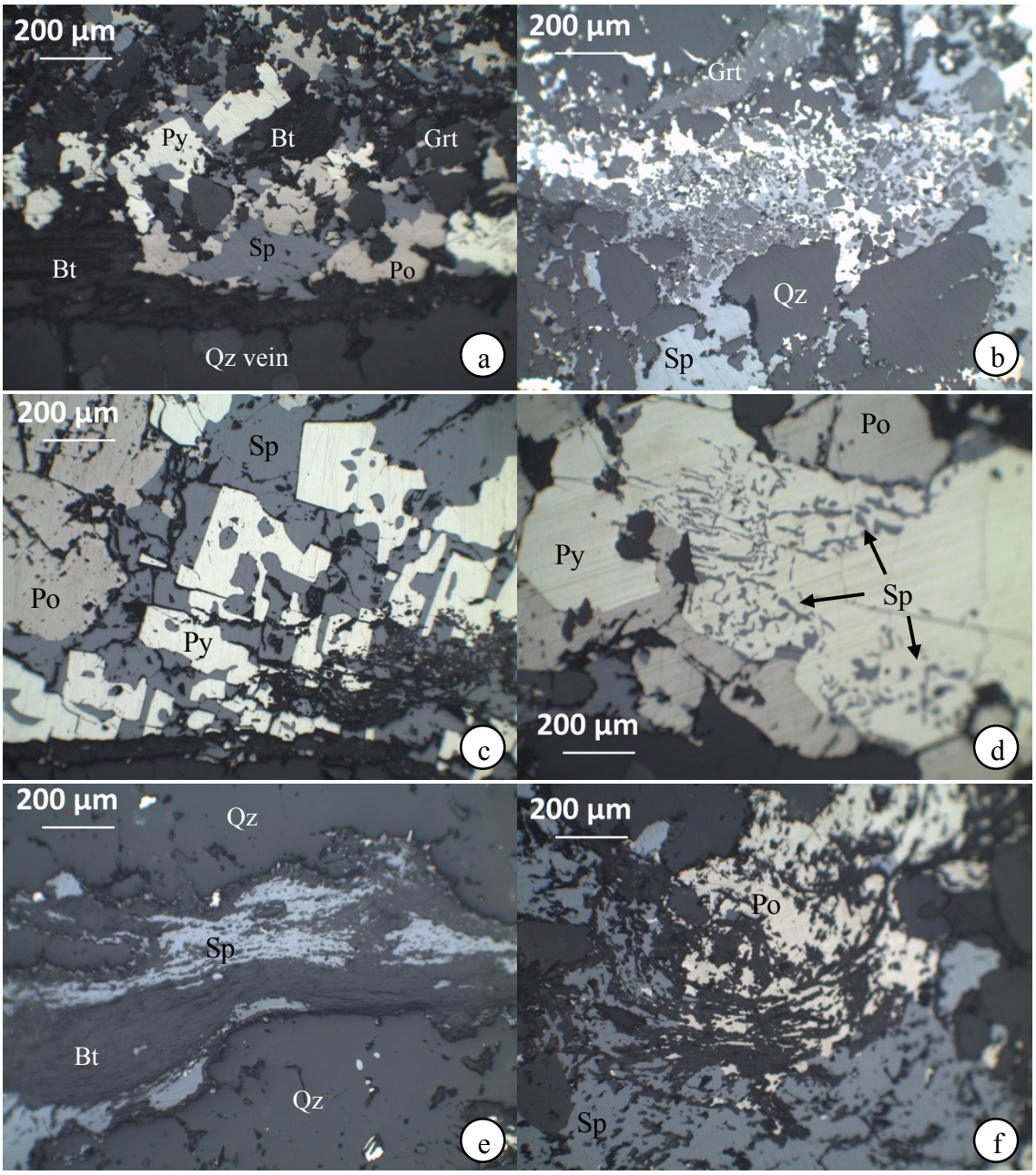

Figure 15: Microscopic photographs in reflected light of: (a) Typical sulfidic package and quartz vein (sample 26A). (b) Breccia texture: sphalerite matrix including fine-grained pyrite and gangue minerals (sample 26A). (c) Annealed to poikiloblastic pyrite grains in coarser sphalerite (sample 26C). (d) Sphalerite in pyrite aggregates (sample 26A). (e) Sphalerite associated with an elongated deformed mica (sample 31A). (f) Complex folded texture of alteration and gangue minerals in sphalerite and pyrrhotite (sample 26B).

4.4 MINERALOGY AND TEXTURES: SQZ UNIT

The sulfidic quartzite (SQZ) unit is a particularity of the Gams Formation occurring in the West and South orebodies. The unit represents a 9 to 10 meter-thick quartzite with intercalated, irregular sulfide-rich meso-bands. Medium- to coarse- grained quartz developed a granoblastic texture showing wavy extinction in the crystals due to deformation. Identifiable by their lighter grey and the multiple sulfide inclusions, garnets are present in minor amounts followed by anhedral fine- to medium-grained micas often altered in chlorite displaying a discrete preferred orientation. The SEM-EDS analysis permitted also the identification of minor manganese oxides containing F, Mg and Ca as minor constituents. The said Mn phase is tentatively interpreted as pyrolusite.

Sulfides are concentrated in meso-bands whose apparent thicknesses in cross-section vary from millimetres to centimeters. Sulfides are mainly fine- to coarse- grained sub-idiomorphic to xenomorphic pyrite, pyrrhotite and sphalerite. The contact between sulfide-rich and sulfide-poor areas can be sharp (Figure 16.a) or gradational. In the latter case, sulfide-poor areas are marked by disseminated very fine- to fine grained sulfides in the granoblastic quartz-dominated entity. The transition towards the sulfide-rich area marks an increase in the proportion and grains sizes of sulfides. Furthermore, sulfide-rich zones possess a higher concentration of slightly elongated mica that accentuates the preferred orientation effect in the meso-bands. Mica and sulfides are in a close relationship exhibited by inclusions and intergrowth patterns of the two minerals displaying wavy micro-structures as encountered in the previous unit (Figure 15.e). The core of the meso-bands is marked by aggregates of coarse sulfides, sphalerite being the main phase (Figure 16.c). Alteration is more clearly seen in coarse crystals, whereby very fine- to medium-sized dark spots are recurrent (Figure 16). Interpreted exsolution features are observed in coarser crystals of sphalerite as blebs of alabandite (Figure 16.e) possibly denoting a geochemical reconstitution of the sulfide ore during metamorphism. Another possible metamorphic texture is the presence of pyrite overgrowths surrounding a sphalerite core (Figure 16.d), denoting phase re-equilibration during the annealing process (Craig and Vaughan 1994). Ductile sulfides (pyrrhotite, sphalerite) are sometimes found interstitial to gangue minerals

and filling micro-fractures in quartz or in coarse-grains sulfides. Chalcopyrite was also observed albeit as a very fine accessory phase.

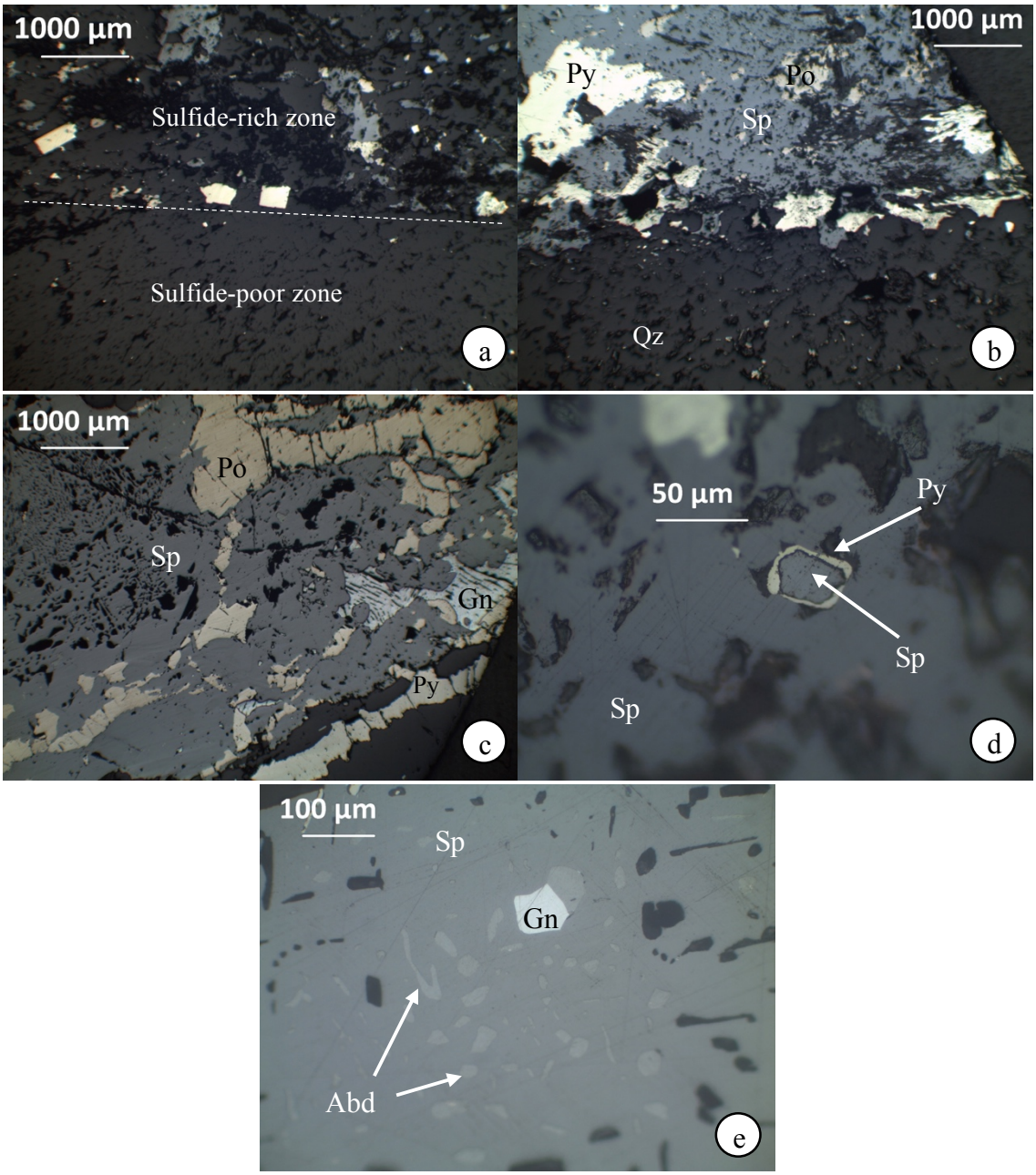

Figure 16: Microscopic photographs in reflected light of: (a) Sharp contact between a sulfide-rich zone and a sulfide-poor zone (sample 34A). (b) Altered coarse sphalerite grain with sulfide inclusion contrasting with quartz dominated zone (sample 38A). (c) Sulfidic package in coarse altered sphalerite (sample 37A). (d) Pyritic phase overgrowth surrounding sphalerite (sample 38A). (e) Bleb exsolutions of alabandite in sphalerite (sample 37A).

4.5 MINERALOGY AND TEXTURES: B1 UNIT

The B1 unit is the lower and less mineralised part of the B member with fundamental difference being the replacement of pyrrhotite from the B2 unit with pyrite as now the predominant iron sulphide phase. In the literature, this unit is called "metapelitic-hosted ore" standing for a fine-grained quartz-sillimanite-muscovite schist bearing major amounts of pyrite and sphalerite with additional substantial amounts of graphite, K-feldspar, sericite, chlorite, biotite, galena and pyrrhotite (Stalder 2004, Rozendaal 1986). In the upper part of the B1 unit, a moderate banding is observable due to corresponding mineralogical variations, and specifically the association of sillimanite, muscovite and sphalerite as elongated grains preferentially orientated and defining an irregular wavy foliation. Deeper in the unit, the gradational contact with the A member is associated with an apparent reduction in the degree of foliation to the benefit of a texturally more massive ore body, until reaching a fine-grained disseminated-sulfide zone characterized as the "PEL unit" by the geologists of Vedanta.

Pyrite is developed as aggregates of sub-euhedral rounded angles grains in the massive domains or as elongated anhedral grains in the foliated ones. Recrystallization of pyrite is displayed by 120° contacts between pyrite grains (Figure 17.f) but association of medium- to coarse-grained pyrite with interstitial softer sulfides (sphalerite, pyrrhotite, galena) is a more common feature (Figure 17.d-e). Breccia-textured zones, produced by intense deformation, have also been found in this unit. These ave apparently resulted in the fracturing of pyrite grains against each other and simultaneous migration and infilling of micro-fractures by more ductile sulfides such as sphalerite and pyrrhotite.

Sphalerite is the second most abundant sulfide in the B1 unit; it occurs as elongated, xenomorphic grains, as apparent fibrous intergrowths with sillimanite and muscovite (Figures 17.a-c, 15.e), or as coarser crystals containing bleb-like inclusions and lamellar exsolutions of alabandite, galena, pyrrhotite (Figure 17.c). By contrast, sphalerite grains are more anhedral in the disseminated sulfide zone as compared with pyrite (Figure 17.a). Accessory minerals in the B1 unit also include also chalcopyrite, apatite, zircon and rutile.

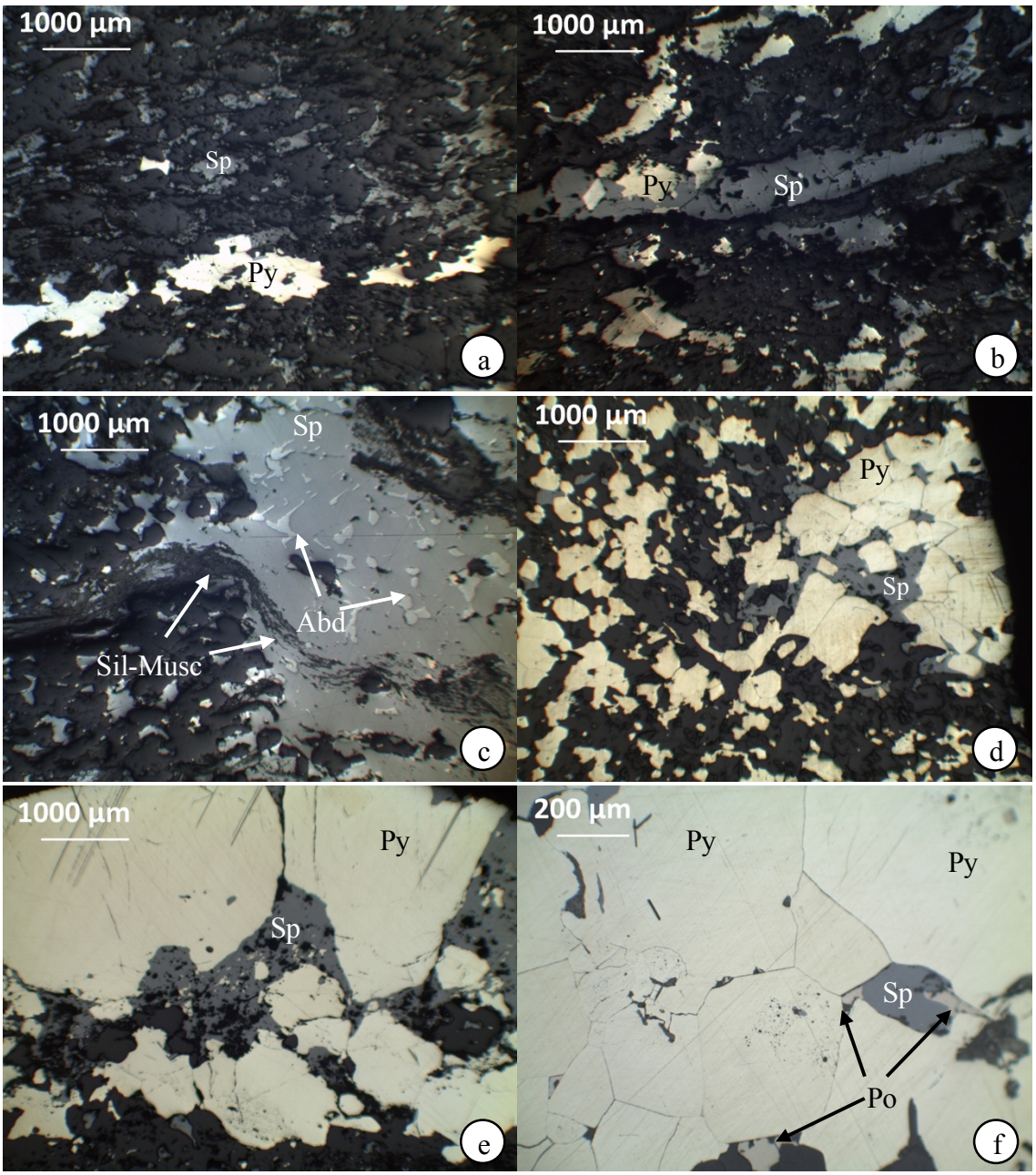

Figure 17: Microscopic photographs in reflected light of: (a) Elongated pyrite and anhedral disseminated sphalerite showin a discrete foliation (sample 40B). (b) Elongated sphalerite and disseminated sub-euhedral pyrite (sample 40C). (c) Coarse sphalerite with alabandite exsolution and associated with wavy fibrolitic sillimanite-muscovite (sample 40A). (d) Massive pyrite-gangue package with interstitial sphalerite (sample 42A). (e) Massive coarse pyrite with interstitial sphalerite (sample 41A). (f) Recrystallized pyrite grains with 120° junctions and interstitial sphalerite and pyrrhotite (sample 42B).

4.6 MINERALOGY AND TEXTURES: A3 UNIT

The A3 unit is significantly poorer in sulfides and is characterized by the presence of manganiferous carbonate and garnet with minor quartz, amphibole and pyroxene/pyroxenoid. The mineralogy of the A3 unit varies as a function of the location in the deposit: the North orebody records the occurrence of K-feldpsar, the South orebody has a larger proportion of clinopyroxene, while in the East orebody the A3 unit appears to be pinching out (Stalder 2004). In some places, the gradual contact between the B member and the A member is marked by a banded garnetiferous quartzite transition unit (A4) but this does not occur in this studied location. According to borehole log information made available by Vedanta, the contact between the A3 unit and the previous one is at 110.4 meters in the GVD038 drillhole. It was decided that sampling would be terminated below that depth mark of 110.4 meters (see Table 2) but the gradational contact permitted the identification of mineralogical features from the A3 unit in the samples 44A, 44B and 44C.

Mn-rich carbonate, mainly maganoan calcite and rhodocrosite, appear as sub-euhedral to anhedral fine crystals with a slight lighter grey tint than other gangue components. Developed as sub-euhedral medium-grained crystals, andratite is the most common species here representing the garnet group. Gangue minerals record both deformation and lower-temperature alteration, with fine-grained kaolinite observable in parts of the section. Deformation effects appear to be manifested by different features such as fracturing of minerals or microscopic sigmoidal deformation structures overprinted on fine-grained pyrite included in garnet (Figure 18.c).

Sulfides are disseminated, fine- to coarse-grained and often interstitial or filling micro-fractures (Figure 18.a). Pyrite, alabandite and sphalerite form the predominant sulfidic phase. Lamellar and irregular exsolution blebs of pyrrhotite are sometimes found in alabandite and sphalerite (Figure 18.e). Alabandite is more abundant here than sphalerite, and this may be used as strong indication of relative abundance of manganese in the palaeo-environmental setting of the A3 unit. Recrystallized sulfide aggregates are denoted by 120° junctions (Figure 18.d) and well-developed overgrowths suggest textural re-equilibration

(Figure 18.e). Corroded textures (Figure 18.f) are interpreted as effects of replacement. Titanite, pyrophanite, wollastonite, mica and apatite are also present as accessory phases.

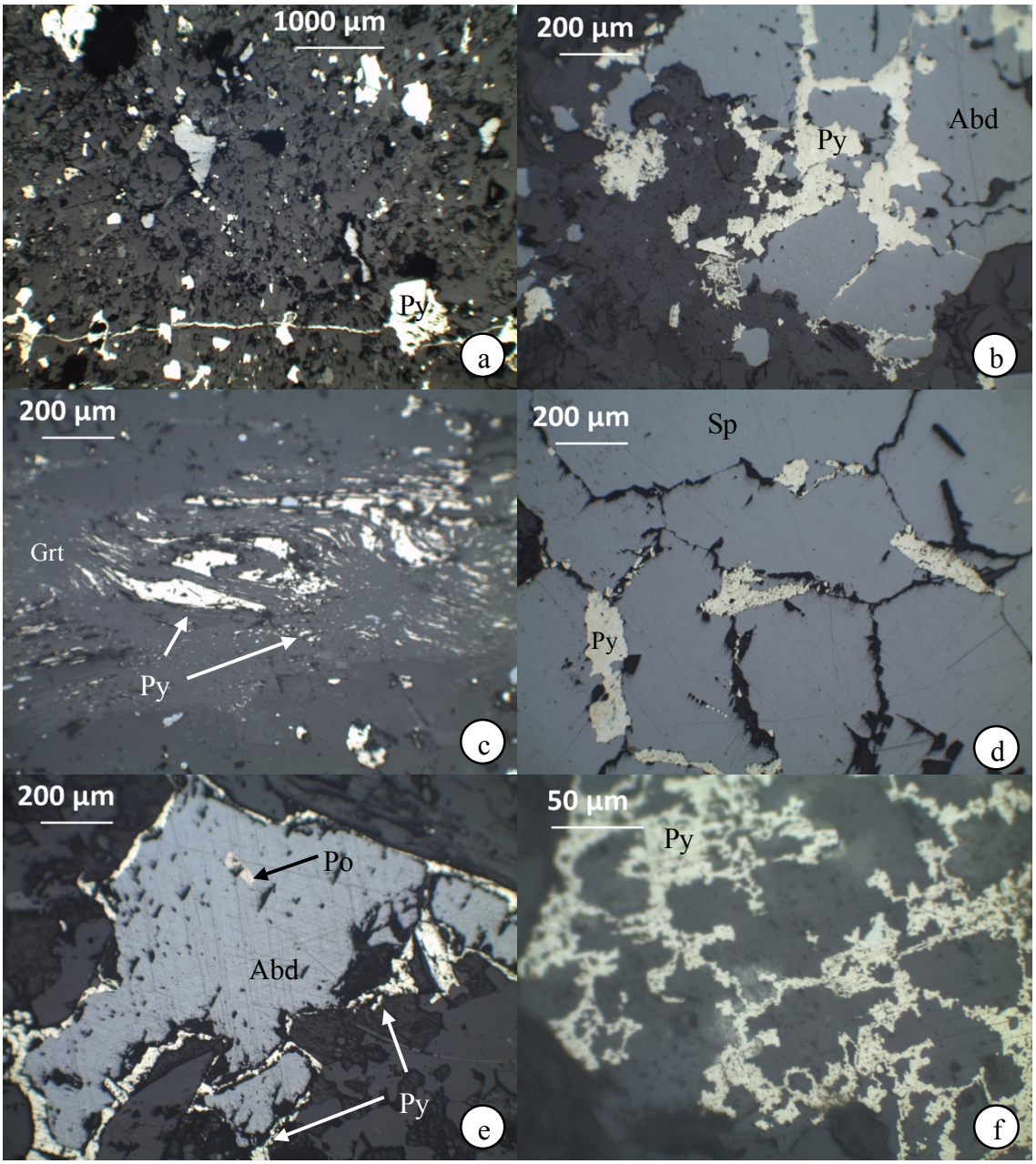

Figure 18: Microscopic photographs in reflected light of: (a) Typical mineralogical assemblage of the A3 unit (sample 44C). (b) Pyrite developed interstitial to sphalerite coarser grain (sample 44B). (c) Microscopic deformational structure recorder by pyrite (sample 44A). (d) 120° junctions of sphalerite associated with pyrite (sample 44B). (e) Pyrite overgrowth surrounding an alabandite grain with pyrrhotite exsolution (sample 44C). (f) Corroded texture of pyrite in a gangue mineral (sample 44C).

4.7 Stratigraphic Overview

The petrographic approach permitted the construction and display of the main mineralogical and textural characteristics of the GVD038 drillhole. Figure 19 displays an overview of the Gams Formation stratigraphy from the section selected for this study, which will be used for the geochemical profiling in the chapter that follows.

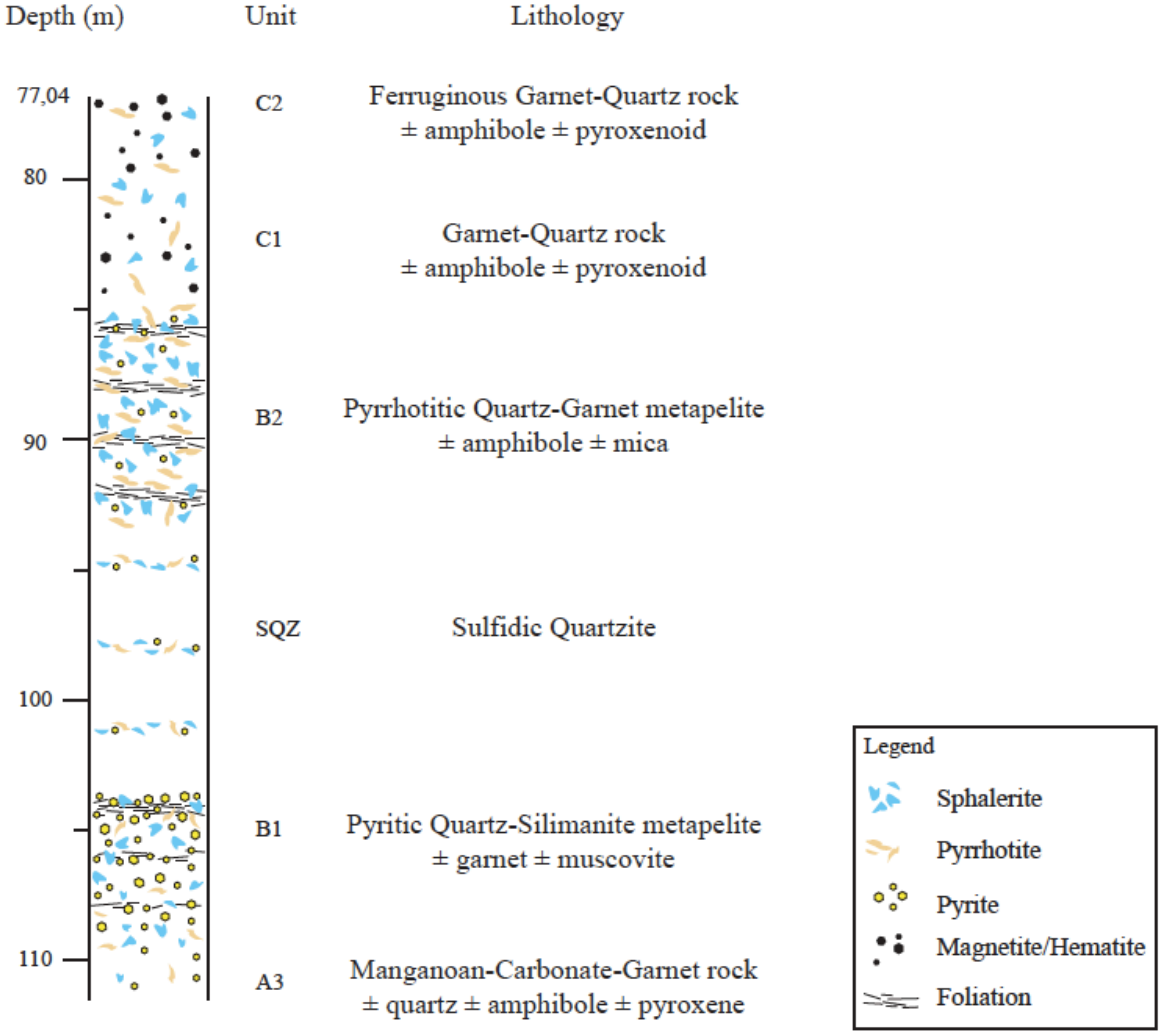

Figure 19: Stratigraphy of the Gams Formation in the West orebody from the GVD038 drillhole based on logging and the petrographic approach of this study.

5 GEOCHEMISTRY

The first section of this chapter is a brief review of sphalerite geochemistry. The section that follows thereafter is a quantitative and qualitative approach to the EPMA analysis as a function of the lithologic members that were logged and petrographically described in the foregoing chapters. The last part of the chapter presents and assesses the chemostratigraphic profiles produced through EPMA data, in conjunction with existing similar data from a previously-studied section.

5.1 BACKGROUND ON SPHALERITE GEOCHEMISTRY

Sphalerite is the main zinc sulfide in base-metal deposits. The wide range of environmental settings forming base-metal deposits combines several genetic processes (seafloor deposition, metal-rich hydrothermal fluids, alteration, etc.) transporting a large range of minor and trace elements which can be incorporated in the sphalerite structure (ZnS). Previous studies on sphalerite (Deer et al 1962, Cook et al 2009, Ye et al 2011) are unanimous concerning the incorporation of other elements in the mineral structure being effected by substitution of Zn^{2+} by other divalent ions (Fe^{2+}, Mn^{2+}, Cd^{2+}, Co^{2+}, etc) or by coupled ionic substitutions ($Zn^{2+} \leftrightarrow Cu^{+}+In^{3+}$). Iron is naturally present in sphalerite as a substitute for Zn in proportions ranging widely from trace levels to more than 15 wt.%. The highest concentration recorded is 26 wt.% (Deer et al 1962). Other key constituents of sphalerite substituting for Zn are manganese and cadmium: their concentrations are also very variable and range from a few hundred ppm to 4 to 5 wt.% but higher concentration have been recorded in certain geological settings. According to Cook and others (2009), Mn substitutions in sphalerite above 2 wt.%, approach the upper limit for MnS incorporation in its structure, thus developing alabandite and wurtzite (Zn, Fe)S. Hg, As, Tl, Ga, In, Co can also be found as trace elements in some sphalerites (Deer et al 1962, Cook et al 2009).

Multiple studies have been conducted on sphalerite geochemistry from base metal deposits due to the economic importance of the mineral and the genetic information which can be

gleaned from the trace and minor element geochemistry. Gottesmann and others (2009) found geochemical similarities between the Turmutjin-ovoo Fe-Mn skarn deposit in Mongolia and the sphalerite-bearing manganiferous skarn iron ores in Sweden. The mineralogical package of the Turmutjin-ovoo deposit went through a first stage of recrystallization, interpreted as directly linked to pre-contact metamorphism, thus producing an overall granoblastic texture. Latter stages of mineralogical replacement enriched the rocks in rhodocrosite, sphalerite, pyrite and bustamite. Sphalerite displays high Fe and Mn concentrations ranging from 0.1 to 6.54 wt.% and from 0.01 to 9.32 wt.% respectively. The two elements are also responsible for zoning patterns inside the sphalerite crystals. A co-genetic crystallization of sphalerite with Mn and Fe has been suggested.

High concentration of iron and manganese in sphalerite have also been noted in other base metal skarn deposits: Majdanpek in Serbia and Lefevre in Canada as documented in the work of Cook and others (2009). The same authors highlighted that this trend is present in some epithermal deposits in Romania showing Mn-rich lamellae in sphalerite. A detailed study (Olivo and Gibbs 2003) on the epithermal Santo Toribio Ag-rich polymetallic deposit, in Northern Peru, focused on brecciated alabandite-rich veins. This study defines the development of an early stage of mineralogical formation leading to Mn-rich sphalerite (14.5 wt.%) with significant Fe concentration (5 wt.%) developing co-genetically with the alabandite veins. The authors suggested that the second formation stage was triggered by condition changes (increase in the CO_2/S ratio and abrupt decrease in H^+ and /or Cl^-) leading to dissolution of alabandite and the deposition of rhodocrosite and a second generation of sulfides.

Various base metal deposits including skarns, Volcanogenic Massive Sulfide (VMS) deposits, SEDEX, Mississippi Valley-type (MVT) deposits and the giant sediment-hosted Jinding deposit were compared based on their sphalerite geochemistry by Ye and others (2011). Manganese concentration in sphalerite is not as high as in previous studies but remains a dominant feature. A high concentration variability has been noted from one sample to the other in the same deposit and in the same samples. Highest variations were recorded for MVT deposits whereas skarn, VMS and SEDEX deposits show the highest

manganese concentrations. The sphalerites from the Jinding sediment-hosted deposit present very low Fe and Mn concentrations. In general, the Mn/Fe ratio is preserved due to a correlation between Fe and Mn. This relationship between Mn and Fe has been detected by others but sometimes as an inversed correlation (Cook et al 2009, Deer et al 1962). The color of sphalerite seems to be directly affected by its geochemistry, as an increase in Mn and Fe concentrations would change sphalerite from yellow to black (Graser 1969, Ye et al 2011).

Previous studies have been conducted on sphalerite from the Gamsberg deposit (McClung and Viljoen 2010, 2011). Their work suggested the occurrence of different populations of sphalerite mainly based on geochemical data without concrete morphological similarities between sphalerites from the same population. The four main sphalerite populations are interpreted to reflect the composition of the primary sulfide mass producing a Fe-rich population, metasomatism produced the Mn-poor and Mn-rich population and finally retrograde metamorphism giving rise to Zn-rich sphalerites.

5.2 EMPA ANALYSIS: QUALITATIVE AND QUANTITATIVE APPROACH

Sphalerites were analysed in the 34 selected polished blocks, with a minimum of 5 analyses per sample performed to obtain a statistically robust average value and range for the mineral chemistry of the corresponding sphalerite populations. In case where the range of values varied more widely, the number of point analyses was increased to enhance the statistical robustness of the data set. Most samples targeted the economic units (C1, B2 and B1) therefore the number of samples and points analysed in those units is higher than in the lithologic units at the stratigraphic extremities (i.e. C2 and A3) (Table 3). The highest standard deviations are associated with the SQZ unit due to one sample (34A) presenting a clear contact between two discrete sulfide populations (Figure 22). Relatively higher standard deviations encountered in the C1 or B2 units are considered to be a response to variability across the said units, although individual sample data appear statistically tighter.

Table 3: Distribution of analysis as a function of lithologic unit and the 1σ standard derivation for the elements Zn, Fe and Mn.

Unit	Number of Samples	Number of Points	Std Dev Zn	Std Dev Fe	Std Dev Mn
C2	2	14	0,67	0,31	0,23
C1	7	41	2,06	0,73	1,62
B2	8	48	1,90	0,58	1,28
SQZ	7	42	4,71	2,38	2,28
B1	6	33	1,18	0,71	0,51
A3	4	17	1,47	0,68	0,79

The data of Table 3 show that the distribution for zinc and iron is relatively homogeneous throughout the stratigraphy (Figure 20) comparatively to a more erratic one for manganese values. A wide range of values can be observed particularly in Figure 20 for the SQZ unit for reasons previously explained. With respect to the Fe and Mn as both elements that substitute for Zn, the range of values is relatively higher for the latter.

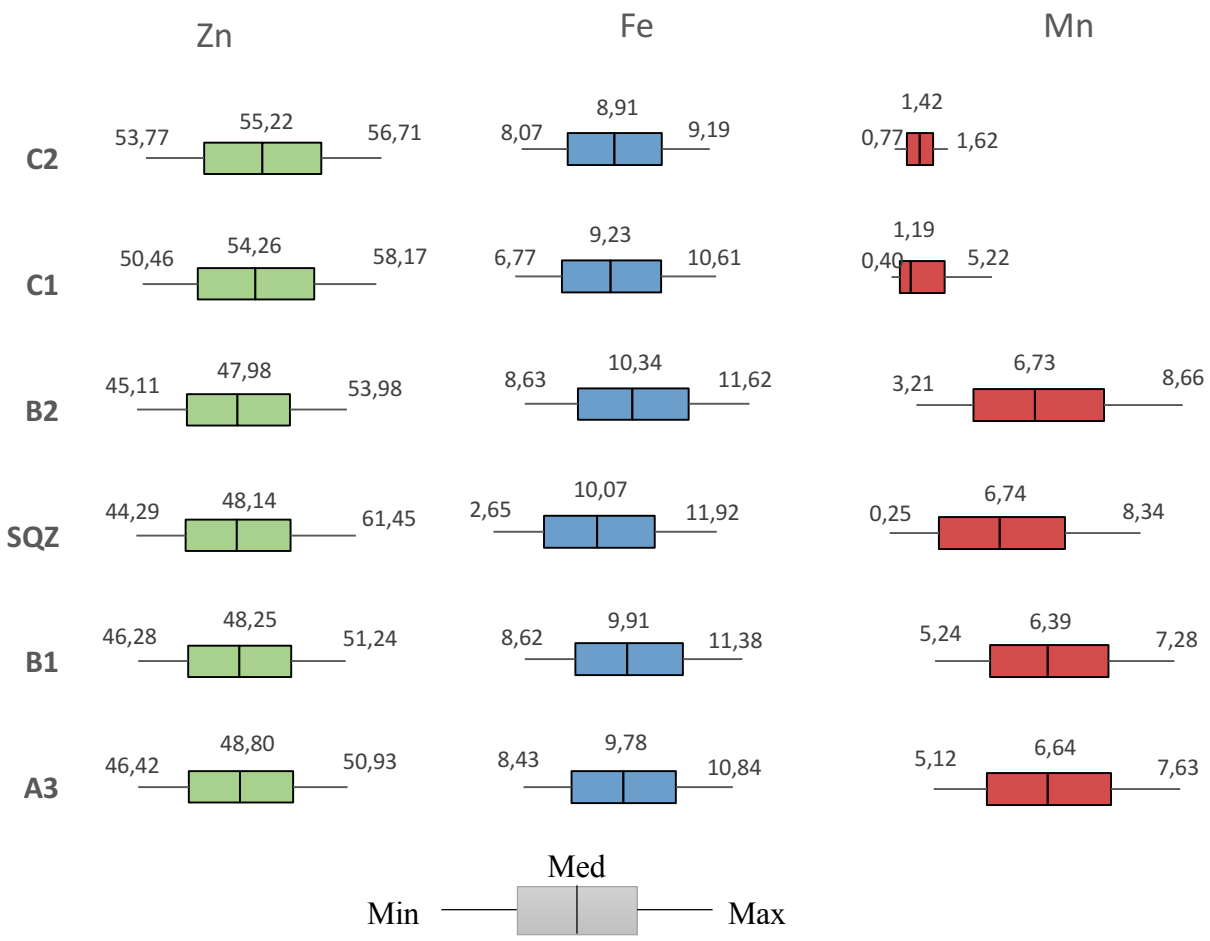

Figure 20: Distribution of zinc, iron and manganese values as a function of lithologic unit. The borders of the boxes are the 1st and 3rd quartiles.

Units C1 and C2 displayed a similarly equigranular, granoblastic mineralogical character (Figures 21.a.b.) and record a closely similar range of values (Figure 20). Unit B2 bears the highest ore grade in the Gams Formation and from a metamorphic texture point of view the ore assemblage appears more enhanced in this unit. Grains are often elongated with a preferential orientation more or less noticeable, whereas sulfides and gangue mineral intergrowths are typically complex (Figures 21.c.d). The EPMA analysis therefore targeted the different morphologies of sphalerites to detect any potential geochemical variation with textural form.

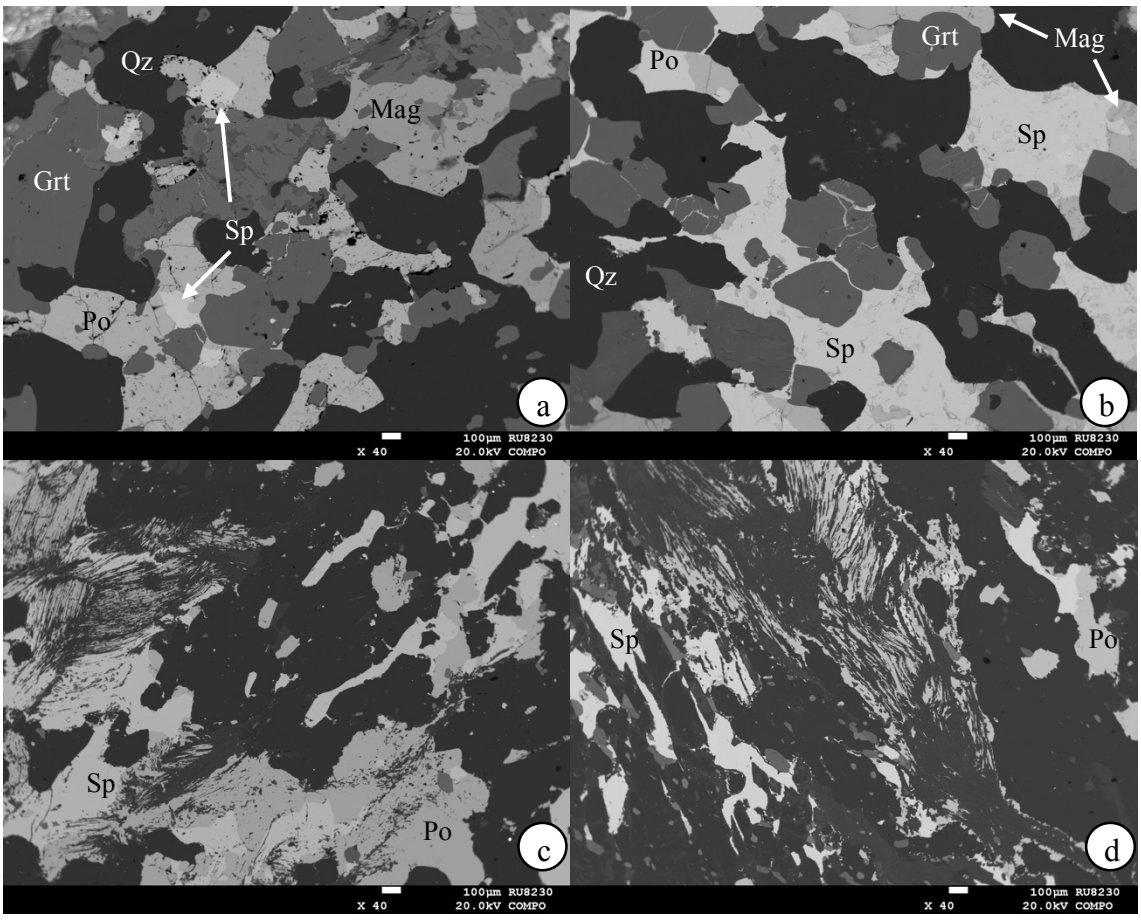

Figure 21: EMPA photography (100µm): Both units display similar morphologies, the proportion of iron oxides is higher in the C2 unit (medium light grey) comparatively to the C1 unit richer in sulfides and sphalerite (lightest grey) (a) C2 unit typical mineralogical package (sample 18A). (b) C1 unit typical mineralogical package (sample 21B). (c) On the left side, sulfide gangue mineral association displaying complex texture. Sphalerite is the main sulfide closely associated with pyrrhotite (sample 29B). (d) Similar complex texture of sphalerite with gangue minerals. Elongated shaped sphalerite on the left side displaying a subtle foliation (sample 31B).

The sulfidic-quartzite contains disseminated, very fine- to fine grained sulfides and meso-bands of coarser sulfides. Sample 34A displays particularly well the sharp contact between sulfide-rich and sulfide-poor zones. EPMA analyses targeted both areas. The geochemical data manifested two populations of sphalerite that are further discussed in the results.

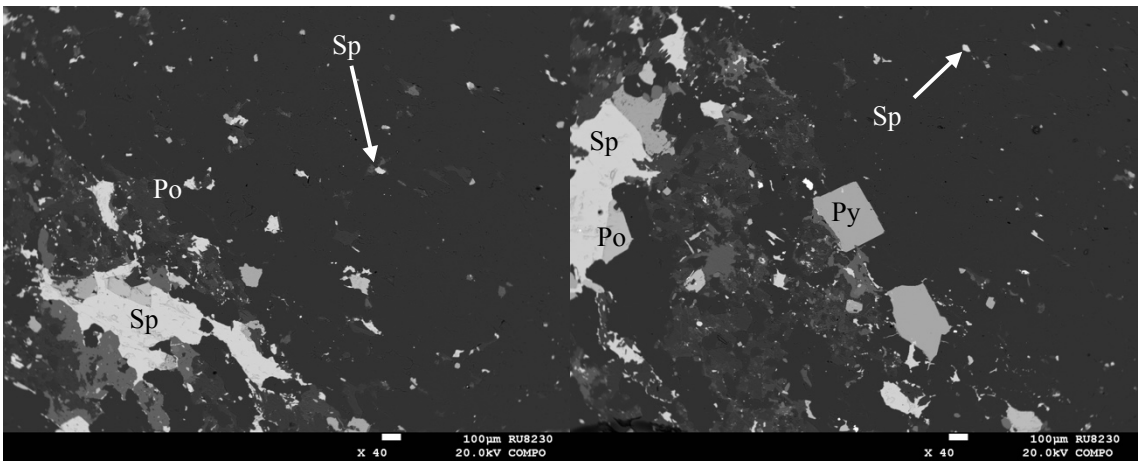

Figure 22: EPMA photography (100µm): Two pictures from the 34A sample presenting the contact between sulfides-rich (bottom-left) with coarse euhedral to anhedral sulfides and sulfide-poor zone with disseminated very fine- to fine grained sulfides (top-right).

The B1 unit is characterized by the absence of pyrrhotite over pyrite as key iron sulphide species. The upper part of the unit is apparently foliated whereas the lower part of the unit gradually becomes more massive. No striking geochemical variation was noted between the upper and lower parts of the B1 unit (see Table 3 and Figure 20).

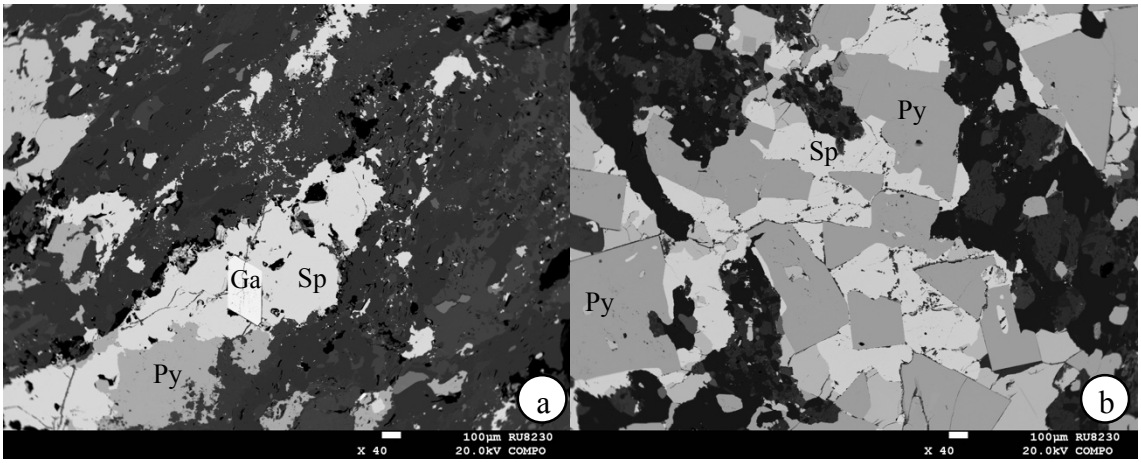

Figure 23: EPMA photography (100µm): (a) Upper B1 unit with elongated sulfides (sample 40C). (b) Lower B1 unit with massive euhedral pyrite and interstitial sphalerite (sample 42B).

The lower part of the B1 unit has a highly gradational contact with the underlying A3 unit. The sulfide-rich samples from this zone contain a predominance of alabandite along with, or instead of, sphalerite (Figure 24). Despite the abundance of Mn denoted by the coarse grained alabandite, sphalerite geochemistry appears to be comparable with the previous units.

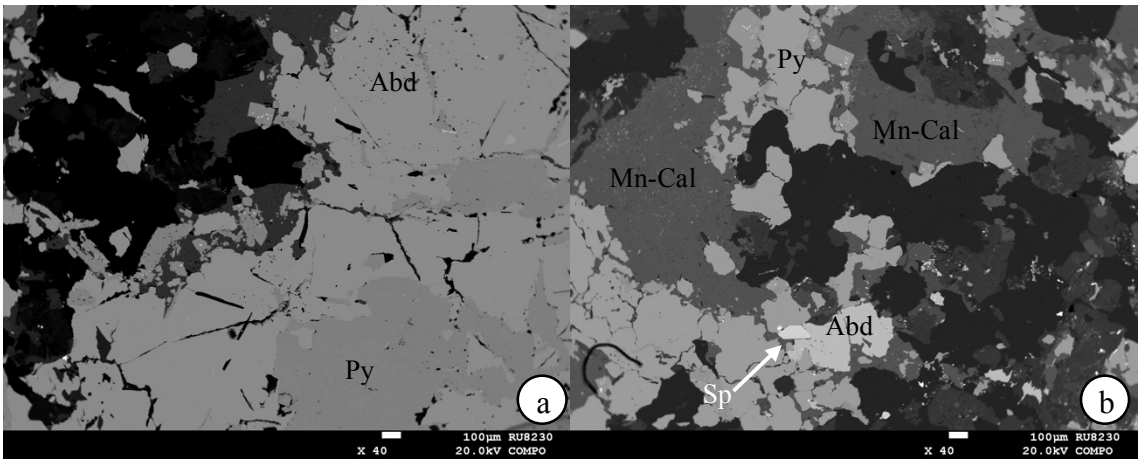

Figure 24: EPMA photography (100µm): Mineralogical package of the B1/A3 units transition. (a) Coarse grained alabandite associated with pyrite (sample 44C). (b) Aggregates of alabandite, pyrite, sphalerite and manganoan-calcite (sample 44C).

5.3 EPMS Analysis: Results

The results of the EPMA analysis performed on sphalerites are presented in Figures 25, and 27. The profiles present the average Zn in sphalerite (wt%), Mn (wt%) and Fe (wt%) (see Appendix A) from each sample and have been plotted against the interpreted lithostratigraphy of the drillhole. Ratio profiles are shown using mean data. The data set producing the earlier geochemical profile which triggered this study (see section 1.2 and Appendix B for the raw data) has been adapted to be compared with the information collected during this work, and is presented in Figures 26 and 27.

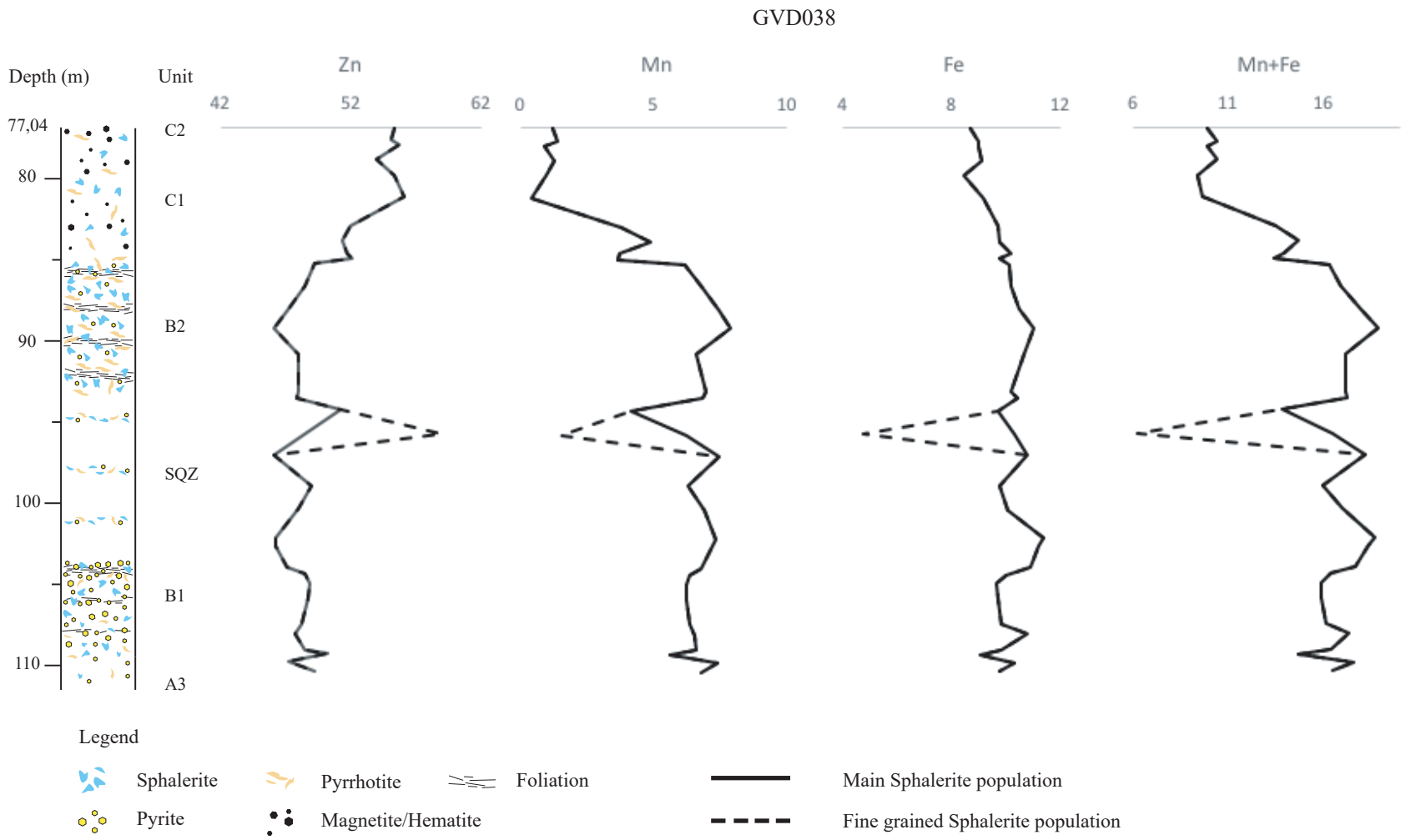

Figure 25: Sphalerite geochemical profiles of Zn, Mn and Fe from the Gams Formation in drillhole GVD038 against lithostratigraphy.

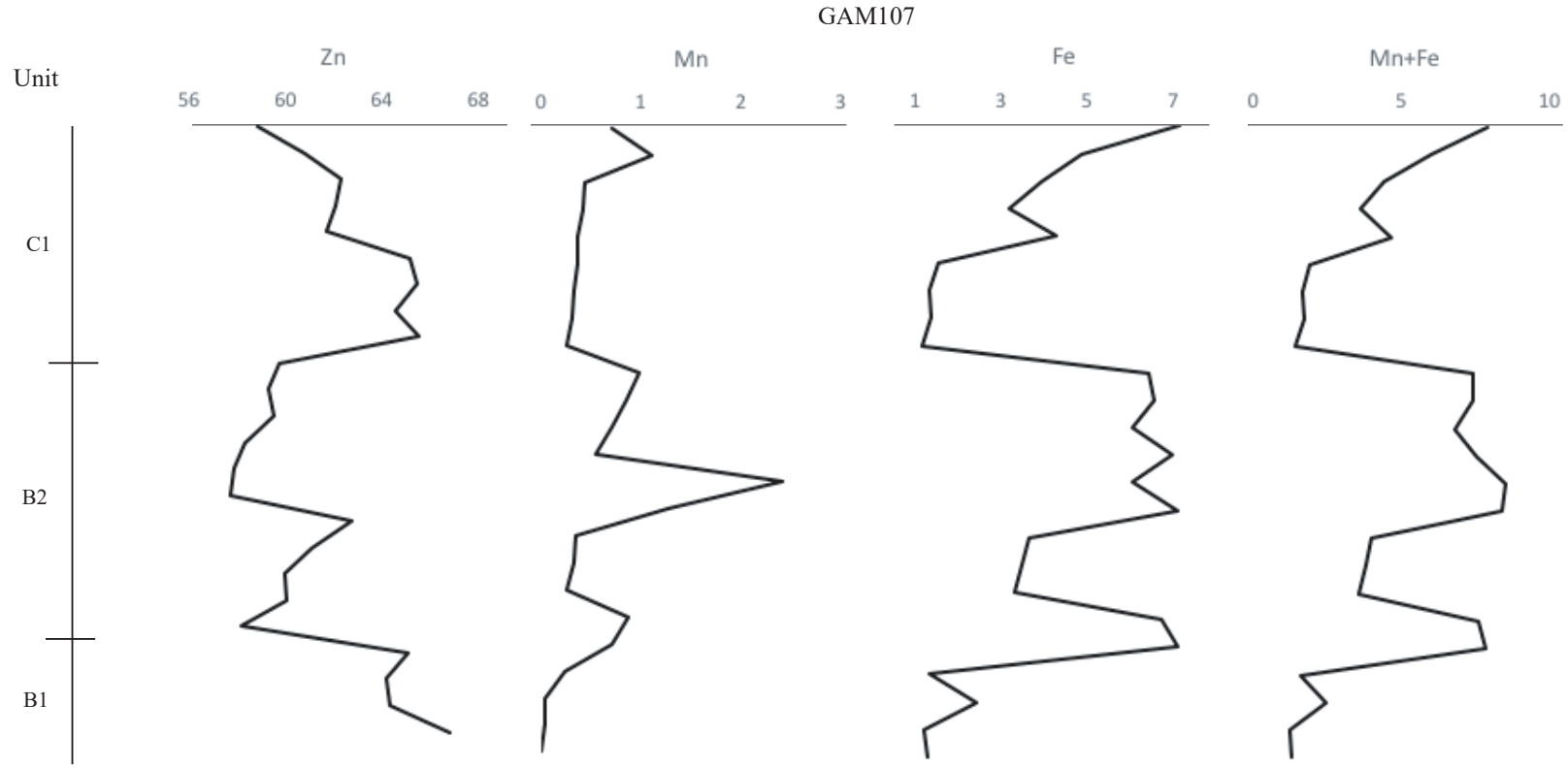

Figure 26: Sphalerite geochemical profiles of Zn, Mn and Fe from the Gams Formation in the GAM107 drillhole against its simplified stratigraphy.

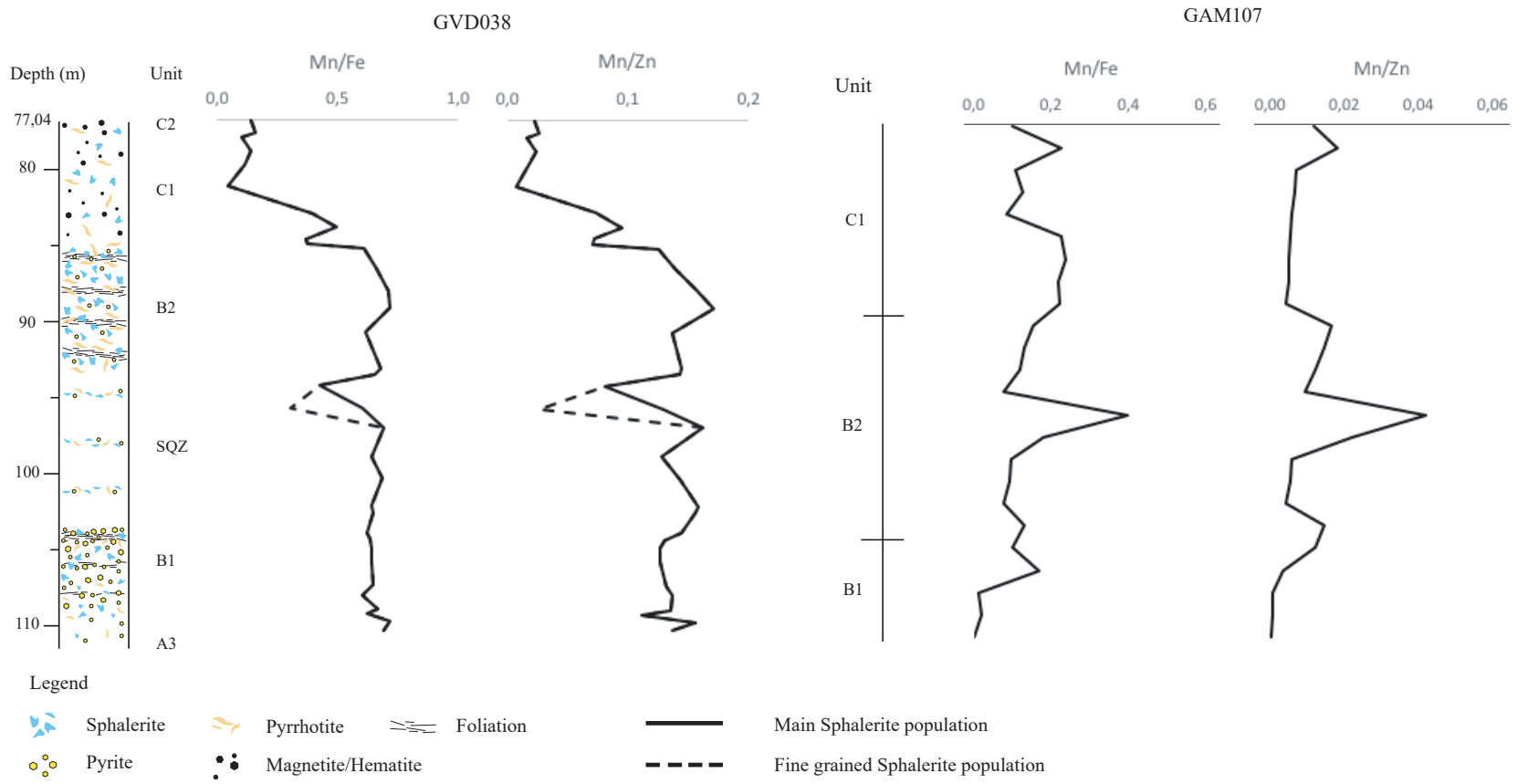

Figure 27: Sphalerite geochemical ratio profiles of Mn from the Gams Formation in the GVD038 and GAM107 drillholes against their respective stratigraphies.

The mean Zn content is higher in GAM107 (61.7 wt.%) than in GVD038 (49.8 w.t%). The highest concentrations come from the oxide-rich units (C1 and C2) for the two drillholes. The B1 unit from GAM107 presents significant Zn-high values which are not recorded in GVD038. The lowest values are recorded in the B2 unit for both drillholes. As expected, the Zn concentration shows an approximatively inverse relationship with Mn+Fe concentration due to closure effects. The combination of high zinc concentration in sphalerite and low Mn+Fe content suggest a propitious environment for mineral growth at minimal substitution by Fe and Mn. This environment typifies the upper units of the Gams Formation (C2 and C1). It is possible that the zinc enrichment in sphalerite in those units is not episodic but rather the expression of a shift in primary basin conditions promoting the development of other Fe/Mn-rich mineral phases such as silicates and oxides (encapsulated in the present assemblages as spessartine garnet and iron oxides), which preferentially took up the available Mn and Fe. This change of environmental conditions between the C1 and B2 units is noticeable in the geochemical profiles by an increase in the Zn concentration of section GAM107, whereas in drillcore GVD038 oxide-rich units show a gradational decrease. This inverse trend might be the result of a lateral primary variation in basin configuration.

The latter feature could also explain the pattern differences in the profiles recorded between GAM107 and GVD038. Indeed, Zn and Fe concentration profiles in section GAM107 show three types of data distribution broadly commensurate to the three main units of the Gams Formation. The contact between C1 and B2 is marked by an abrupt Zn decrease and a corresponding Fe increase while the contact between B2 and B1 presents a significant Zn increase associated with Fe decrease. This variability is not noticeable in GVD038 where the distribution of data is more invariant except for the gradational changes between the C1 and B2 units. Nonetheless, in GVD038 slight “spikes” are recorded in all profiles close to the interpreted boundaries between lithologic units, which may represent episodic changes in basin conditions.

A more focused comparison by lithologic unit is attempted for iron in Figure 28. The vertical iron distribution in the sphalerites of section GVD038 presents a largely invariant

concentration around 9-10 wt.% throughout the Gams Formation, whereas GAM107 displays values with high variability ranging from 1 to 7 wt.%. A variability within the same unit is noticeable in the B2 unit for GAM107 and is slightly visible in the B1 unit for GVD038. This information shows that the sphalerites from the West orebody are iron-enriched compared to the sphalerites from the North orebody, pointing to correspondingly diverse paleo-environmental conditions permitting diverse iron uptake over short distances.

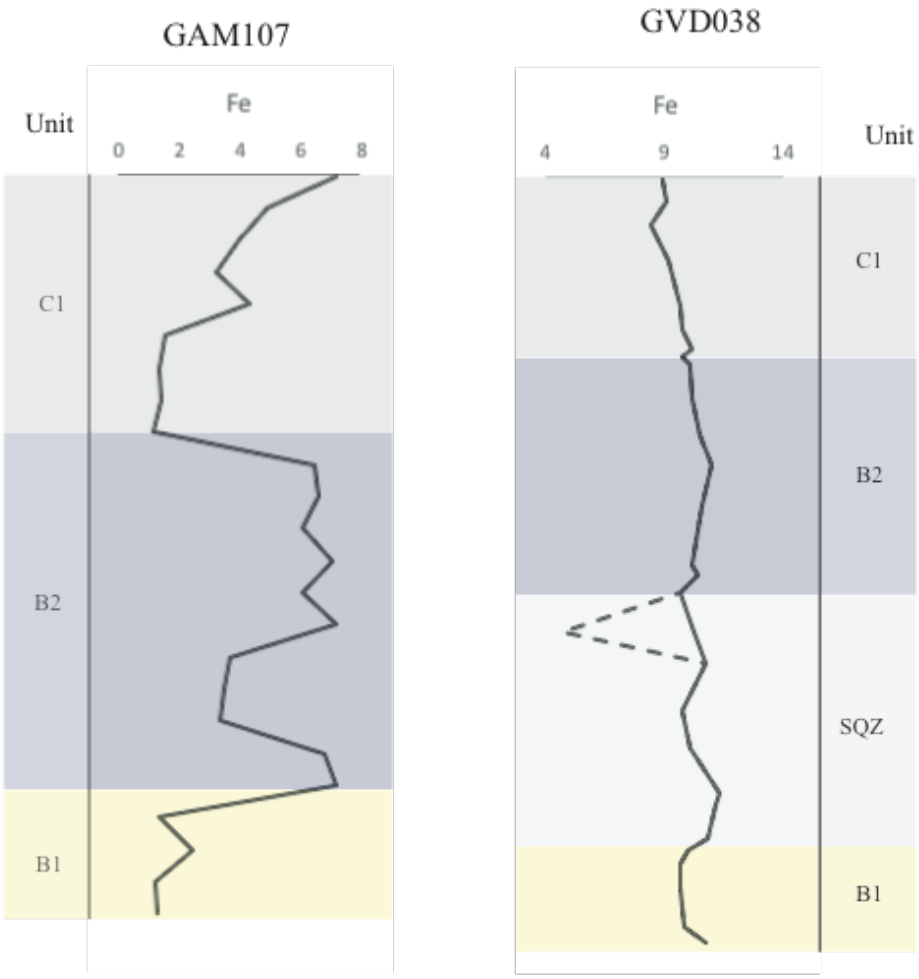

Figure 28: Comparison of iron distribution in sphalerite from GAM107 and GVD038 by unit. Data from C1 and A3 units have been removed from GVD038 for visualization purposes.

Similar to Figure 28, a comparison diagram of vertical distribution "geometry" is attempted in Figure 29 for sphalerite-hosted manganese between the two drillholes. Similarly to iron data, Mn concentration is clearly higher in GVD038 (mean concentration of 5.33 wt.%) comparatively to GAM107 Mn concentration (mean concentration of 0.57 wt.%).

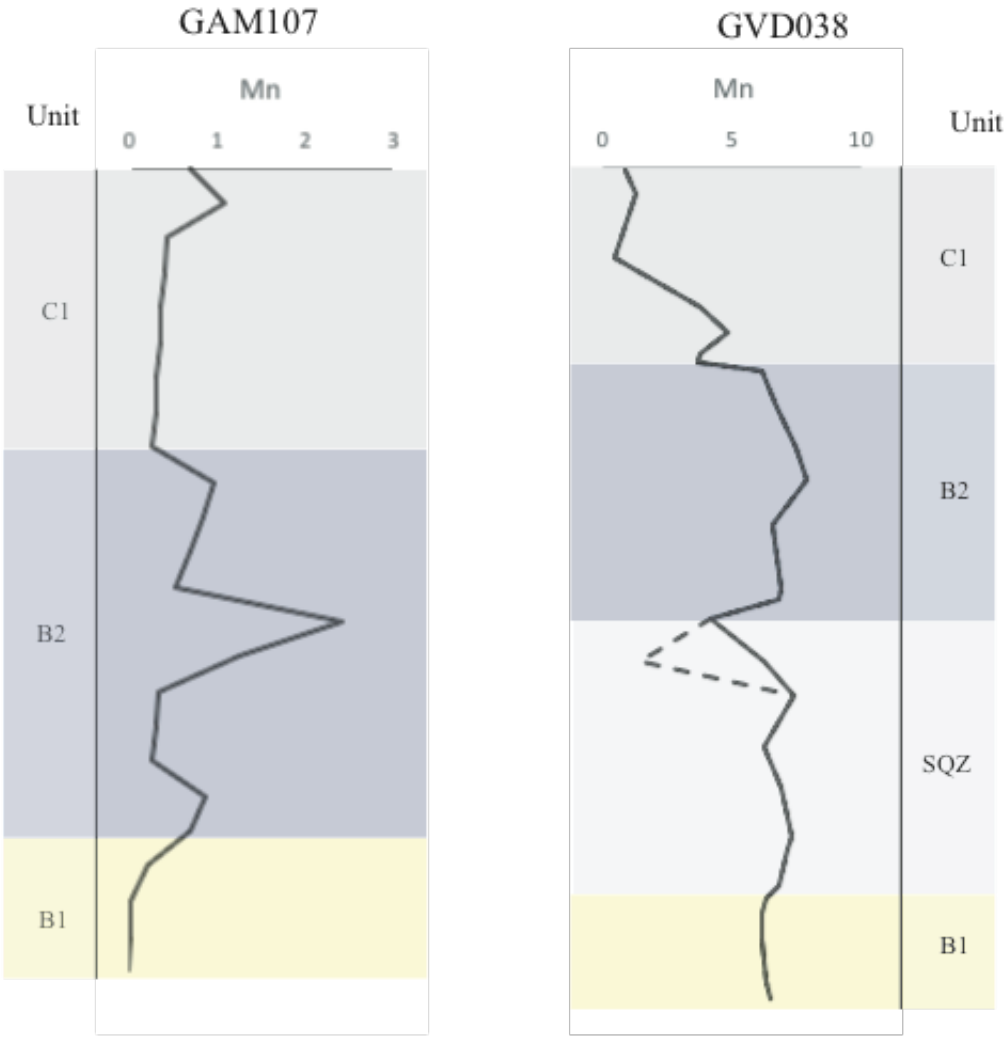

Figure 29: Comparison of manganese distribution in sphalerite from GAM107 and GVD038 by unit. Data from C1 and A3 units have been removed from GVD038 for visualization purposes.

The vertical manganese profile in GVD038 presents a gradational decrease in the oxide-rich units to the stratigraphic top and a broadly invariant distribution around 6.6 wt.% in the underlying units. In GAM107, manganese distribution of little fluctuation is recorded

with slight increases at the geochemical boundaries defined by Fe and Zn distributions mentioned previously. The highest detected manganese concentrations are both located in the B2 unit: 2.41 wt.% in GAM107 and 7.89 wt.% in GVD038. The high variability recorded in the iron distribution of GAM107 is not replicated in terms of manganese distribution, while GVD038 presents a wider range of Mn values (0.25 to 7.89 wt.%) by comparison to its narrow range of Fe values. Based on this data set, Mn-poor sphalerites from the North orebody could reflect a Mn-depleted initial environment contrasting to the West orebody where Mn-rich sphalerite formed in environmental conditions of clearly enhanced manganese availability.

The boundaries defining the contacts between the units in the previous figures (28 and 29) are based on logging interpretation of the corresponding lithological assemblages. Overall, the geochemical profile geometries are hard to reconcile qualitatively, as a result of data distribution and inherently different absolute values over most part of the examined sections. Perhaps a higher number of data and sections across the orebody could potentially reveal stratigraphic patterns of similarity. For example, the low-Mn sphalerite from the C1 units are predominant in GAM107 but only discernible in the upper part of the C1 unit from GVD038 (see Figure 29). Additionally, the slight increase in manganese in the B1 unit toward the top from GVD038 is clearer in the GAM107 B1 unit. This very broad correspondence between distinct qualitative elements of the profiles might be the expression of overall similar basinal conditions of primary chemogenic sulphide precipitation overprinted, for example, by variable degrees of siliciclastic input.

To this end, one obvious difference between the two drillholes is the presence of the intercalated quartzite in the B member of GVD038 which does not occur in GAM107. In the section of the Gams Formation presented by GVD038, this quartzite unit is located between the B1 and B2 units but it has been recorded to be mostly interbedded within the B1 unit in the South orebody (Stalder 2004). The quartzite holds a significant amount of sulfides represented by pyrrhotite, sphalerite, pyrite some galena and trace of alabandite. Sulfides are mostly concentrated in millimetre- to centimeter-scale sulfide-rich bands, or as very fine to fine-grained disseminated crystals. Sphalerites from the meso-banding are

coarser and display a geochemical signature relatively similar to the sphalerites recorded in the B member. On the contrary, disseminated sphalerites are by comparison impoverished in manganese and iron and thus enriched in zinc. Only one sample (34A) captured well the contact between sulfide-rich and sulfide-poor zones. The geochemical distinction was quantified and is represented on the result profiles as two populations of sphalerite (Figures 25, 27). In addition, the scatter plot distribution of Figure 30 displays effectively the two populations of sphalerite from the sulfidic-quartzite; the main sphalerite population is located with the bulk of the data while the fine-grained sphalerite population has a geochemical composition closer to the sphalerite from GAM107 and the C2 unit from GVD038, suggesting that basinal conditions during the primary deposition of those units could have been transiently similar.

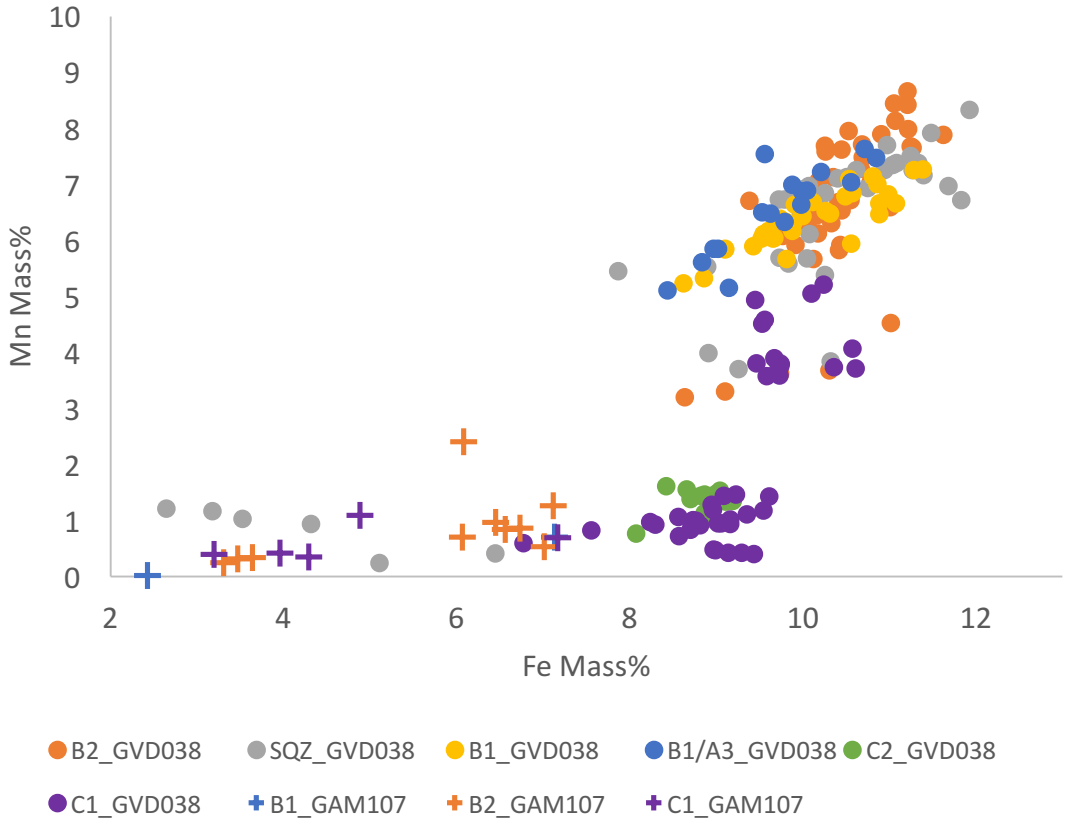

Figure 30: Scatter plot presenting the distribution of Mn in function of Fe in sphalerite from GVD038 and GAM107.

To enhance the visualization of the geochemical distribution displayed in Figure 27, the scatter plot of Mn as a function of Fe clearly reveals two populations of sphalerite. The **Mn-poor** sphalerites (0 to 2 w.t%) are represented by the upper units of the Gams Formation from GVD038 (C2 and partially C1 units), the fine-grained population of sphalerite from the SQZ unit and sphalerites from the GAM107 drillhole. In the same group, the sphalerite from C2 and C1 units are Fe-enriched and therefore closer to the second population. The latter is defined by its **Mn-rich** signature (3.5 to 8.5 wt.%) and comprises mainly sphalerite underlying the oxide-rich units in the Gams Formation from GVD038. In Figure 27, the transition from one population to the other is expressed by the increase in Mn/Fe ratio encountered at the gradational contact between the C1 and B2 units.

In summary, comparing the profiles from the GVD038 drillhole and the GAM107 drillhole reveals the following:

- The GAM107 section is richer in Zn and poorer in Mn+Fe contrasts with GVD038 richer in Mn+Fe and poorer in Zn.

- The GAM107 section presents relatively sharp geochemical changes corresponding to the contacts of interpreted lithologic units and has a higher vertical variability in the data.

- Section GVD038, by contrast, displays a more gradational transition between the oxide-rich and sulfide-rich units and the overall vertical profile shows far less variability of values.

- Finally, the sulfidic-quartztite in section GVD038 is absent from GAM107, but contains sphalerites with geochemical signature close to the sphalerites from GAM107.

The data presented by Moses (2015) investigates the manganese concentration in sulfides and more specifically alabandite and sphalerite from the East orebody. Sphalerite

analysis on the East orebody present similarities with the EPMA analysis from GVD038 (West orebody). Those similarities are particularly conspicuous via the geochemical distribution in sphalerites between the two orebodies and are displayed below in Figures 31, 32 and 33. Mn contents range from 1.5 to 8.5 wt.% with a higher density of values for Mn-rich sphalerite which is analogous to the geochemical signature of sphalerite from the West orebody. The Fe content has a normal distribution centered on 10.5 wt.%, and is thus slightly enriched compared to the distribution recorded at the West orebody (mean Fe content of 9.7 wt.%). Finally, the Zn content in sphalerite ranges from 46 to 57 wt.% with a higher density of values around 49 wt.% which is also very closely analogous to the West orebody sphalerite signature. The similar geochemical distributions of sphalerite from the East and West orebodies suggest an analogous environment with similar conditions of primary precipitation of the mineralization.

Adjacent to the investigation on sphalerites, some EPMA analysis have revealed the presence of coarse alabandite in the lower part of the B1 unit and in the A3 unit. The analysis performed on alabandite in this study present a homogeneous geochemistry (see Table 4). Alabandite analysis from the work of Moses (2015) revealed two populations based on their sulfur content. The limited number of analysis performed on alabandite in this study does not confirm or refute this.

Table 4: EPMA analysis from alabandite in GVD038.

Sample ID	S(Mass%)	Zn(Mass%)	Fe(Mass%)	Mn(Mass%)	Total(Mass%)
36A_1	36,72	0,00	5,66	56,63	99,00
44B_1	36,72	0,00	5,97	56,70	99,39
44B_5	36,82	0,00	5,74	56,74	99,30
44C_10	36,87	0,00	5,77	56,63	99,27
44C_11	36,76	0,00	5,27	57,29	99,32
44C_4	36,62	0,00	5,72	57,18	99,52
44C_6	36,66	0,00	5,98	56,38	99,02
44C_9	36,80	0,05	5,86	56,92	99,63
Mean	**36,75**	**0,01**	**5,75**	**56,81**	**99,31**
St Dev	**0,09**	**0,02**	**0,22**	**0,30**	**0,22**

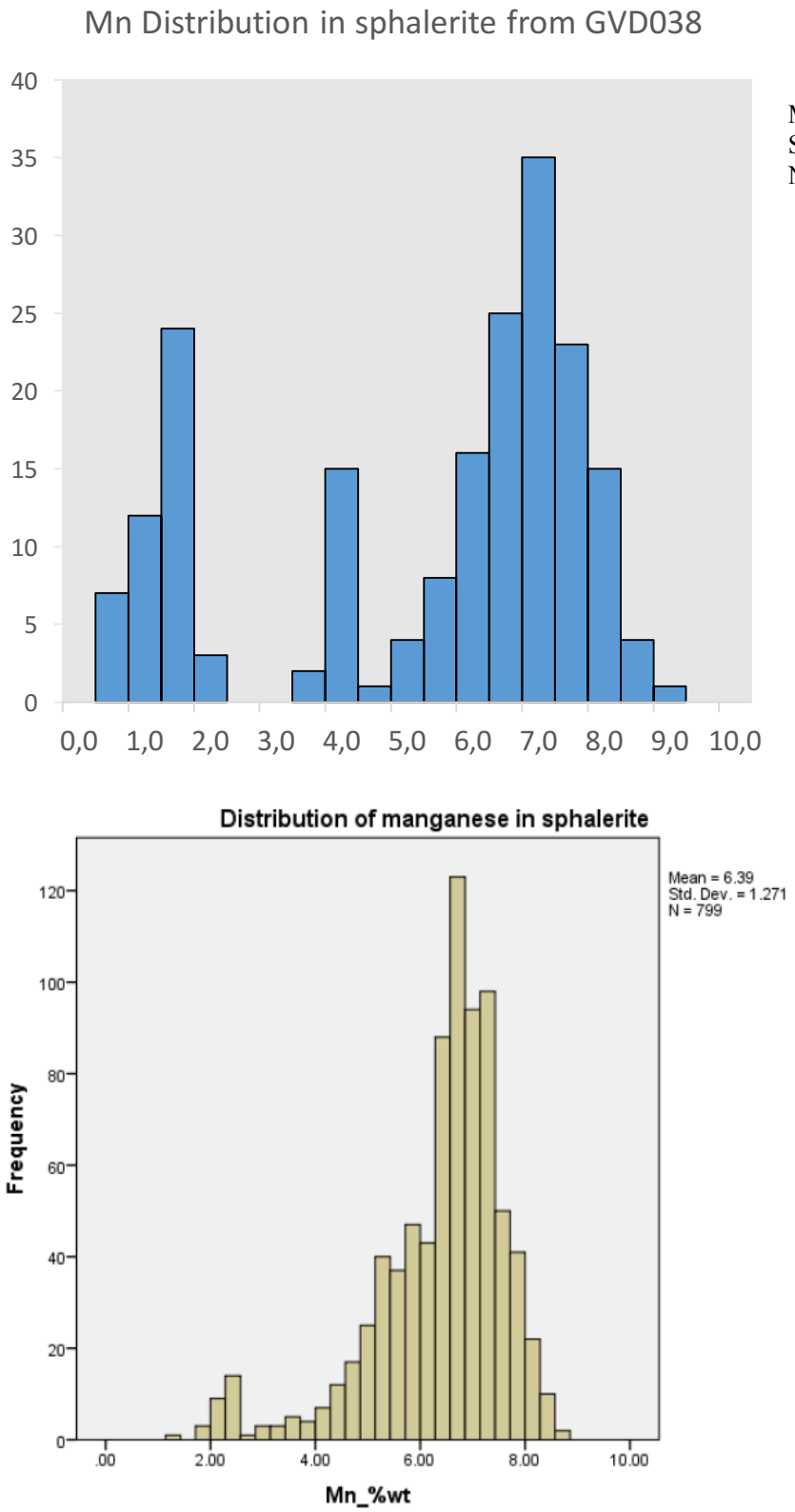

Figure 31: Histograms presenting manganese distribution in sphalerite from the West orebody (this study) and the East orebody (Moses 2015).

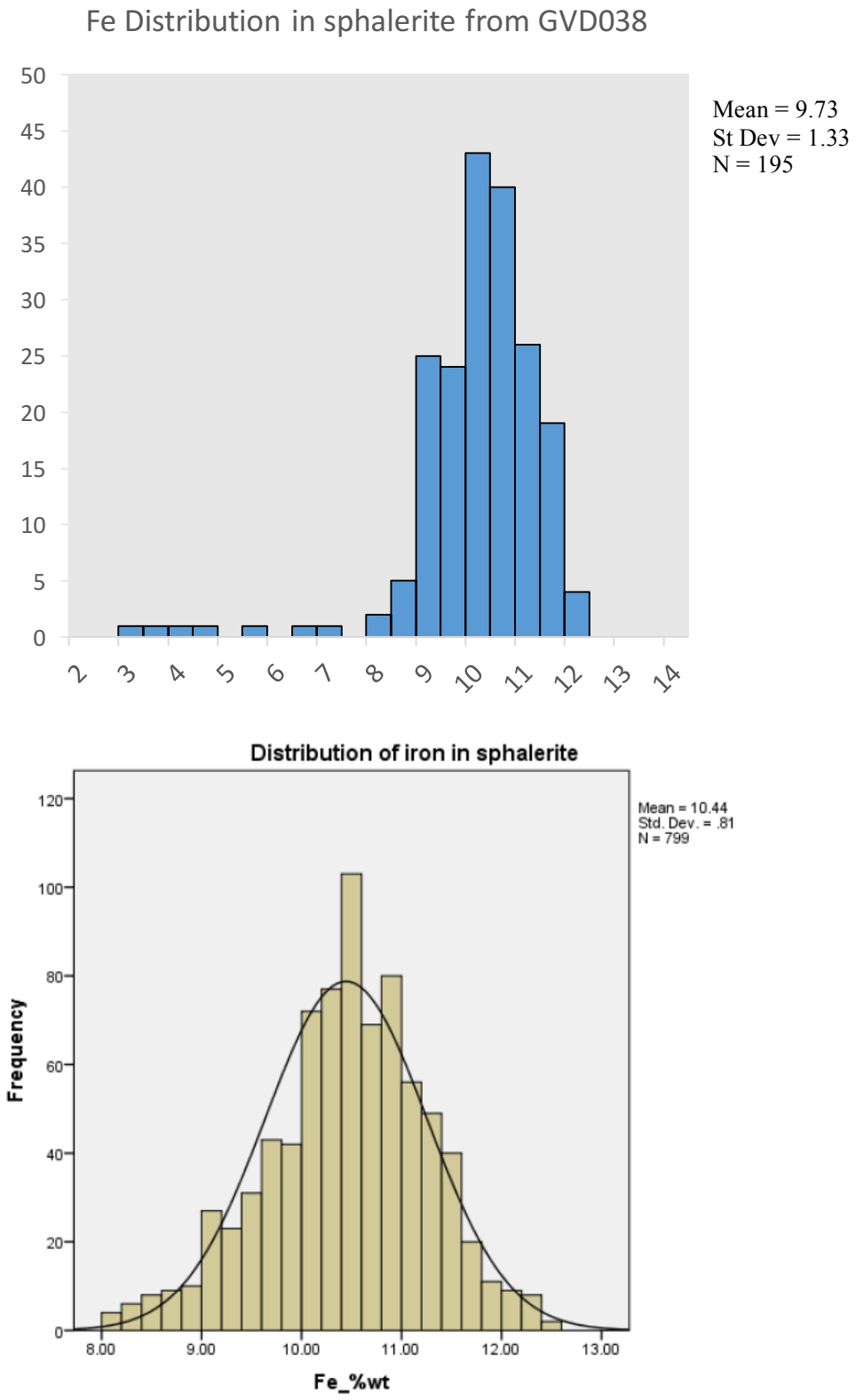

Figure 32: Histograms presenting iron distribution in sphalerite from the West orebody (this study) and the East orebody (Moses 2015).

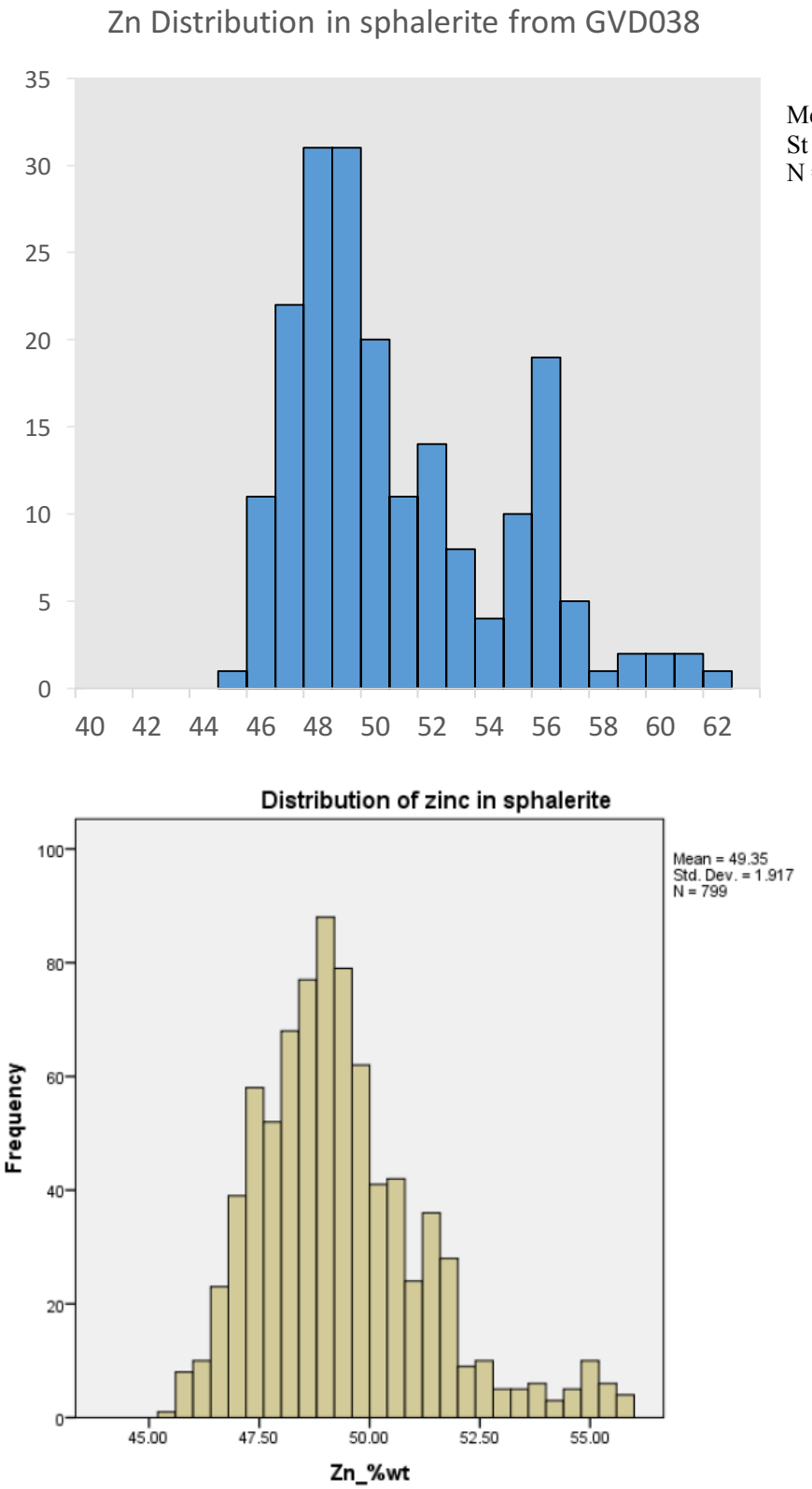

Figure 33: Histograms presenting zinc distribution in sphalerite from the West orebody (this study) and the East orebody (Moses 2015).

6 SYNTHESIS

This section provides a comprehensive summary of proposed genetic processes which formed the Aggeneys-Gamsberg mining district and more specifically the Gamsberg zinc deposit. The information collected during this study is then incorporated into the models to reinforce the understanding of the primary environmental setting.

6.1 CURRENT GENETIC MODELS

A regional-scale genetic model interpreting the formation of the four base metal deposits mineralization of the studied area has been suggested by McClung (2006). The author interprets the selection of lithologies from the Aggeneys-Gamsberg district (graphitic and pyritic units, metaconglomerates, carbonates lenses) to have been developed in secondary and tertiary basins in an intracontinental rift system. The accepted concept of enrichment for SEDEX deposits via metal-bearing brines (see Section 2) is used to introduced Fe and Mn into those basins with low clastic sediment input. This model constrained the hydrothermal fluid conditions to low-temperature (<250°C), buoyant Fe/Mn-rich brines, mixing with the seawater column to finally precipitate as Fe-Mn-rich rocks and hydrothermal sediments (massive barite, tourmalinites, massive sillimanite, massive sulfide bodies, quartz-magnetite rocks, base metal-rich silicates). Based on REE patterns from Fe-Mn-rich rocks, the author suggests a syn-diagenetic hydrothermal alteration caused by acidic, saline, hot (>250°C), crustally derived, metal-rich fluids which developed the mineralized horizons. The infiltrating fluids do not bear the same geochemical signature resulting in the regional zonation observable from west to east (Ryan et al 1986). The last stage of the genetic model proposes a later mobilization of Fe, Na, Ca and Cu introduced by metamorphic fluids derived from prograde metamorphism during the Namaquan Orogeny, and possibly by magmatic fluids derived from the intrusion of the Little Namaqualand suite.

The genetic model proposed by Stalder (2004) gives a closer look on basin development of the Gamsberg deposit comparatively to the broader picture painted in the previous

genetic model. The tectonic settings are similar, with a regional rift system of active normal faulting which led to the development of the main basin with secondary and tertiary basins. It is in the latter basins where particular units were deposited, such as the metapelitic schist, the quartzite and the Gams Formation. With respect to the latter, the author subdivided the basin development in four stages: before activation of tectonic extension, marine deposition was dominated by stable chemical sedimentation developing the A2 and A3 units overlying the intact continental basement (Figure 34). The rift triggered the development of the basin resulting in additional clastic material influx and the formation of the A4 unit (Figure 34). Due to tectonic pressures and constant clastic supply from the southern source, the basin grew into an asymmetric depocenter; shallow nearby the sedimentary source while deeper further away. The main basinal phase is marked by a decrease in vertical circulation in the restricted basin which eventually turned marine conditions into an anoxic environment. The latter mixed with hydrothermal fluids infiltrated through the normal faults or by migration on the seafloor supported the deposition of iron sulfides and sphalerite associated with clastic material forming the B1 unit (Figure 35). In the overlying stratigraphy, the apatite nodule horizon is explained by a change of conditions toward a suboxic environment. Additional mixing of hydrothermal brines with the suboxic basin precipitated elements remaining in solution (Mn, Ba and P) as base metal sulfides and oxides to form the B2 units. The basin gradually evolved into an oxic environment promoting the development of oxide-rich unit C1 and C2. Brines were subsequently discharged of their metals and the ore forming processes terminated.

The above model is not devoid of weaknesses. The Hoogoor Gneiss represents a small reservoir for metal-bearing fluids compared to classic SEDEX deposits. Based on geochronology, Baillie and others (2007a, 2007b) also stressed that the granitic gneisses cannot have been a potential source of base metals for district-wide mineralization. Finally, even if S-isotopes of barite may indicate evaporitic origin (Stalder and Rozendal 2005) the presumed lack of evaporites in the sequence is noted.

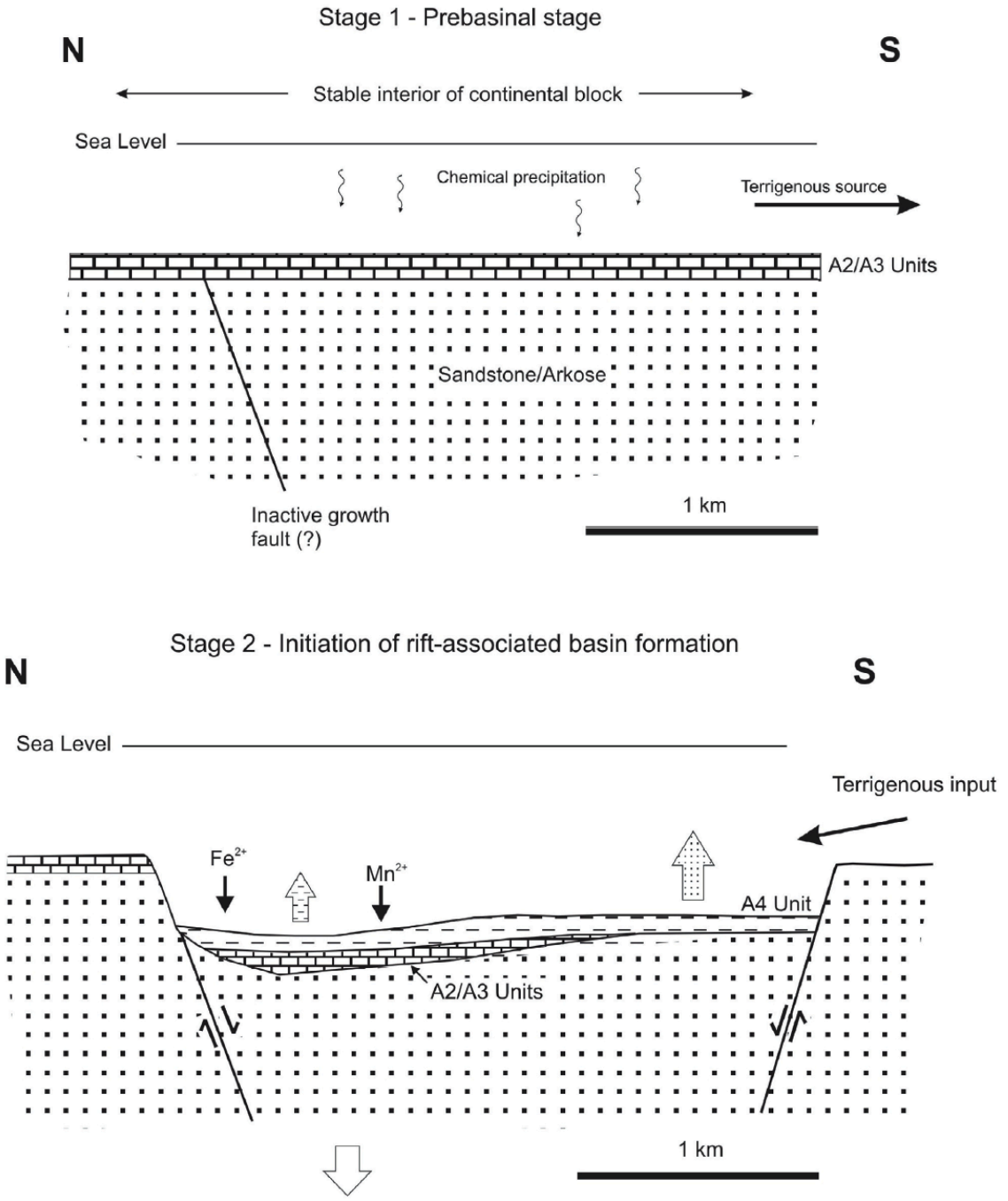

Figure 34: Genetic models representing the first stages of development of the Gamsberg basin. Stage 1 presents the original intact continental basement while Stage 2 shows the changes after initiation of expansion. Dotted and dashed arrows represent coarse- and fine-grained clastic sedimentation, respectively. Downward open arrow represents subsidence. (adapted from Stalder 2004).

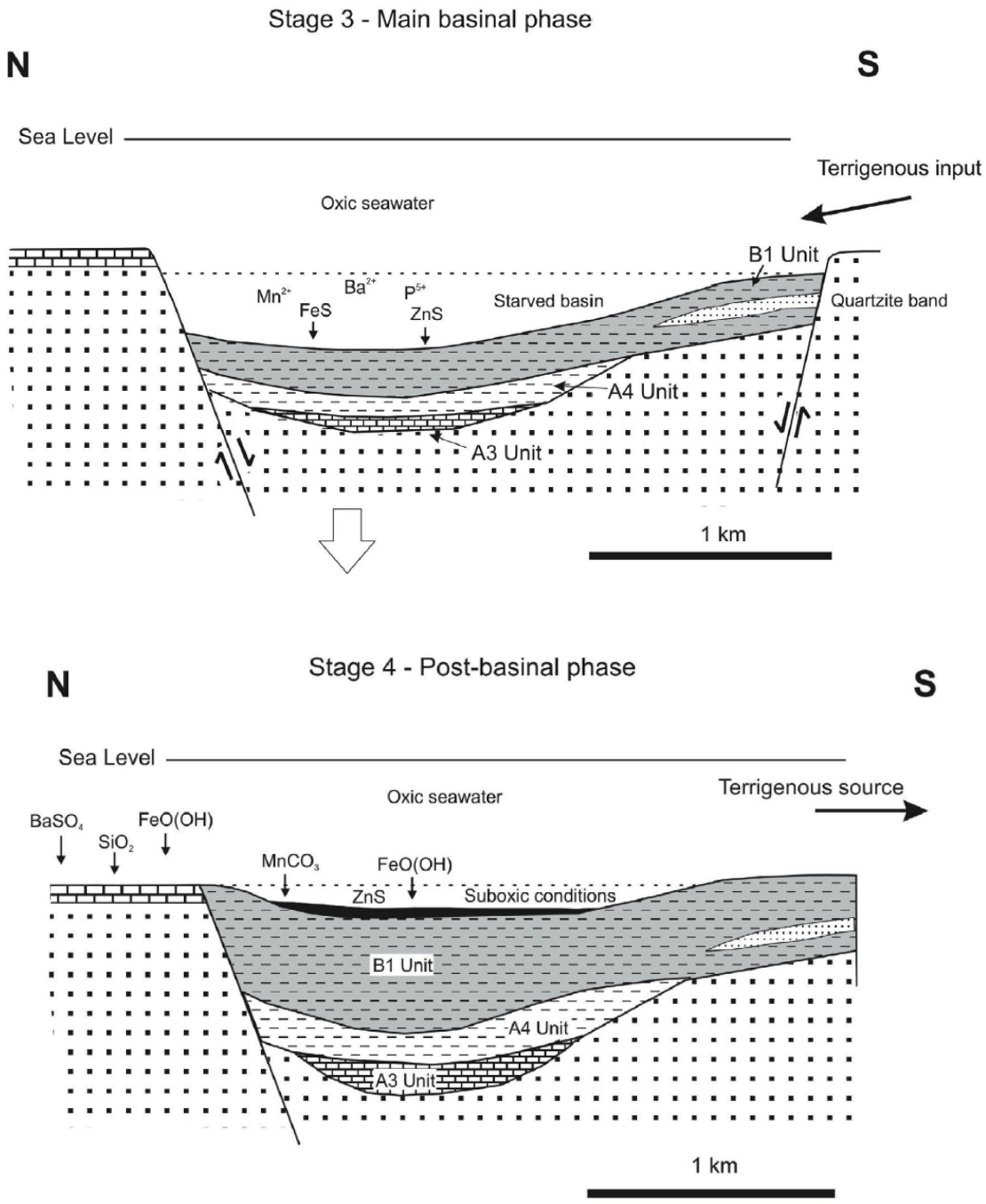

Figure 35: Genetic models representing latter stages of the Gamsberg basin development. Stage 3 displays the precipitation of sulfides contemporary with clastic sediments and the remaining of Mn, Ba and P in solution. Stage 4 is marked by the shift from a suboxic basin (predominated by sphalerite, Mn- and Fe-rich rocks) to an oxic basin (predominated by Fe oxyhydroxides, chert and barite). Downward open arrow represents subsidence (adapted from Stalder 2004).

These factors generally point to insufficient understanding of the ultimate metal source. An adjustment of the genetic model includes deep-seated magmas and amphibolites as heat source driving meteoric and/or connate fluid flow to leach metals from the granitic gneisses, and/or as the primary source of magmatic-derived brines which enriched the existing hydrothermal fluids in the granitic gneisses.

6.1 CONSTRAINTS OF THIS STUDY

This section aims to adapt the previous genetic models to incorporate the high variability in Zn, Fe and Mn concentrations in sphalerite throughout the Gamsberg deposit and within the different units of the Gams Formation discovered during this study.

The substitution of elements in crystal lattice of minerals is governed by three environmental factors: the abundance of the equal size substitutive elements, temperature and pressure. In the present case, pressure is not a prominent factor, as quasi-constant low pressure conditions are expected from the submerged basinal environment during precipitation. Temperature seems like a more influential factor, as an increase in ambient temperature would enhance the substitution process. Hot brines infiltrating the seafloor are already part of the genetic model precipitating the mineralization of the Gams Formation. A potential source of temperature increase introducing hotter fluids could be the presence of a deep-seated magmatic body heating and driving convective fluid-flow upward to the seafloor. Deer and others (1962) questioned the influence of temperature since equilibrium is generally not attained but suspected the original composition of the source as the main factor for minor elements distribution. Therefore, the abundance of iron and manganese in solution during the precipitation of the Gams Formation units is certainly a crucial factor to the Mn+Fe enrichment or depletion in sphalerite.

To identify the source of iron and manganese, several lithological and geochemical components influencing the composition of the basin are taken in consideration. In a context of rifting, the **sedimentary input** bringing the clastic material dictate the lithological composition of the sedimentary sequences. Moreover, the intensity and

orientation of terrigenous sedimentary input influence the overall volume and thickness of the various stratigraphic units, and it is in turn influenced by the geomorphology of the basin. Considering the terrigenous input coming from the south in Stalder's (2004) model, the asymmetric depocenter being deeper away from the source may suggest that iron and manganese were brought by the sedimentary input and were incorporated in sphalerite lattice closer to the source rather than in sphalerite from the northern part of the basin. Therefore, the distance from the clastic source could have had an impact on the variation of sphalerite geochemistry. Indeed, during intensive terrigenous influx, areas of the basin closer to the source will most likely present metal depleted rocks comparatively to areas distanced from the source. The exclusive occurrence of the intercalated quartzite in the South and West orebodies can potentially be the expression of an intensive clastic material import.

The meso-banding characterizing the sulfidic-quartzite would thus be the result of intermittent clastic input episodes. During intensive clastic influx, the dense terrigenous material mixed with the ambient metal-rich submerged basin resulted in perturbations of ore mineral precipitation and was probably accompanied by a decrease in temperature. This would have resulted in the formation of very fine to fine-grained disseminated sulfides enriched in zinc and depleted in more mobile elements remaining in solution (Mn and Fe). During periods of low clastic influx, the stable conditions allowed the metal-rich bottom environment to precipitate ore minerals in the sediment pores, with coarse Mn- and Fe-enriched sphalerite and other sulfides developing into sulfide-rich bands in the quartzite.

Nonetheless, the primary source of iron and manganese being from terrigenous sediment input is unlikely. Indeed, it would first of all assume the primary erosion of a Mn- and Fe-rich geological body. Furthermore, the distribution of Mn- and Fe-bearing minerals (i.e. spessartine, alabandite, manganoan-carbonate) in the Gams Formation is not exclusively restricted to the West, East or South orebodies but recorded throughout the whole deposit which suggest an overall distribution of iron and manganese from a lithological point of view. It seems more likely that non-detrital geochemical factors are responsible for the distribution of iron and manganese in sphalerite.

Metal-bearing hot brines leading to Zn+Pb minearalisation are a far more appealing source for iron and manganese. It is reasonable to assume that if saline, acidic hot fluids leached gneisses for zinc, the enrichment in the fluid of other soluble metallic elements as chlorides such as manganese and iron is most probable. Enriched fluids in Zn, Fe and Mn ascending via normal faults, would have discharged their metals in the basin and caused the precipitation as key component of the Gams Formation.

One mineralization process forming vent-distal SEDEX-deposits suggests that "bottom-hugging" fluids would discharge onto the seafloor as a metal-rich plume and mix with the primitive permeable clastic sediments to precipitate ore minerals (Sangster 2002). The manganese concentrations are typically increasing away from the vent-complex. In this scenario, the distance from the vent-complex could have had major importance considering mobility contrasts between Zn, Fe and Mn in solution. As metal-rich fluids migrated on the seafloor and deposited the mineralized horizon, a large scale zonation would have developed with Zn/Mn+Fe ratios decreasing away from the vent-complex. This would imply that the North orebody (GAM107) was closer to the vent-complex than the West (GVD038) and East orebodies. Still, with the introduction of "bottom-hugging" fluids it remains difficult to explain that the occurrence of manganese is detected right through the mineralogy of the Gams Formation units while Mn-rich sphalerite is only seen away from the vent-complex.

The other component influencing the geochemistry of the minerals in the basin is the **environmental conditions of the basin** itself. The different mineralogical package of the A, B and C members of the Gams Formation has been interpreted as a transition of the basin condition from a reduced, to suboxic and finally to an oxic environment, respectively (Stalder 2004). However, this shift in seawater conditions is not sufficient to explain the enrichment in zinc and manganese of the Gams Formation. The occurrence of alabandite (MnS) at the gradational contact between the A3 and B1 unit, commonly absent in most natural environments (Roy 2006), is evidence of unusually very reducing conditions. The introduction of reduced, metal-bearing hot brines mixing with the ambient anoxic water column could explain the formation of alabandite and the onset of the mineralization event.

To resolve the variability in sphalerite geochemistry throughout the deposit, additional features are included in the genetic model. Coupled with the transition of environmental conditions, the anoxic basin would have developed a chemocline after mixing with the hot brines. This would have led to a geochemical stratification of the water column displaying Mn-enrichment in the deeper reduced zones contrasting with a shallower Mn-depleted zone (Figure 36). This interpretation is based on the manganese behavior requiring reduced conditions to remain in solution. Additionally, it is suggested that the geometry of the basin was such that Mn-rich sphalerite may have formed in relatively deeper parts (topographic lows) while Mn-poor sphalerite precipitated in topographic highs with respect to the ambient chemocline. The end product is the repartition of different orebodies with distinct geochemical profiles. A broadly similar interpretation was previously suggested to genetically explain the presence of alabandite in the East orebody (Moses 2015). The suggested geometry of the primitive basin is fundamentally different from the asymmetric depocenter with higher topography in the southern part of the basin proposed by Stalder's model (2004). To be coherent with the sedimentary input coming from the south an element of subsidence in the gneissic basement was included in the model.

Even if iron and manganese are closely associated because of similar affinities in variable redox conditions, in the present study the distribution of the two elements is in itself informative. This is especially observable in the data from the the North orebody where the iron variability is significantly higher than that of manganese. The fact that iron and manganese do not have similar responses in the same environment may be explained by the flexibility of iron to be incorporated into a discrete mineral phase (iron sulfides, iron oxides, Fe-rich silicates, etc) comparatively to manganese which is less compliant at least to sulphides. In the West orebody the geochemical profiles of the two elements follow the same trend except for a steeper decrease in manganese concentration in sphalerite from the C member. It is thought that oxic conditions supported the incorporation of manganese in the trivalent state in silicates rather than sulfides. This is consistent with the higher manganese content in silicates recorded in the top of the Gams Formation (Stalder 2004, Foulkes 2015) and with the Mn-poor character of sphalerite in the same units, and not so consistent with the asymmetric basin drawn in the current model (Stalder 2004).

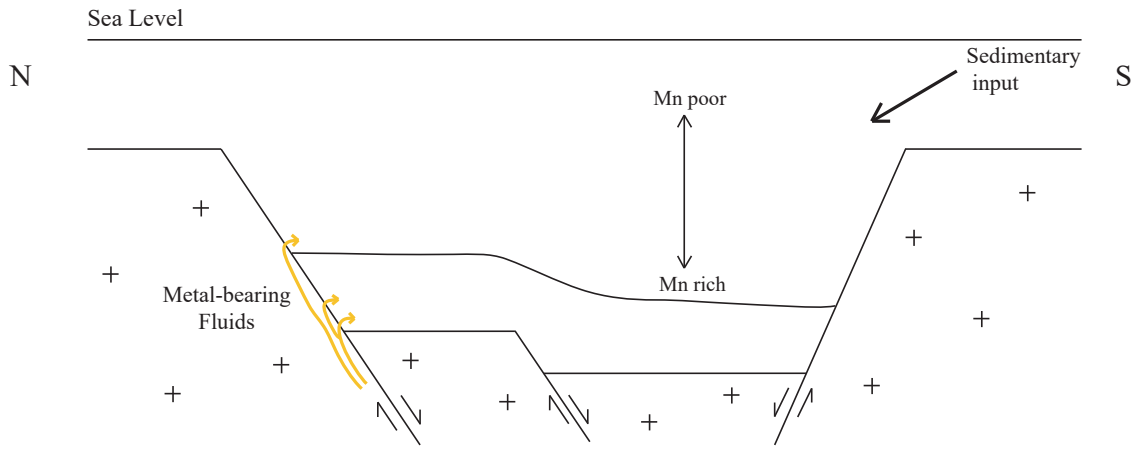

Figure 36: Simplified genetic model of the Gamsberg basin.

Finally, the polyphase **metamorphism** which affected the Gamsberg deposit might have contributed to the manganese enrichment of the Gams Formation. Manganese in SEDEX deposits is commonly hosted in Mn-rich carbonate as an alteration halo around the mineralization (Emsbo 2010, Large et al 2002, Leach et al 2005). This feature seems to be recorded well at Gamsberg with the Mn+Fe-rich rocks enveloping the Gams Formation (Stalder 2004). The petrography of the Gams Formation (see Section 4) shows that every unit discloses significant alteration features such as remobilization and recrystallization textures. It would thus not be implausible to assume that polyphase metamorphism has, at least to some degree remobilized manganese from the surrounding rocks to concentrate manganese in ductile sulfide phases, in this case sphalerite. This, however, does not comply with the large difference in Mn abundance in sphalerite over short distances (i.e. between the North and West orebodies), which must be controlled to a large degree by pre-metamorphic processes of Mn uptake by Zn sulphide.

7 CONCLUSIONS

7.1 SUMMARY OF RESULTS

The Gamsberg deposit is subdivided into four orebodies (North, South, West and East) and the eastern Overturned Limb which is enriched in Ba. Based on the investigation of sphalerite from a drillhole localized in the West orebody, this study identified the main units of the economic Gams Formation: lower manganoan-carbonate-garnet-rich rocks composing the A3 unit; overlying this is the pyritic metapelitic B1 unit. A quartzite characterized by mesobands of sulfides separates B1 unit from the upper pyrrhotitic metapelitic B2 unit. The overlying C1 and C2 units are enriched in iron oxides and gradually depleted in base metal sulfides with stratigraphic height. The core of the Gams Formation (B1, B2 and C1) represents the economic layers. Microscopic petrography of the enriched-zones shows a recurrent simple sulfide package (sphalerite, pyrrhotite, pyrite and galena) associated with quartz and garnet and secondary amphibole, pyroxene and mica. Primary textures have been overprinted by polyphase metamorphic ones which left recrystallization, replacement, breccia, and deformational textures as main microscopic features. EPMA analyses revealed that sphalerite grains are in most cases enriched in iron and manganese. Geochemical profiles permit the visualization of the distribution of sphalerite as a function of mineral chemical composition. Mn+Fe-rich sphalerite is localized in the lower units of the Gams Formation (A3, B1, SQZ and B2) while sphalerite from the overlying C1 and C2 records a progressive depletion in the concentration of Mn+Fe. This signature is interpreted as a shift in basin conditions resulting in the development of other primary mineral phases taking up Mn and Fe as trivalent species, thus limiting the substitution of Mn^{2+} and Fe^{2+} in sphalerites. The geochemical profiles were also compared with sphalerite data from the North and East orebodies: analogous signals are clear with the East orebody whereas the North orebody presents different geochemical patterns. Changes are detected in the overall Zn, Mn and Fe concentration and between units; those differences have been interpreted as the result of geomorphological and environmental controls variation within the primary basin in which the Gams Formation developed. Deep, relatively more Mn-rich reduced waters and Mn-poor shallow

waters define the chemocline of the basin. This feature is coupled with a variation in basin topography, namely higher in the northern part than in the southern part, which therefore produced the variation in geochemistry of sphalerite recorded in the different orebodies.

7.2 RECOMMENDATIONS FOR FUTURE WORK

This study reveals the existence of a lateral discontinuity in the basin development reflected by geochemical variations throughout the same units of the metal-bearing Gams Formation. One obvious extension of this study would be to investigate an increased number of drillholes covering the Gams Formation in the four orebodies of the deposit. This refinement would provide essential information on Zn and lateral variation in Mn+Fe concentration which could be used to categorise different ore grades and the host lithofacies. An advanced study could produce a detailed map characterizing the geochemical distribution of Fe and Mn in the Gams Formation throughout the deposit. Of utmost importance here is the thorough understanding of the lateral and vertical distribution of Fe and Mn in a mineral-specific context, i.e. not just in the sulphide fraction but in all mineral phases present, which requires advanced speciation methodology. This would help define the variety of basin conditions in which the different orebodies and associated lithofacies developed. A genetic reconstruction of the formation of the entire basin and its contained sediments could then become possible, and this would naturally permit consideration of potential extensions of this system beyond the Aggeneys-Gamsberg District and the possible discovery of new mineralisation further afield.

Another feature which has not been discussed much in this study but has tremendous potential to shed light on the origin of the Gamsberg deposit is the regional sulfur isotope pattern in sulphides and sulphate (barite) as detected in the Aggeneys-Gamsberg mining district (Foulkes 2015). Whereas the source of sulfur in the four base metal deposits is not thoroughly understood, i.e. whether it is carried with the hydrothermal fluid or is available in the ambient water column, the distinct sulfur isotope variation in space from low $\delta^{34}S$ at Aggeneys to high $\delta^{34}S$ at Gamsberg, may point to either a single evolving mineralising system with distance from the hydrothermal source, or the punctuated development of

discrete SEDEX deposits through time against a common isotopically evolving sulphur source. The possible deposition of SEDEX mineralisation diachronously has profound implications with respect to understanding the placement of the Gamsberg deposit in the entire Aggeneys-Gamsberg District. So far, the Gamsberg deposit has been thought of as the latteral termination, i.e. the “tail” of a broader system of SEDEX mineralisation. If it is SEDEX deposit in its own right (albeit a metamorphosed one), then the possibility emerges that it may not be the last one to be found and exploited. Additional investigation on sulfur isotopes currently being carried out on the same sample set by the Rhodes Research group, could hold the key in understanding SEDEX ore formation in the Aggeneys-Gamsberg District and environs.

REFERENCE LIST

- Bailie, R. Armstrong, R. and Reid, D. (2007a) The Bushmanland Group supracrustal succession, Aggeneys, Bushmanland, South Africa: Provenance, age of deposition and metamorphism. *South African Journal of Geology*, 110, p. 59-86.
- Bailie, R. Armstrong, R. Reid, D. (2007b) Composition and single zircon U-Pb emplacement and metamorphic ages of the Aggeneys Granite Suite, Bushmanland, South-Africa. *South African Journal of Geology*, 110, p. 87-110.
- Carne, R.C. and Cathro, R.J. (1982) Sedimentary exhalative (sedex) zinc-lead-silver deposits, northern Canadian Cordillera. *Canadian Institute of Mining Bulletin*, 75, p. 66-78.
- Cook, N.J. Ciobanu, C.L. Pring, A. Skinner, W. Shimizu, M. Danyushevsky, L. Saini-Eidukat, B. Melcher, F. (2009) Trace and minor elements in sphalerite: A LA-ICPMS study. *Geochimica et Cosmochimica Acta 73,* 4761-4791.
- Cooke, D.R. Bull, S.W. Large, R.R. McGoldrick, P.J. (2000) The Importance of oxidized brines for the formation of Australian Proterozoic stratiform sediment-hosted Pb-Zn (Sedex) deposits. *Economic Geology*, 95, p. 18.
- Cornell, D.H., Thomas, R.J., Moen, H.F.G., Reid, D.L., Moore, J.M. and Gibson, R.L. (2006) The Namaqua-Natal Province. *In*: Johnson, M.R. Anhaeusser, C.R. and Thomas, R.J. (Eds.), The Geology of South Africa. *Geological Society of South Africa, Johannesburg and The Council for Geoscience, Pretoria*, p. 325-379.
- Deer, W.A. Howie, R.A. Zussman, J. (1962) Sphalerite. *In: Longman Group Ltd* (Eds.) Rock Forming minerals. Vol.5 Non-Silicates. *London*, p. 166-179.
- Dewey, J.F. Robb, L. Van Schalkyck, L. (2006) Did Bushmanland extensionally unroof Namaqualand? *Precambrian Research*, 150, p. 173-182.
- Du Toit M.C. (1998) Zinc. *In:* Wilson M.G.C. and Anhaeusser C.R (Eds) The Mineral Resources of South Africa: Handbook, *Council for Geoscience*, 16, p. 676-681.
- Emsbo, P. (2009) Geologic Criteria for the Assessment of Sedimentary Exhalative (Sedex) Zn-Pb-Ag Deposits. *Open-File Report 2009-1209, USGS,* p. 25.
- Emsbo, P. Seal, R.R. Breit, G.N. Diehl, S.F. Shah, A.K. (2010) Sedimentary Exhalative (Sedex) Zinc-Lead-Silver Deposit Model. *In: Mineral Deposit Models for Resource Assessment, Scientific Inverstigations Report 2010-5070-N, USGS,* p. 72.
- Foulkes, S.E. (2015) New geochemical constraints on the genesis of the Gamsberg zinc deposit, Namaqualand Metamorphic Province, South Africa. *MSc thesis (published), Rhodes University,* p. 172.
- Gottesmann, W. Gottesmann, B. and Seifert W. (2009) Sphalerite composition and ore genesis at the Tumurtjin-ovoo Fe–Mn–Zn skarn deposit, Mongolia. *Neues Jahrbuch für Mineralogie Abhandlungen Journal of Mineralogy and Geochemistry*. 185, 249–280.

- Graeser S. (1969) Minor elements in sphalerite and galena from Binnatal. *Contributions to Mineralogy and Petrology*. 24, 156–163.
- Holland H.D. (2005) Sedimentary mineral deposits and the evolution of Earth's near-surface environments. *Economic Geology, 100th Anniversary Special Paper,* 100, p. 1489-1509.
- Huston, D.L. Stevens, B. Southgate, P.N. Muhling, P. Wyborn, L. (2006) Australian Zn-Pb-Ag ore-forming systems: a review and analysis. *Economic Geology*, 101, p. 1117-1157.
- Jébrak, M. and Marcoux, E. (2008) Géologie des ressources minérals. *Ministère des Ressources naturelles et de la Faune, Québec,* p. 685.
- Joubert, P. (1971) The regional tectonism of the gneisses of part of the Namaqualand. *Bulletin of the Precambrian Research Unit, University of Cape Town*, 10, p. 220.
- Joubert, P. (1972) Geological survey of part of Namaqualand and Bushmanland. *Bulletin of the Precambrian Research Unit, University of Cape Town,* 7-9, p. 4-11.
- Joubert, P. (1974) The gneisses of Namaqualand and their deformation. *Transactions of the Geological Society of South Africa*, 77, p. 339-346.
- Joubert P. (1986) The Namaqualand Metamorphic Complex - A Summary. *In*: Anhaeusser, C.R. and Maske, S. (Eds.) Mineral Deposits of Southern Africa, p. 1395-1420 Vol II.
- Large, R. Bodon, S. Davidson, G. and Cooke, D. (1996) The chemistry of BHT ore formation - one of the keys to understanding the differences between SEDEX and BHT deposits. *In:* Pongratz, J. and Davidson, G. (Eds.) New developments in Broken Hill Type deposits, *Proceedings of a workshop on "New Developments in Broken Hill Type Deposits" CODES, University of Tasmania, July 1996*, Special Publication 1, p. 105-111.
- Large, R.R. Bull, S.W. Yang, J. Cooke, D.R. Garven, G. McGoldrick, P.J. and Selley, D. (2002) Controls on the formation of giant stratiform sediment- hosted Zn-Pb-Ag deposits with particular reference to the north Australian Proterozoic. *University of Tasmania, Centre for Special Ore Deposit and Exploration (CODES) Studies Publication* 4, p. 107−149.
- Large, R.R., Bull, S.W., McGoldrick, P.J., Derrick, G., Carr, G., and Walters,S. (2005) Stratiform and strata-bound Zn-Pb-Ag deposits of the Proterozoic sedimentary basins of northern Australia. *Economic Geologic 100th Anniversary Volume*, p. 931−963.
- Leach, D.L. Sangster, D.F. Kelley, K. D. Large, R. R. Garven, G. Allen, C.R. Gutzmer, J. and Walters, S. (2005) Sediment-hosted lead-zinc deposits: A global perspective. *Economic Geologic 100th Anniversary Volume*, p.561−608.
- Leach, D.L. Bradley, D.C. Huston, D. Pisarevsky, S.A. Taylor R.D. Gardoll, S.J. (2010) Sediment-hosted lead-zinc deposits in Earth history. *Economic Geology*, 105, p. 593-625.
- Lydon, J.W. (1996) Gîtes de sulfures exhalatifs dans des roches sédimentaires (gîtes SEDEX). *In:* Eckstrand, O.R. Sinclaire W.D. Thorpe, R.I. (Eds) Géologie des types de gîtes minéraux du Canada. *Canadian Geological Survey*, p. 714.

- Moses, A.M. (2015) The deportment of manganese of the Gasmberg East orebody, South Africa. *MSc thesis (unpublished), University of Pretoria,* p. 193.
- McClung, C.R. (2006) Basin Analysis of the Mesoproterozoic Bushmanland Group of the Namaqua Metamorphic Province, South Africa. *PhD thesis* (*unpublished), University of Johannesburg,* p. 509.
- McClung, C.R. and Viljoen, F. (2010) Ore mineralogy of the world-class Gamsberg zinc sulfide deposit, South-Africa. *GSA Denver Annual Meeting (Oct-Nov 2010),* Paper N°226-3, Abstract
- McClung C.R. and Viljoen F. (2011) A detailed mineralogical assessment of sphalerites from the Gamsberg zinc deposit, South Africa: The manganese conundrum. *Minerals Engineering,* 24, 930-938.
- McCourt, S. Armstrong, R.A. Grantham, G.H. Thomas, R.J. (2006). Geology and evolution of the Natal belt, South Africa. Journal of African Earth Sciences 46, 71-92.
- Olivo, G.R. and Gibbs, K. (2003) Paragenesis and mineral chemistry of alabandite (MnS) from the Ag-rich Santo Toribio epithermal deposit, Northern Peru. *Mineralogical Magazine,* 67, 95-102.
- Robb, L.J. Armstrong, R.A. Waters, D.J. (1999) The History of Granulite-Facies Metamorphism and Crustal Growth from Single Zircon U-Pb Geochronology: Namaqualand, South-Africa. *Journal of Petrology*, v.40, n.12, 1747-1770.
- Robb, L. (2005). Introduction to ore-forming processes. *Blackwell Publishing*, p. 386.
- Roy, S. (2006) Sedimentary manganese metallogenesis in response to the evolution of the Earth system. *Earth-Science Reviews,* 77, 273-305.
- Rozendaal, A. (1975) The Geology of Gamsberg, Namaqualand*, South Africa*. *M.Sc. thesis (unpublished), University of Stellenbosch*, p. 109.
- Rozendaal, A. (1977) Geological structure of the Gamsberg zinc deposit, Namaqualand, South Africa. *Annals of the University of Stellenbosch*, M.S. Taljaart Volume, 1-32.
- Rozendaal, A. (1986) The Gamsberg Zinc Deposit, Namaqualand District. *In*: Anhaeusser, C.R. and Maske, S. (Eds.) *Mineral Deposits of Southern Africa* (1986), 1477-1488. Geological Society of South Africa.
- Rozendaal, A. Rudnick, T-K. Heyn, R. (2017) Mesoproterozoic base metal sulphide deposit in the Namaqua Sector of the Namaqua-Natal Metamorphic Province, south Africa: a review. *South African Journal of Geology* (2017) 120 (1): 153-186.
- Ryan, P.J. Lawrence, A.L. Lipson R.D. Moore, J.M. Paterson, A. Stedmen, D.P. Van Zyl, D. (1986) The Aggeneys Base Metal Sulphide Deposits, Namaqualand District. In: Anhaeusser, C.R. and Maske, S. (Eds.) Mineral Deposits of Southern Africa (1986), 1447-1473. Geological Society of South Africa.
- Thomas, R.J. Agenbacht, A.L.D. Cornell, D.H. Moore, J.M. (1994) The Kibaran of southern Africa: Tectonic evolution and metallogeny. Ore Geology Reviews 9, 131-160.

- Sangster, D.F. (2002) The role of dense brines in the formation of vent-distal sedimentary-exhalative (SEDEX) lead-zinc deposits: field and laboratory evidence. *Mineralium Deposita,* 37, 149-157.
- Schouwstra, R. de Vaux, D. Hey, P. Malysiak, V. Shackleton, N. Bramdeo, S. (2010) Understanding Gamsberg – A geometallurgical study of a large stratiform zinc deposit. *Minerals Engineering,* 23, 960-967.
- Siivola, J. and Schmid, R. (2007) 12. List of Mineral Abbreviation. IUGS Subcommission on the Systematics of Metamorphic Rocks (SCMR), pp. 14.
- Stalder, M. Rozendaal, A. (2002) Graftonite in phosphatic iron formations associated with the mid-Proterozoic Gamsberg Zn-Pb deposit, Namaqua Province, South-Africa. *Mineralogical Magazine,* 66, 915-927.
- Stalder, M. and Rozendaal, A. (2004) Apatite nodules as an indicator of depositional environment and ore genesis for the Mesoproterozoic Broken Hill-type Gamsberg Zn-Pb deposit, Namaqua Province, South Africa. *Mineralium Deposita*, 39, 189-203.
- Stalder, M. and Rozendaal, A. (2005a) Distribution and geochemical characteristics of barite and barium-rich rocks associated with the Broken Hill-type Gamsberg Zn-Pb deposit, Namaqua Province, South Africa. *South African Journal of Geology,* 108, 35-50.
- Stalder, M. and Rozendaal, A. (2005b) Calderite-rich garnet and franklinite-rich spinel in amphibolite-facies hydrothermal sediments, Gamsberg Zn-Pb Deposit, Namaqua Province, South Africa. *The Canadian Mineralogist,* 43, 585-599.
- Spry, P.G. Teale, S.G. Steadman, J.A. (2009) Classification of Broken Hill-Type Pb-Zn-Ag deposits: a refinement. *Eos Transactions AGU, v. 90 (22), Joint Assembly Supplement*, Abstract, V21A-01.
- Craig, J.R. Vaughan, D.J. (1994) Chapter 7: Ore Mineral Textures. *In:* Ore Microscopy & Ore Petrography, 2nd Edition, p. 446.
- Walters, S.G. (1998) Broken Hill-type deposits. *AGSO Journal of Australian Geology & Geophysics,* 17(4), 229-237.
- Williams N.R. and Holtzhausen S. (2001) The impact of ore characterization and blending on metallurgical plant performance. *The Journal of The South African Institute of Mining and Metallurgy.* 437-446.
- Willner, A.P. (1995) Pressure-temperature evolution of a low-pressure amphibolite facies terrane in central Bushmanland (Namaqua-Natal Mobile Belt; South Africa). *Communications of the Geological Survey of Namibia*, 10, 5-19.
- Ye, L. Cook, N.J. Ciobanu, C.L. Yuping, L. Qian, Z. Tiegeng, L. Wei, G. Yulong, Y. Danyushevskiy, L. (2011) Trace and minor elements in sphalerite from base metal deposits in South China: A LA-ICPMS study. *Ore Geology Review,* 39, 188-217.

Appendices

Appendix A - Raw GVD038 sphalerite EPMA data.

Sample ID	S(Mass%)	Zn(Mass%)	Fe(Mass%)	Mn(Mass%)	Total(Mass%)
20A_3	33,253	55,391	9,156	0,946	98,746
20A_4	33,271	56,05	8,563	0,73	98,614
20A_5	33,045	55,748	9,051	0,955	98,799
20A_6	33,19	55,386	9,016	0,951	98,543
20A_7	33,282	55,601	8,812	0,915	98,61
20A_8	33,268	55,661	9,155	1,024	99,108
18B_5	33,552	55,351	8,653	1,557	99,113
18B_6	33,868	55,466	8,817	1,444	99,595
18B_7	34,01	54,753	9,188	1,353	99,304
18B_8	33,844	54,918	8,996	1,478	99,236
18B_9	34,046	55,366	8,861	1,463	99,736
18B_10	33,721	55,09	8,697	1,392	98,9
18A_2	34,056	55,539	9,108	1,345	100,048
18A_3	33,624	55,488	8,963	1,026	99,101
18A_4	34,065	56,711	8,069	0,769	99,614
18A_5	33,801	53,766	8,418	1,621	97,606
20B_1	32,238	54,156	8,945	1,29	96,629
20B_2	32,366	55,213	8,698	0,837	97,114
20B_3	32,653	52,625	8,955	1,189	95,422
20B_4	32,806	53,706	9,61	1,438	97,56
20B_5	32,716	54,264	9,226	1,464	97,67
20B_6	32,396	54,066	9,083	1,444	96,989
21A_1	33,099	55,151	8,562	1,066	97,878
21A_2	32,989	54,26	9,54	1,185	97,974
21A_3	33,073	58,168	6,767	0,599	98,607
21A_4	33,178	57,154	7,552	0,83	98,714
21A_5	33,308	55,71	8,768	1,003	98,789
22A_1	33,379	56,176	9,138	0,432	99,125
22A_2	33,45	55,983	9,431	0,403	99,267
22A_3	33,651	56,126	9,293	0,432	99,502
22A_4	33,347	55,569	8,99	0,472	98,378
22A_5	33,5	56,296	8,968	0,489	99,253
24A_2	33,686	52,327	9,713	3,694	99,42

24A_3	33,656	52,079	9,464	3,81	99,009
24A_4	33,934	51,846	9,666	3,902	99,348
24A_5	34,021	51,604	9,741	3,8	99,166
24A_6	33,807	51,694	9,732	3,751	98,984
25A_1	33,921	50,521	10,235	5,22	99,897
25A_2	33,677	51,829	9,449	4,942	99,897
25A_3	33,929	50,576	10,097	5,054	99,656
25A_4	33,659	51,818	9,558	4,592	99,627
25A_5	33,905	52,128	9,531	4,521	100,085
25B_2	33,613	50,459	10,569	4,07	98,711
25B_3	33,789	52,605	9,725	3,594	99,713
25B_4	33,615	52,684	9,581	3,579	99,459
25B_5	34,051	51,382	10,605	3,717	99,755
25B_7	33,583	51,331	10,356	3,747	99,017
26A_1	33,576	53,981	8,633	3,208	99,398
26A_2	33,494	50,252	11,014	4,534	99,294
26A_3	33,757	51,006	10,303	3,685	98,751
26A_4	33,586	51,982	9,732	3,629	98,929
26A_5	33,608	53,045	9,099	3,311	99,063
26B_1	34,406	49,432	9,912	5,919	99,669
26B_2	34,567	48,928	10,171	6,459	100,125
26B_4	34,255	48,968	10,429	5,924	99,576
26B_5	34,535	49,165	10,324	6,316	100,34
26B_7	34,487	49,825	9,765	6,283	100,36
26C_1	34,338	47,429	10,776	7,026	99,569
26C_2	33,813	47,951	10,175	7,068	99,007
26C_4	33,815	48,925	10,036	6,335	99,111
26C_5	33,72	48,507	10,446	6,545	99,218
26C_6	33,95	49,518	9,381	6,712	99,561
27A_1	34,159	46,951	10,255	7,694	99,059
27A_2	33,922	47,8	10,346	7,13	99,198
27A_3	34,357	47,32	10,668	7,285	99,63
27A_4	34,128	46,868	10,446	7,63	99,072
27A_5	34,174	47,049	10,686	7,492	99,401
29A_1	33,856	45,684	11,048	8,447	99,035
29A_2	33,881	45,528	11,209	8,419	99,037
29A_3	33,942	46,379	10,526	7,957	98,804
29A_4	34,019	46,306	11,068	8,137	99,53
29A_5	33,686	49,039	10,412	5,833	98,97
29B_2	33,939	47,887	11,005	6,593	99,424

29B_3	34,109	46,114	11,242	7,683	99,148
29B_4	33,602	49,366	10,122	5,669	98,759
29B_5	34,014	47,994	10,549	6,725	99,282
29B_6	33,759	48,548	10,168	6,131	98,606
31A_1	33,723	48,086	10,045	6,698	98,552
31A_2	34,173	47,875	9,996	6,821	98,865
31A_3	34,23	48,274	10,152	6,897	99,553
31A_4	33,823	48,315	10,083	6,73	98,951
31A_5	34,797	47,012	10,681	7,72	100,21
31A_6	33,948	47,91	10,172	6,789	98,819
31B_1	34,154	47,011	10,791	7,065	99,021
31B_3	34,174	49,244	9,764	6,084	99,266
31B_7	34,192	48,646	10,199	6,56	99,597
31B_8	34,241	45,863	11,619	7,891	99,614
31B_9	34,095	46,994	10,258	7,594	98,941
33A_2	33,913	52,508	9,253	3,709	99,383
33A_3	34,087	51,92	9,725	3,818	99,55
33A_4	33,902	48,964	10,255	5,39	98,511
33A_5	34,069	51,288	10,318	3,845	99,52
33A_7	33,313	51,213	8,904	3,996	97,426
29A_7	33,734	45,506	11,207	8,659	99,106
34A_1	34,073	47,082	10,94	7,254	99,349
34A_2	34,417	47,176	10,751	6,936	99,28
34A_3	34,018	49,146	9,832	5,597	98,593
34A_4	34,345	48,911	10,042	5,684	98,982
34A_5	33,648	59,904	5,106	0,246	98,904
34A_6	33,916	51,838	7,866	5,455	99,075
34A_8	33,996	58,597	6,444	0,417	99,454
34B_1	33,728	46,897	10,404	7,114	98,143
34B_2	34,187	48,079	9,783	6,735	98,784
34B_3	33,63	45,422	10,614	7,262	96,928
34B_4	34,312	45,639	10,969	7,701	98,621
34B_5	34,479	44,285	11,924	8,336	99,024
35A_1	34,221	48,523	9,966	6,549	99,259
35A_2	34,034	49,148	9,626	6,132	98,94
35A_3	34,205	47,768	10,067	6,972	99,012
35A_4	33,681	50,521	8,889	5,539	98,63
35A_5	34,025	48,643	10,075	6,118	98,861
36A_2	33,102	48,573	9,722	6,739	98,136
36A_3	33,431	47,518	10,506	7,135	98,59

36A_4	33,112	47,61	10,024	6,927	97,673
36A_5	33,629	48,205	9,904	6,895	98,633
36A_6	34,203	47,987	10,158	6,778	99,126
37A_1	33,857	46,338	11,825	6,725	98,745
37A_2	34,631	46,035	11,388	7,173	99,227
37A_3	33,962	45,653	11,483	7,918	99,016
37A_4	33,947	46,551	11,079	7,389	98,966
37A_5	33,963	46,63	11,038	7,351	98,982
38A_1	33,72	45,366	11,336	7,388	97,81
38A_2	33,213	47,206	10,252	6,846	97,517
38A_3	33,53	46,087	11,682	6,973	98,272
38A_4	33,644	46,589	11,264	7,265	98,762
38A_5	33,836	46,039	11,245	7,515	98,635
40A_1	34,317	47,196	10,881	6,66	99,054
40A_2	34,808	46,932	11,074	6,671	99,485
40A_3	34,806	46,713	10,985	6,831	99,335
40A_4	34,446	47,586	10,49	6,792	99,314
40A_5	34,566	47,101	10,862	7,003	99,532
40B_1	33,672	47,407	10,574	6,848	98,501
40B_2	33,216	49,238	9,668	6,045	98,167
40B_3	33,153	49,219	9,651	6,034	98,057
40B_4	33,539	48,11	10,314	6,481	98,444
40B_5	33,157	48,485	9,811	6,31	97,763
40C_1	34,364	46,857	10,808	7,142	99,171
40C_5	34,435	51,241	8,62	5,237	99,533
40C_6	34,195	48,644	10,257	6,53	99,626
40C_7	35,227	48,791	9,735	6,39	100,143
40C_9	33,946	50,975	8,857	5,331	99,109
41A_1	33,622	49,233	9,422	5,896	98,173
41A_2	33,628	48,252	9,874	6,169	97,923
41A_3	33,505	49,318	9,1	5,849	97,772
41A_4	33,859	49,025	9,803	6,337	99,024
41A_5	33,808	47,6	10,113	6,688	98,209
42A_1	33,66	48,77	9,541	6,119	98,09
42A_2	33,963	46,962	10,534	7,104	98,563
42A_3	33,899	48,67	9,883	6,296	98,748
42A_4	33,714	47,785	9,603	6,174	97,276
42A_5	33,653	49,205	9,523	6,042	98,423
42B_1	34,219	46,281	11,384	7,275	99,159
42B_2	34,013	48,217	10,556	5,948	98,734

42B_3	34,221	47,885	10,881	6,466	99,453
42B_4	33,775	49,581	9,809	5,672	98,837
42B_5	34,236	46,723	11,283	7,257	99,499
43A_1	33,553	47,301	10,558	7,039	98,451
43A_4	33,667	48,291	9,98	6,644	98,582
43A_5	33,752	50,361	9,02	5,852	98,985
43A_6	33,637	47,736	10,049	6,899	98,321
43A_7	34,023	48,953	9,526	6,506	99,008
44A_1	33,854	50,73	8,835	5,62	99,039
44A_2	33,758	50,124	8,969	5,859	98,71
44A_3	33,787	50,928	8,43	5,117	98,262
44A_6	34,116	48,874	9,783	6,333	99,106
44A_7	33,631	50,606	9,145	5,163	98,545
44B_2	33,54	46,424	10,708	7,631	98,303
44B_4	33,819	46,765	10,843	7,476	98,903
44B_6	33,721	47,357	10,205	7,225	98,508
44B_7	34,17	48,191	9,985	6,878	99,224
44B_8	33,421	47,267	9,561	7,545	97,794
44C_2	33,726	49,519	9,622	6,478	99,345
44C_5	33,522	48,801	9,878	6,999	99,2
44C_9	36,803	0,054	5,857	56,915	99,629
18B_7	32,754	54,709	8,962	1,43	97,855
18B_8	33,265	54,697	9,166	1,412	98,54
18B_9	33,028	54,502	9,038	1,537	98,105
18B_10	33,228	55,407	8,861	1,142	98,638
21A_6	33,498	52,183	8,295	0,933	94,909
21A_7	33,894	54,431	9,351	1,11	98,786
21A_8	33,574	55,178	8,729	1,014	98,495
21A_9	33,509	55,95	8,233	0,974	98,666
29A_8	34,156	45,551	10,904	7,899	98,51
29A_9	34,013	45,257	11,266	7,66	98,196
29A_10	34,165	45,106	11,215	7,989	98,475
31B_10	33,919	47,959	10,408	6,684	98,97
31B_11	33,831	48,058	10,284	6,464	98,637
31B_12	34,125	49,105	10,051	6,255	99,536
34A_9	32,04	61,448	2,645	1,212	97,345
34A_10	34,081	60,526	3,176	1,176	98,959
34A_11	33,532	60,84	3,523	1,029	98,924
34A_12	33,767	59,192	4,314	0,948	98,221
34A_13	33,94	49,923	9,731	5,699	99,293

40C_10	32,37	47,129	9,097	5,844	94,44
40C_11	34,107	48,357	9,905	6,64	99,009
40C_12	34,313	49,067	9,992	6,435	99,807

Appendix B – Raw GAM107 sphalerite data (from Vedanta).

Interval	S	Mn	Fe	Zn	Unit
1	31,98	0	1,30	66,82	**PEO_Py**
2	33,19	0,02	1,21	64,35	**PEO_Py**
3	33,12	0,02	2,43	64,19	**PEO_Py**
4	33,02	0,22	1,33	65,12	**PEO_Py**
5	34	0,7	7,13	58,20	**PEO_Py**
6	32,23	0,86	6,73	60,02	**PEO_Po**
7	32,68	0,25	3,31	59,99	**PEO_Po**
8	32,59	0,31	3,47	61,13	**PEO_Po**
9	32,95	0,34	3,64	62,77	**PEO_Po**
10	32,67	1,26	7,12	57,74	**PEO_Po**
11	33,14	2,41	6,08	57,84	**PEO_Po**
12	32,93	0,53	7,01	58,34	**PEO_Po**
13	32,96	0,7	6,07	59,51	**PEO_Po**
14	32,67	0,84	6,56	59,27	**PEO_Po**
15	32,82	0,97	6,45	59,73	**PEO_Po**
16	32,68	0,25	1,14	65,57	**MPO**
17	32,68	0,3	1,38	64,55	**MPO**
18	32,55	0,31	1,31	65,46	**MPO**
19	32,82	0,35	1,56	65,16	**MPO**
20	32,24	0,35	4,29	61,68	**MPO**
21	32,46	0,4	3,20	62,10	**MPO**
22	32,91	0,42	3,96	62,32	**MPO**
23	32,94	1,09	4,88	60,83	**MPO**
24	33,05	0,69	7,17	58,85	**MPO**